Synthesis and photoluminescence properties of alkali metal salt-doped zinc tungstates

アルカリ金属塩添加タングステン酸亜鉛の合成および発光特性

A dissertation submitted in partial fulfillment of the requirements for the Degree of Doctor of Engineering

by

Lorchirachoonkul Prinya

Academic advisor: **Assoc. Prof. Tomoichiro Okamoto**

Department of Materials Science
Nagaoka University of Technology
Niigata, JAPAN
March, 2019

ACKNOWLEDGEMENTS

The author would like to express his profound gratitude to Assoc. Prof Tomoichiro Okamoto, his advisor, for his excellent guidance, strong support, supervision, encouragement, inspiration, support and constructive criticism throughout his study. He provided not only all the requirements for the accomplishment of his study but also gave invaluable advice in the personal concerns. Without his help in both academic and personal concerns, this dissertation work could not have been completed.

The author's great thanks are given to the Japanese Government (Ministry of Education, Culture, Sports, Science and Technology, MEXT) for granting the scholarships and financial support to study the Doctoral program in Material science.

Finally, the author always keeps in mind the true love, support encouragement and provision of whatever he needs throughout his whole life from his beloved family members.

Lorchirachoonkul Prinya
Nagaoka University of Technology, Japan

ABSTRACT

In this work, we found the significant improvement of photoluminescence of zinc tungstate doped with alkali metal salts.

First, this work focused on the different concentrations of potassium salts doped $ZnWO_4$. The samples were prepared by solid-state reaction using ZnO, WO_3, KNO_3, K_2SO_4, and KCl as starting powders. The powders were mixed with the molar ratios of ZnO: WO_3: potassium salts = 1: 1: x (x = 0, 0.02, 0.04, 0.1) and sintered at 800˚C for 3 h in air. The zinc tungstate phase was confirmed from the samples by X-ray diffraction. The emission peak of photoluminescence excited at 275 nm was observed at 465 nm. With increasing potassium salts content, the intensity increased reached its maximum at x = 0.02 and decreased. The order of each maximum intensity was $KNO_3 > K_2SO_4 > KCl$.

After that, alkali metal nitrate and sulfate doped $ZnWO_4$ was prepared and investigated. The samples were prepared in the same method as the previous experiment. From the samples, the grain size of the doped samples was large compared with undoped one image. Lattice parameters of zinc tungstate phase was calculated by Rietveld refinement and found that they increased with increasing ionic radius of alkali metal ions. Compared with undoped sample, the samples doped with alkali metal salts exhibited the higher emission intensity except $LiNO_3$, Li_2SO_4, and Na_2SO_4 doping. It was considered that alkali metal ions replacing Zn ions in the crystal lattice enhanced the intrinsic luminescence in the blue wavelength region. Moreover, different anions doping had the different effect of the enhancement of the luminescence.

TABLE OF CONTENTS

LIST OF TABLES

LIST OF FIGURES

CHAPTER 1

INTRODUCTION

1.1 GENERAL

The demands of photoluminescence devices continuously occur, while the material resource is limited. Therefore, the improvement of the photoluminescence device has become an alternative way because it will be better if the device have the same size but higher performance. Generally, the doping method can be applied.

Furthermore, the major problem of photoluminescence projects, which are challenging for researchers, is low performance. Hence, many studies about optical properties including absorption, light yield, emission wavelength, and the afterglow of luminescence have been investigated and reported [1, 2, 3]. Minh et al. [4] have reported that doping phosphor material with Er^{3+} shows a significant optical transition. Ishwar Prasad Sahu et al. [5] has reported that the photonic properties such as photoluminescence intensity, afterglow, and mechanoluminescence intensity significantly increased after Dy^{3+} co-doping on $Sr_2MgSi_2O_7:Eu^{2+}$ phosphor material. Jie et al. [6] have reported that compared with $CaMoO_4:Eu^{3+}$ without

charge compensation, charge compensated $CaMoO_4:Eu^{3+}$ phosphor material shows the significant enhancement of red light emission excited at 393 and 467 nm wavelength. Singh et al. [7] have reported that Luminescence intensity of $CaMoO_4:Eu^{3+}$ increases significantly with co-doping of Gd^{3+}. Hee Sang Kang et al [8] has reported that the photoluminescence intensities of co-doped $(Ba,Sr)_2SiO_4$:Eu phosphor material increased about 120~143% of the sample without co-dopant. Dafinova et al. [9] have reported that the addition of ammonium and sodium salts into the phosphor material leads to a substantial increase in the intensity of the intrinsic blue emission. Sheng Deng et al. [10] reported that co-doping of Ca and Dy showed higher UV absorption efficiency of the sample. For alkali metal and alkali earth metal doping, it was reported that co-doping of Li, Sm and Bi improved the white light emission which is the extrinsic photoluminescence properties of phosphor material [11]. The enhanced luminescence comes from the improved crystalline and from the charge compensation of Li^+ ions by the co-doping of Li and Pr [12]. And for sodium salts doping, the decreasing of photoluminescence activities in the phosphor material occurs because Na^+ hamper the transition [9].

For phosphor material, the scintillator is the famous application for these fields. The scintillator is a material that exhibits scintillation when excited by ionizing radiation.

Scintillators have also been used in many applications such as particle detectors, x-ray security, computed tomography scanner, resource exploration such as oil

Generally, famous materials that are used in the scintillator application such as Polyethylene naphthalate, Tl doped NaI, Tl doped CsI, Na doped CsI, CsI, CsF, Tl doped KI, Eu doped LiI, BaF_2, Eu doped CaF_2, Ag-doped ZnS, Ce doped $Y_3Al_5O_{12}$, bismuth germanate (BGO), Cerium doped Gadolinum ortho-silicate (GSO) and lutetium oxyorthosilicate (LSO).

1.2 STATEMENT OF THE PROBLEMS

As mentioned in the previous section, there are three major problems that are widely found when we use the famous materials which are aforementioned as following items:

- Hygroscopic
- Toxic
- Cost

Hygroscopic property is the phenomena which absorb moisture into the material. When they absorb moisture, some material surface has the possibility to be damaged. Some materials such as Tl doped NaI, Na doped CsI, pure CsI, Tl doped CsI, and BaF_2 have hygroscopic property.

For example, in Na doped CsI, the surface of the materials will be deactivated by hydration. Damage which occurs from the small amount of hydration

is not clearly seen but it affects in the photoluminescence properties at low energies. Moreover, the drops of moisture or excessive condensation easily damage the surface of pure CsI, Tl doped CsI, and BaF_2 which decrease the photoluminescence properties of the material.

For the toxic problem, many heavy metal elements were used as starting powder or dopant on the scintillator materials. Some heavy metal is toxic which is a danger for human health or the environment. For example, thallium iodide as a pure chemical is toxic. From MSDS datasheet, the amounts of more than 1 gram per person can cause death.

For cost problem, Because of some famous scintillator material has a heavy metal compound, the price of the materials is high.

For scintillator application, photoluminescence properties are important. Many studies have been investigated about the improvement of photoluminescence in various methods such as doping some material. Doping in the materials has been investigated for a long time. Some dopant was doped in materials can improve its performance in photonic fields but some cannot. Some researchers have been reported that the photoluminescence was related to band gap and deformation of materials. Kowalski et al. [13] explained that the introducing of additional levels to the band gap of samples can make the material a good phosphor. The energy levels of dopants needed for emission process must lie in the gap of the host material. Kalinko et al. [14] reported that the deformation of the WO_6^{6-} structure of the samples was related to the enhancement of photoluminescence in the $ZnWO_4$.

The aforementioned problem has led to the intensive study of the new material for replacing with other materials. $ZnWO_4$ is a good choice because it is less hygroscopic, less toxic and cheaper than other materials, a widely used scintillation crystal. To improve the performance of $ZnWO_4$, the doping method is chosen to use in this work. For dopant, alkali metal salts were chosen to use in this work. From the related researches, alkali metal ions are supposed to substitute with Zn^{2+} of $ZnWO_4$. The charge difference between alkali metal ions (Li^+, Na^+, K^+, Rb^+, Cs^+) and Zn^{2+} has the possibility to distort the symmetric of the crystal structure and the energy level for the photoluminescence which resulted to the enhancement of photoluminescence of the samples.

Moreover, because ionic radius of alkali metal ions is larger than Zn^{2+} [15, 16, 17, 18, 19, 20, 21]. Therefore, doping the $ZnWO_4$ with alkali metal should deform the crystal structure which might result in the increasing of photoluminescence activities of $ZnWO_4$.

1.3 RESEARCH OBJECTIVES

The purpose of this study is to improve the photoluminescence properties of zinc tungstate. The study emphasizes the following objectives:

(1) To investigate the effect of alkali metal salts doping using nitrate, sulfate, chloride on photoluminescence property of zinc tungstate.

(2) To make clear the effect of the alkali metal salts doping

(3) To validate the performance of the photoluminescence activities.

(4) To determine the relationship between crystal structure and photoluminescence of the samples.

1.4 ORGANIZATION OF THE DISSERTATION

The organization of the dissertation includes the following chapters:

Chapter 1 describes the overview of the photoluminescence and scintillator device. The statement of the problem is realized and discussed. The objectives of the study are also mentioned.

Chapter 2 explains briefly about the material background on the zinc tungstate and equipment experimental.

In Chapter 3, the effect of potassium doping using nitrate, sulfate, chloride on photoluminescence property of zinc tungstate was investigated and explained. The analysis by SEM and XRD were carried out. The performance of the samples was examined.

In Chapter 4, the effect of alkali metal doping using nitrate on photoluminescence property of zinc tungstate was done and discussed. The analysis by SEM and XRD were carried out. The performance of the samples was examined.

In Chapter 5, the effect of alkali metal doping using sulfate on photoluminescence property of zinc tungstate was investigated and discussed. The analysis by SEM and XRD were carried out. The performance of the samples was examined.

The conclusions of the research and recommendations for further research are drawn in chapter 6.

References

[1] T. Oi, K. Takagi and T. Fukuzawa, Scintillation study of $ZnWO_4$ single crystals, Appl. Phys. Letts. 36 (1980) 278-279.

[2] W. Kolbe, K. Petermann, and G. Huber, Optical properties of planar waveguides on $ZnWO_4$ formed by carbon and helium ion implantation and effects of annealing, IEEE J. Quantum Electron. 21(10) (1985) 1596–1599.

[3] W. Klamra, T. Szczesniak, M. Moszynski, J. Iwanowska, L. Swiderski, A. Syntfeld-Kazuch, V. N. Shlegel, Y. V. Vasiliev, E. N. Galashov, Journal of Instrumentation 7 (2012)

[4] P. Belli, R. Bernabei1, F. Cappella, R. Cerulli, F. A. Danevich, S. D'Angelo, A. Incicchitti, V. V. Kobychev, D. V. Poda and V. I. Tretyak, Final results of an experiment to search for 2β processes in zinc and tungsten with the help of radiopure $ZnWO_4$ crystal Scintillators, J. Phys. G 38 (2011) 115107

[5] I. P. Sahu, D. P. Bisen, N. Brahme, and M. Ganjir, Enhancement of the photoluminescence and long afterglow properties of $Sr_2MgSi_2O_7:Eu^{2+}$ phosphor by Dy^{3+} co-doping, Luminescence 30 (2015) 1318–1325

[6] J. Liu, H. Lian, and C. Shi Improved optical photoluminescence by charge compensation in the phosphor system $CaMoO_4:Eu^{3+}$, Optical Materials 29 (2007) 1591–1594.

[7] B. P. Singh, A. K. Parchur, R. S. Ningthoujam, A. A. Ansari, P. Singh, and S. B. Rai, Enhanced Photoluminescence in $CaMoO_4:Eu^{3+}$ by Gd^{3+} co-doping, Dalton Trans. (2013).

[8] H. S. Kang, S. K. Hong, Y. C. Kang, K. Y. Jung, Y. G. Shul and S. B. Park, The enhancement of photoluminescence characteristics of Eu-doped barium strontium silicate phosphor particles by co-doping materials, J. Alloys Compd. 402 (2005) 246–250.

[9] R. Dafinova, K. Papazova, and A. Bojinova, The influence of sulphate, chloride and iodide ions of the zinc tungstate blue emission band, J. Mater. Sci. Lett. 17 (1998) 237-239.

[10] S. Deng, W. Zhang, Z. F. Hu, Z. Y. Feng, L. Ma, Y. M. Pan, X. Sheng and L. Luo, Photoluminescence and Photocatalytic Activity in Ca^{2+} and Dy^{3+} Co-doped $ZnWO_4$ System, 2017 Joint International Conference on Materials Science and Engineering Application (ICMSEA 2017) and International Conference on Mechanics, Civil Engineering and Building Materials (MCEBM 2017).

[11] W. Ran, Q. Wang, Y. Zhou, S. Ding, J. Shi, and J. H. Jeong, Fabrication of $ZnWO_4$:Sm^{3+}, Bi^{3+}, Li^{+} with tunable white light-emitting properties for W-LEDs, Materials Research Bulletin 64 (2015) 14.

[12] K. Wang, W. Feng, X. Feng, Y. Li, P. Mi, and S. Shi, Synthesis and photoluminescence of novel red-emitting $ZnWO_4$: Pr^{3+}, Li^{+} phosphors, Spectrochim Acta A Mol Biomol Spectrosc. 154 (2016) 72-75.

[13] Z. Kowalski, S. M. Kaczmarek, M. Berkowski, M. Głowacki, Y. A. Zhydachevskii and A. Suchocki, Growth and optical properties of $ZnWO_4$ single crystals pure and doped with Ca and Eu, J. Cryst. Growth 457 117-121.

[14] A. Kalinko and A. Kuzmin, Raman and photoluminescence spectroscopy of zinc tungstate powders, J. Lumin. 129 1144-1147

[15] The Materials Project: $ZnWO_4$, https://materialsproject.org/materials/mp-602297/

[16] P. Tabero and A. Frackowiak, Reinvestigations of the Li_2O–WO_3 system, J Therm Anal Calorim 130 (2017) 311–318

[17] The Materials Project: Na_2WO_4, https://materialsproject.org/materials/mp-641114/

[18] The Materials Project: K_2WO_4, https://materialsproject.org/materials/mp-772367/

[19] Detail information of Rb_2WO_4, http://www.catalysthub.net/materials.php?id=1819676

[20] The Materials Project: Rb_2WO_4, https://materialsproject.org/materials/mp-761354/

[21] H.D.B. Jenkins and K.P. Thakur, Reappraisal of thermochemical radii for complex ions, J. Chem. Educ. 56 (1979) 576-577.

CHAPTER 2

FUNDAMENTAL ASPECT

2.1 ZINC TUNGSTATE

Zinc tungstate ($ZnWO_4$) is one of the famous materials which use for the photonic field applications such as scintillators [1-4], laser host [5], photocatalyst [6-8], and optical recording [9-10]. Its structure consists of ZnO_6 octahedral and WO_6 octahedral or Wolframite crystal structure which has the intrinsic blue emission wavelength between 460 and 490 nm [11]. In scintillation field, zinc tungstate is interested as detectors. Generally, it is used in such principal investigations as searches for neutrinoless double beta decay [12, 13] and searches for dark matter [14-17] where the anisotropic properties of $ZnWO_4$ crystals are used. Compared with other material which used for scintillation crystals, the main advantages of $ZnWO_4$ are less hygroscopic, less toxic and low cost [11].

2.1.1 STRUCTURE OF ZINC TUNGSTATES

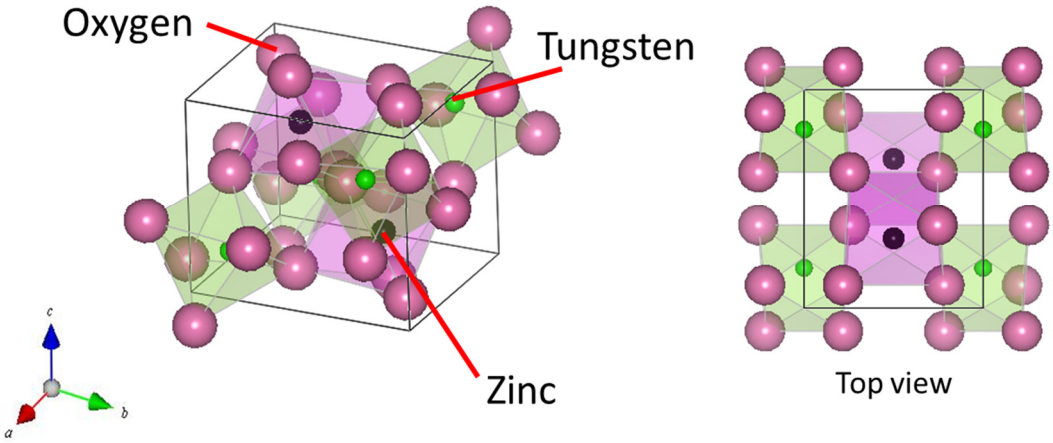

Fig. 2.1 The crystal structure of $ZnWO_4$.

$ZnWO_4$ consisting of ZnO_6 and WO_6 octahedral complexes (Wolframite crystal structure) with C_{2h} point group symmetry and P 2/c space group. Fig. is the top view of the unit cell. 1 unit cell consisting of 8 oxygen atoms, 2 tungsten atoms, and 2 Zinc atoms. WO_6 octahedral has 2 shared oxygen. Its crystal structure is monoclinic which has lattice parameters a = 4.69263 Å, b = 5.72129 Å, c = 4.92805 Å and $\beta = 90.6321^0$ [18]. Figure 2.1 shows that Zn and W cations are surrounded by the hexagonal-close packed (hcp) 6 oxygen atoms with octahedral sites.

Table 2.1 The fundamental properties of Zinc tungstate

Formula weight	313.22
Appearance	White powder or crystalline solid
Melting Point	1875 °C
Density	7.62 g/cm^3
Crystal system	Monoclinic
Water Solubility	Insoluble in water

Lattice constant	a = 4.69 Å
	b = 5.72 Å
	c = 4.93 Å
axial angle	α = 90.00°
	β = 90.63°
	γ = 90.00°

2.1.2 PHOTOLUMINESCENCE OF ZINC TUNGSTATES

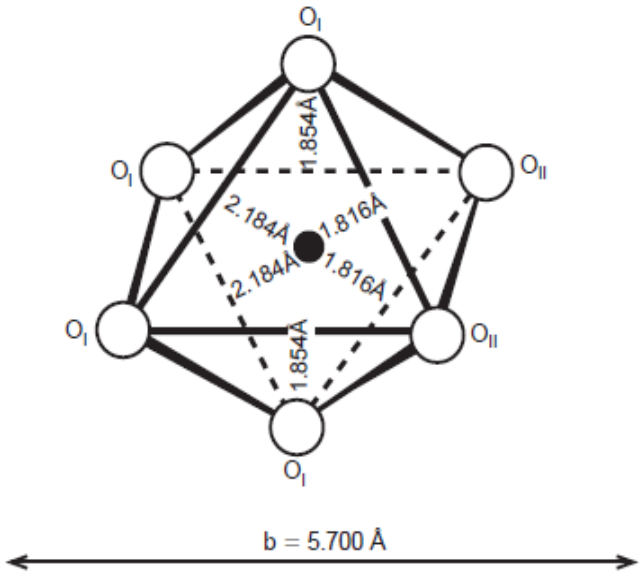

Fig.2.2 WO_6^{6-} complex structure of zinc tungstate. [11]

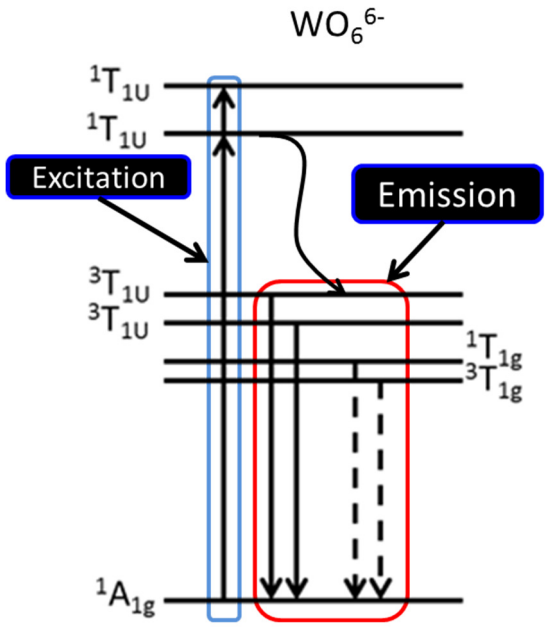

Fig.2.3 The energy level for the photoluminescence in the WO_6^{6-} complex of zinc tungstate. [11]

From zinc tungstate, photoluminescence of Zinc Tungstate occurs from the presence of WO_6 structures. WO_6 structure consists of W atom surrounded by 6 Oxygen atoms. 2 Oxygen atoms will share with other WO_6 and related with emission as shown in Figure 2.2.

Generally, the emission occurs from a charge-transfer transition takes place between the free d orbitals of W and the p orbitals of the O atoms of WO_6^{6-} complex. Figure 2.3 shows the energy level diagram for the photoluminescence in the WO_6^{6-} complex of zinc tungstate [11]. Oosterhout [12] explained that the highest occupied state with t_{1g} symmetry is associated with the $2p$ orbital of the oxygen atom and the excited state consists of an electron at the d orbital of tungsten atom with t_{2g} symmetry. The absorption in the WO_6^{6-} complex is assigned to the ${}^1A_{g1} \rightarrow {}^1T_{1u}$ level and emission is assigned to two ${}^3T_{1u}$ levels $\rightarrow {}^1A_{g1}$ level. Moreover, the long decay time of the photoluminescence of zinc tungstate may occur from the spin-forbidden transitions are partly allowed by spin-orbit coupling. The deformation of the WO_6 octahedron that leads to the changing in the site symmetry may result in T_{1g}-levels and effect to the photoluminescence properties in the long wavelength side.

2.2 SOLID-STATE REACTION METHOD

The solid-state reaction method is the important method for preparing the polycrystalline solids from the mixture of solid starting materials which cannot have the reaction between the starting materials at room temperature. Hence, they are necessary to heat them at high temperature in order to the creating the reaction at an appreciable rate.

2.3 MATERIAL ANALYSIS METHOD

2.3.1 X-RAY DIFFRACTION (XRD)

X-ray diffraction (XRD) is a method that displays the crystallographic structure of materials. This method uses X-ray beams to strikes on the surface of the sample and detects the diffraction pattern of scattered beams. The angles (2θ) and intensities of the scattered beams can show the density of electrons within the crystal structure of samples which can explain their chemical bonds, their disorder and other information.

For XRD principle, Bragg diffraction is the most important knowledge. Bragg diffraction occurs when waves, which have a wavelength comparable to atomic spacings, are scattered by the atoms and undergo constructive interference. For a crystalline solid, the interplanar distance between planes (d) scatter the waves. When x-ray wave strikes a crystalline solid, the difference between the path lengths of the two x-ray waves is equal to an integer multiple with the wavelength (n λ).

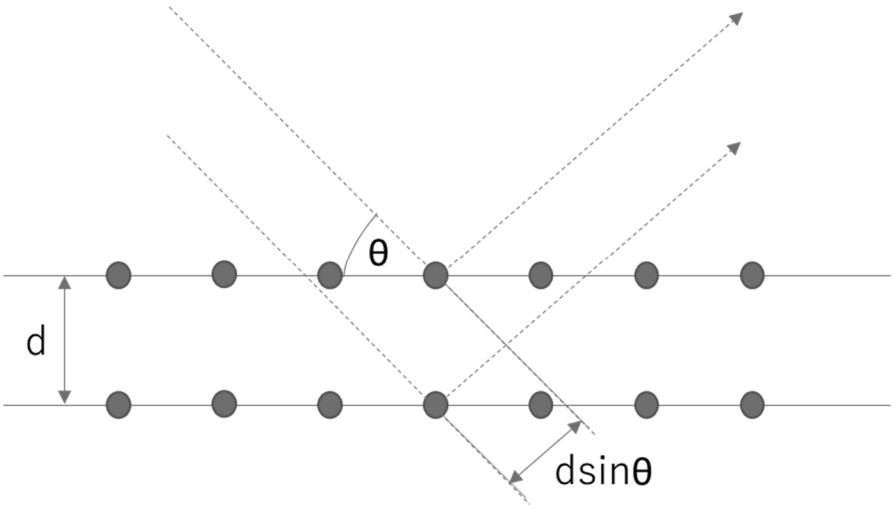

Fig 2.4 Bragg diffraction

From Fig. 2.4, the path difference between the two waves is equal to $2d\sin\theta$, where θ is the incident angle. From these phenomena, Bragg's law is created to describes the condition on θ for constructive interference.

$$n\,\lambda = 2d_{hkl}\sin\theta$$

, where n is an integer number, λ is the wavelength of the x-ray wave and hkl is lattice planes of the sample.

Generally, x-ray diffraction pattern shows the peak intensity vs. measured diffraction angle 2θ. It has the series of peaks in the various intensities. Each XRD peak is related to the x-rays which diffracted from lattice planes in the sample. The peak intensity is related to the number of x-ray photons from beams which is detected by the detector in each angle (2θ). The positions of the peaks (2θ) in x-ray diffraction (XRD) pattern depend on the crystal structure of the sample.

Moreover, the size of particles of crystals in the form of powder can be determined by the Scherrer equation which relates to the size of particles or crystallites. It can be written as:

$$\tau = \frac{K\lambda}{\beta\sin\theta}$$

, where τ is the crystalline size (Å), K is a dimensionless shape factor which has a typical value about 0.9, λ is the X-ray wavelength (Å), β is the FWHM (degrees) and θ is the Bragg angle (degrees).

For XRD pattern analysis, the observed XRD pattern must be compared with the standard XRD pattern to confirm their crystal structure and phase. The standard XRD pattern is called that International Centre for Diffraction Data (ICDD) pattern. The position of each peak of XRD pattern will show the lattice planes of the sample.

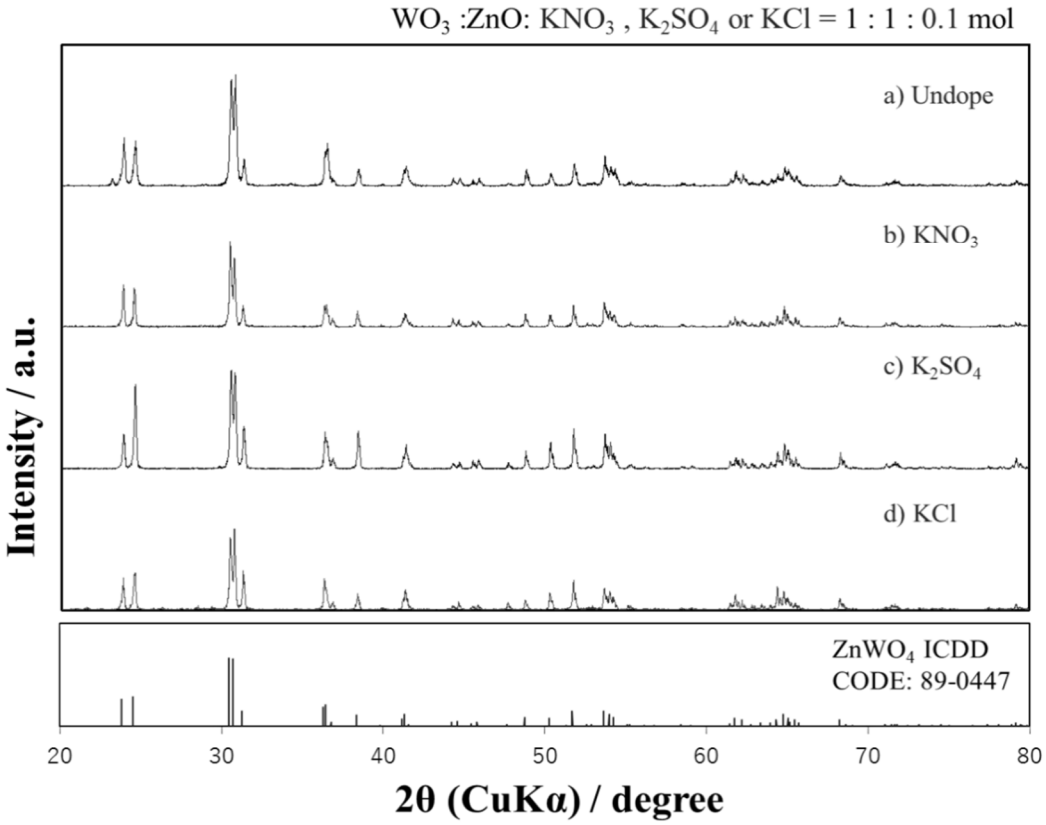

Fig. 2.5 XRD patterns and ICCD pattern

XRD instrument which use in this experiment is RIGAKU Multiflex.

2.3.2 SCANNING ELECTRON MICROSCOPY (SEM)

Scanning Electron Microscopy (SEM) is used to observe the morphologies of the samples. In this method, the SEM images of the sample are obtained from the high-energy beam of electrons which interact with the atoms of the sample and

produce signals which contain the details about the morphology of the sample such as composition, surface microstructure, and topography. When electron incident beams strike the sample, both photons and electrons are emitted.

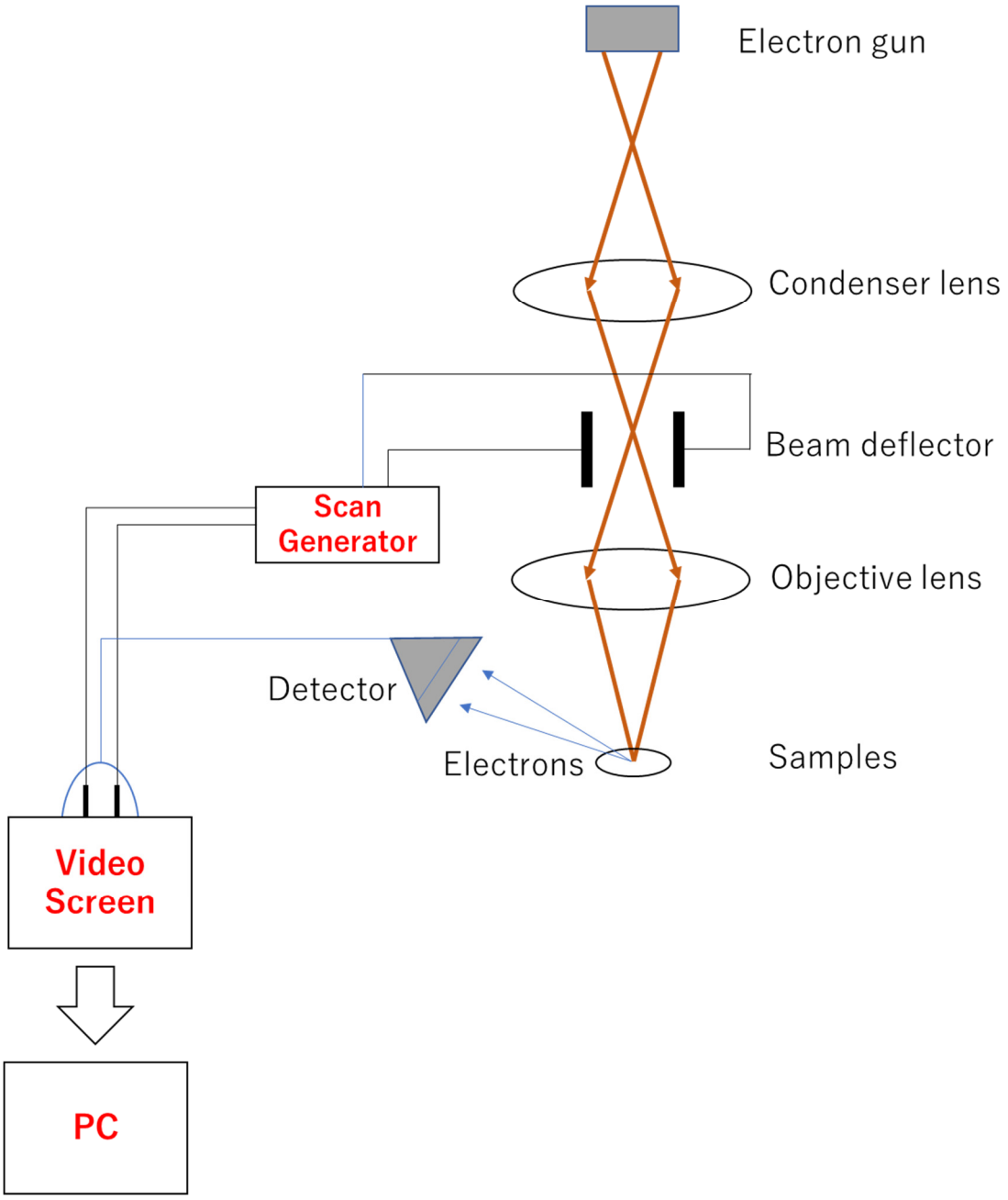

Fig. 2.6 Structure of SEM

Advantages and disadvantages of SEM

Advantages

· Detailed 3D and topographical imaging and the useful information collected from different detectors are obtained.

· Works very fast.

· Can generate data in digital form.

· Require minimal actions for sample preparation.

Disadvantages

· Expensive and large.

· Need special training to operate.

· Samples must be solid.

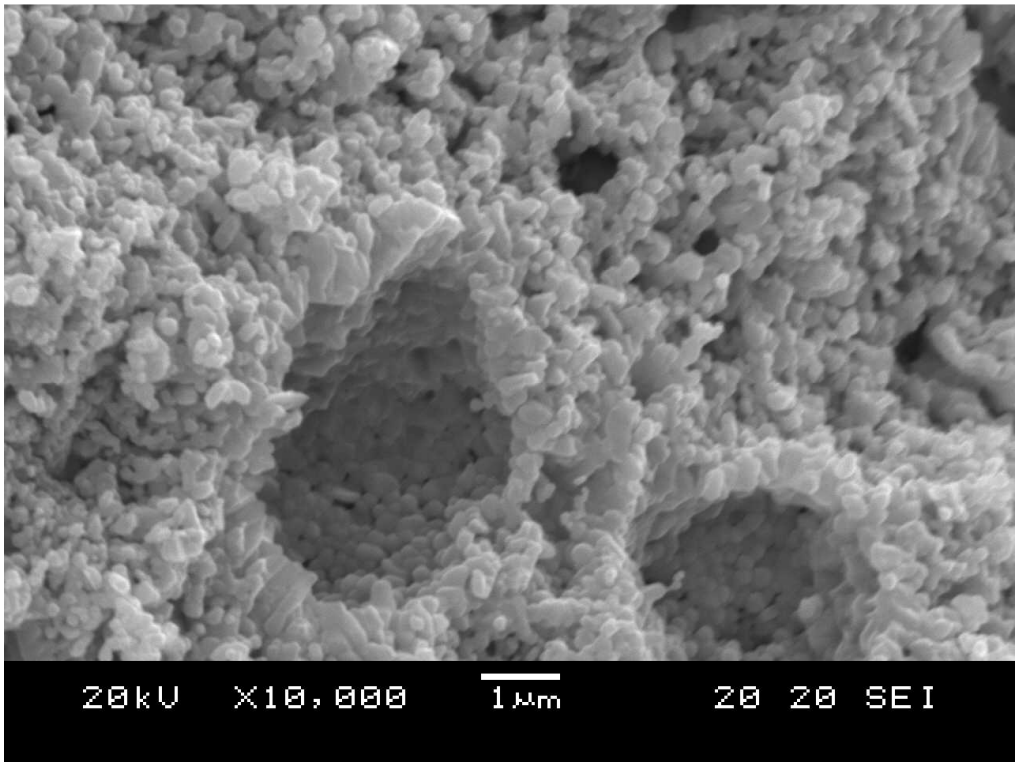

Fig. 2.7 SEM image of potassium sulfate doped zinc tungstate

SEM instrument which use in this experiment is JEOL JSM-5510.

2.3.3 FLUORESCENCE SPECTROSCOPY

Fluorescence spectroscopy is an analytical tool for photoluminescence properties. Its process consists of the excitation of molecules from low energy state to high energy state with a high energy source (excitation process) and the recording of the released energy when excited molecules move back to low energy state as fluorescence energy (emission process).

2.3.3.1 Principle

Fluorescence spectroscopy consists of

- Light source

- Two monochromators for selection of the excitation wavelength and for analysis of the emitted light

- Sample holder

- Detector

After the sample are excited by excitation wavelength, the light is emitted in all directions from the sample and is detected by the detector. Normally, the lamp source which emits radiation in the UV, visible and near-infrared regions is the Xenon arc lamp. The light is released to the excitation monochromator, which allows either preselection of wavelength or scanning of certain wavelength range. When the excited wavelength impacts the sample, the sample in the sample holder is excited and emit light. Light emitted is analyzed by the emission monochromator.

The wavelength analysis of emitted light is carried out by measuring the intensity of fluorescence.

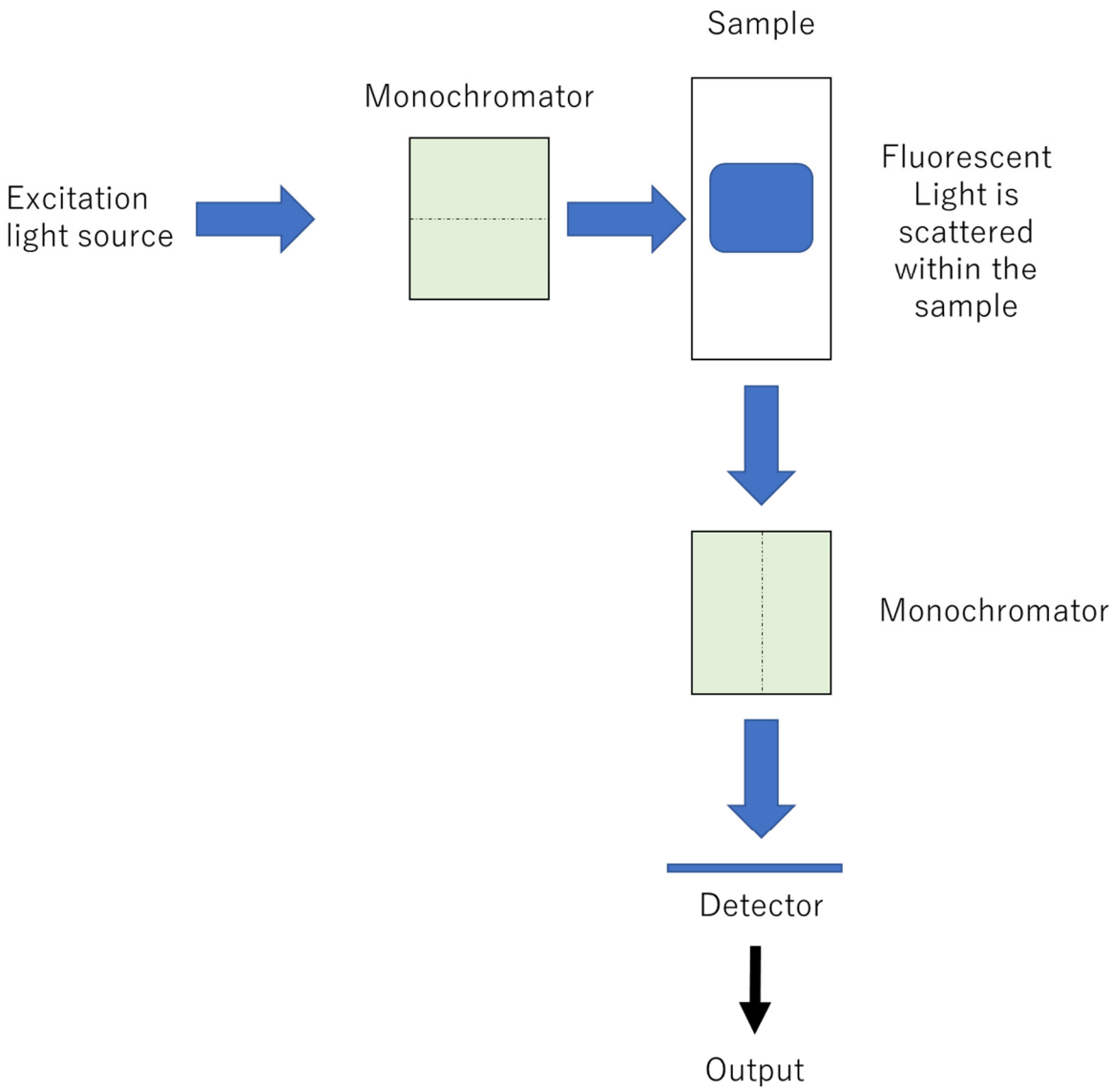

Fig. 2.8 Structure of fluorescence spectroscopy

Fluorescence spectroscopy instrument which use in this experiment is Hitachi F-7000.

2.3.4 RIETVELD REFINEMENT

The Rietveld refinement is the method which refines the parameters to minimize the difference between an observed XRD data (experimental pattern) and theoretical XRD pattern (ICDD pattern) which comes from the model based on the hypothesized crystal structure and the parameters of the instrument.

Rietveld refinement can do the quantitative phase analysis (crystalline and amorphous), lattice parameters calculation, Atomic coordinates, and occupancies, temperature vibrations, Grain size, stacking and twin faults and magnetic moments.

2.3.4.1 PROFEX

Profex is a graphical user interface for evaluating X-ray diffraction pattern of the powder sample using Rietveld refinement. It can analyze the identification and quantification of crystalline phases and crystal structure refinement.

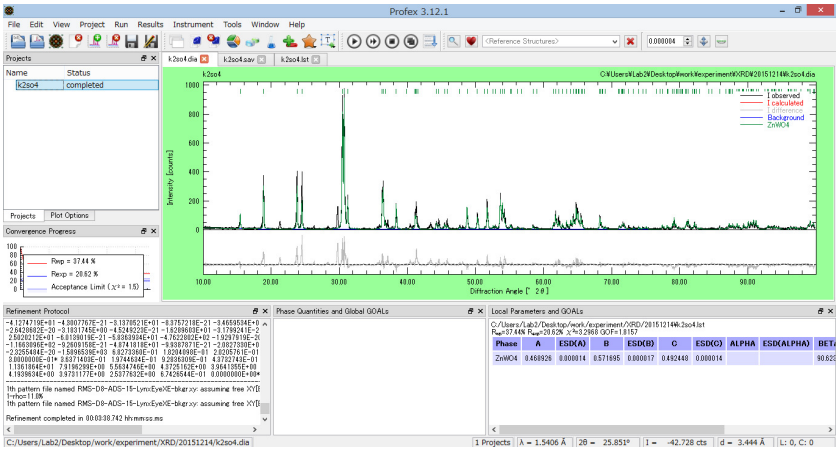

Fig. 2.9 Screenshot of profex program

2.3.5 LASER RAMAN SPECTROSCOPY

Raman spectroscopy is a useful analytical technique which is used for the identification of the materials.

In this technique, photons from infrared ray will interact with materials by absorption or scattering processes. Scattering process can separate to Rayleigh scattering (elastically scattering) and Raman scattering (inelastic scattering). The photon of scattering disturbs the electron of the molecule and excited the molecular vibrations, phonons or other excitations in the system to a virtual energy state. In Rayleigh scattering, photons drop from virtual energy state to the same level of incident photon state of vibrational energy state. Raman scattering or the Raman effect is the inelastic scattering of a photon by molecules which are excited to higher or lower vibrational or rotational energy levels. Raman shift is the frequency shift related to the energy difference between the incident and scattered photon, as following equations (1), (2):

$$\Delta\omega(nm^{-1}) = \left(\frac{1}{\lambda_0(nm)} - \frac{1}{\lambda_1(nm)}\right) \quad (1)$$

$$\Delta\omega(cm^{-1}) = \left(\frac{1}{\lambda_0(nm)} - \frac{1}{\lambda_1(nm)}\right) \times \frac{(10^7 nm)}{(cm)} \quad (2)$$

, where $\Delta\omega$ is the Raman shift expressed in wavenumber, λ_0 is the excitation wavelength, and λ_1 is the Raman spectrum wavelength.

In vibrational transitions, the wavenumber changes in proportion to $k^{1/2}$ as shown in Eq. (3)

$$\nu = \frac{1}{2\pi}\left(\frac{k}{m}\right)^{\frac{1}{2}} \tag{3}$$

, where ν is the wavenumber, k is the force constant and m is mass.

Raman shift occurs as an up- or down-shift of the scattered photon frequency which is related to the incident photon state. The down-shifted which the photons drop from virtual energy state to a higher level of incident photon state of vibrational energy state is called the stoke Raman scattering. And the up-shifted which the photons drop from virtual state to lower level of incident photon state of vibrational energy state is called anti-Stokes Raman scattering. Spectrum obtains from the graph between the detected number of photons and Raman shift from the incident laser energy. Raman spectra are the unique characteristic which shows that different materials have different vibrational modes.

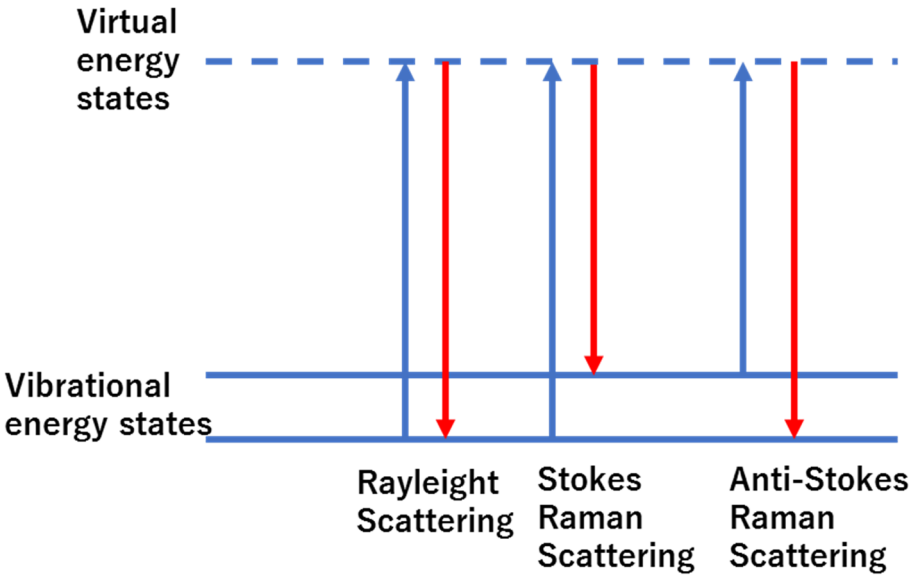

Fig. 2.10 Type of scattering

In the present, lasers are used as a photon source because of their highly monochromatic nature, and high beam fluxes. When the Raman effect is weak, typically the Stokes lines are ~10^5 times weaker than the Rayleigh scattering, the laser is an appropriate source to use.

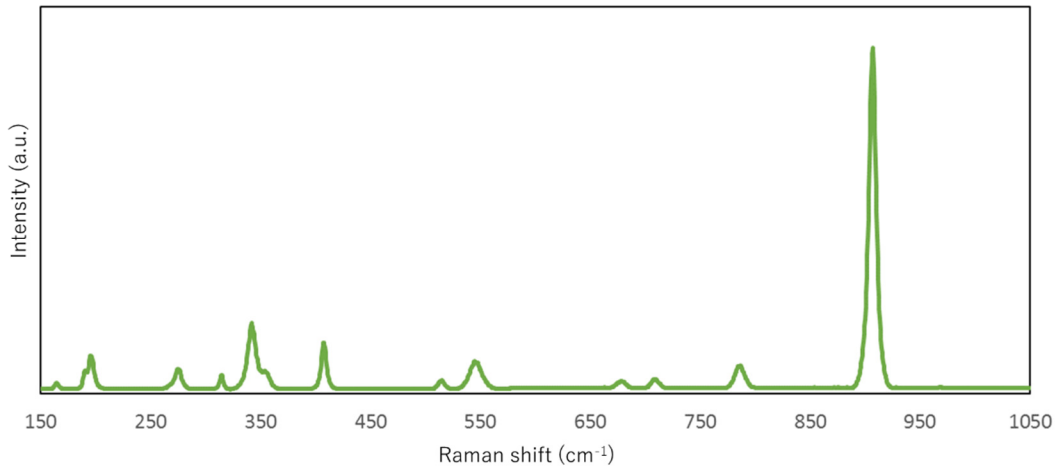

Fig. 2.11 The result of Laser Raman spectroscopy

Laser raman spectroscopy instrument which use in this experiment is JASCO, NRS-7200.

2.3.6 X-RAY FLUORESCENCE

X-ray fluorescence (XRF) is an x-ray equipment used for analyzing the material. It works on wavelength-dispersive spectroscopic principles that are nearly the same as electron microprobe (EPMA). Normally XRF cannot generally analyze at the small spot sizes (about 2-5 microns) but it is typically used for analyzing the large geological materials.

2.3.6.1 Principle of X-ray fluorescence

High energy X-rays from X-ray source irradiate at the sample. When X-ray of sufficient energy, which is greater than the atom's K or L shell binding energy, hit an atom in the sample, an electron from the inner orbital shells of the atom is displaced. To recover the stability, atom fills the vacancy left in the inner orbital shell, which occur from displacement of electron, with an electron from the higher energy orbital shells. When the electron moves to the lower energy state, it releases a fluorescent X-ray. The energy of fluorescent X-ray is equal to the specific difference in energy between two quantum states of the electron. The measurement of this energy is the basis of XRF analysis.

For interpretation, most atoms have several electron orbitals such as K shell, L shell, M shell. When x-ray energy causes electrons to transfer in and out of these shell levels, XRF peaks with varying intensities are created and will be present in the spectrum, a graphical representation of X-ray intensity peaks as a function of energy peaks. The peak energy identifies the element, and the peak intensity is generally indicative of its concentration.

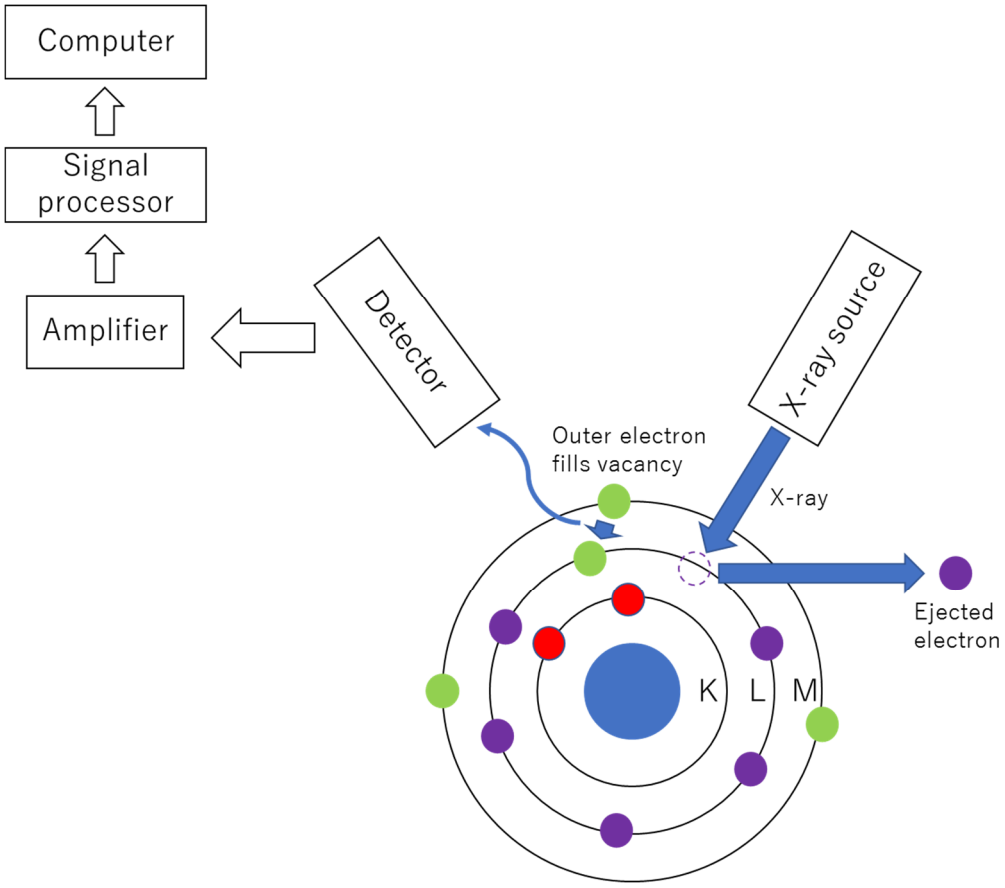

Fig. 2.12 Principle of an x-ray fluorescence

X-ray fluorescence instrument which use in this experiment is ZSX Primus II.

2.3.7 X-RAY PHOTOELECTRON SPECTROSCOPY

X-ray photoelectron spectroscopy (XPS) is a technique that measures and analyzed the elemental composition at empirical formula, chemical state and electronic state of the elements that exist within a material.

XPS spectra are obtained by irradiating a material with a beam of X-rays while simultaneously measuring the kinetic energy and number of electrons that escape from the surface of the material being analyzed.

XPS concept

A monoenergetic x-ray beam emits photoelectrons from the from the surface of the sample. The X-Rays either of two energies such as Al Ka (1486.6eV) and Mg Ka (1253.6 eV). The x-ray photons The penetration about a micrometer of the sample. The XPS spectrum contains information only about the top 10 - 100 Å of the sample. Ultrahigh vacuum environment to eliminate excessive surface contamination. Cylindrical Mirror Analyzer (CMA) measures the KE of emitted e^-s. The spectrum plotted by the computer from the analyzer signal. The binding energies can be determined from the peak positions and the elements present in the sample identified.

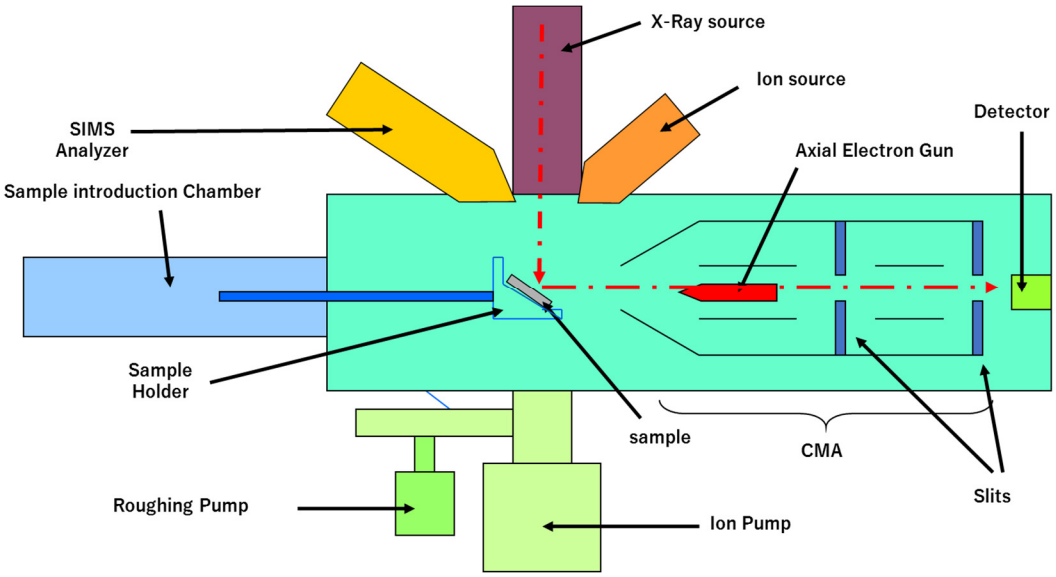

Fig. 2.13 Diagram of an X-ray photoelectron spectroscopy

X-ray photoelectron spectroscopy instrument which use in this experiment is JEOL JPS-9010TR.

2.3.8 UV VIS SPECTROPHOTOMETER

It is the instruments to measure the amount of light and intensity in the range of UV and visible light which transmit or absorb. Wavelength is related to the quantity and type of element in the samples, which can absorb the light in this wavelength.

The absorbance properties of the samples occur when the suitable energy of light in the wavelength of UV or visible light interacts with the molecules of the sample. The electron inside the atom absorbs the light and change state to the higher energy level. Then measure the amount of light which transmit or reflect from the sample compared with light from the source base on Beer-Lambert law, absorbance of samples is proportional with the amount of light absorbed molecules. Hence, the type and amount of elements in the sample can be identified by this technique.

Generally, this technique can analyze in:

- Absorptance

- % Transmittance

- % Reflectance

- Percent of the coefficient of transmittance)Diffuse %T)

- Percent of the coefficient of Reflectance)Diffuse %R)

- Percent of Variable Angle (%T)

- Percent of Specular Reflectance)Specular %R)

- Percent of Total Reflectance)Total %R)

2.3.8.1 Beer's law

For the ray which is parallel beam and monochromatic radiation, the ray transmits through the sample which is the homogeneous solution and has the same pathlength. Absorbance is proportional with the concentration of the solution as shown in below equation.

$$A \alpha c$$

, where A is absorbance of sample, α is proportional symbol and c is the concentration of sample (gL^{-1})

2.3.8.2 Lambert's law

For the ray which is parallel beam and monochromatic radiation, the ray transmits through the sample which is the homogeneous solution and has the same concentration. Absorbance is proportional with the pathlength as shown in below equation.

$$A \alpha l$$

, where A is absorbance of sample, α is proportional symbol and l is the thickness of the sample or pathlength (cm)

2.3.8.3 Beer-Lambert law

For the ray which is parallel beam and monochromatic radiation, the ray transmits through the sample which is a homogeneous solution. Absorbance is proportional with the pathlength and concentration of sample as shown in below equation.

$$A = a l c$$

, where a is the absorptivity of sample ($L.g^{-1}.cm^{-1}$)

If concentration of sample is molarity ($molL^{-1}$), absorptivity is called the molar absorptivity (ε) of solution which has the following equation:

$$A = -\log T = \log \frac{I_0}{I} = \varepsilon l c$$

, where c is concentration of sample (molL-1) and ε is molar absorptivity ($L.cm^{-1}.mol^{-1}$)

UV VIS spectrophotometer which use in this experiment is Solidspec - 3700DUV.

2.3.9 VESTA [19]

VESTA is the program which displays the 3D visualization model for crystal structure, volumetric data, and crystal morphologies.

2.3.9.1 Feature of VESTA

1. Visualization of structural models

1.1 For structural models

VESTA can present the crystal structures as ball & stick, space filling, polyhedral, stick, and wireframe.

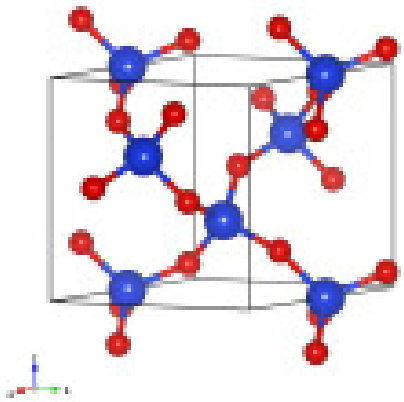

Fig. 2.14 Ball & stick of crystal structure [19]

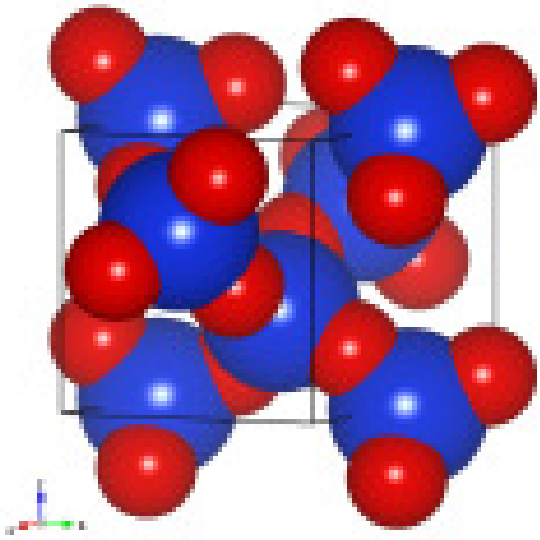

Fig. 2.15 Space filling of the crystal structure [19]

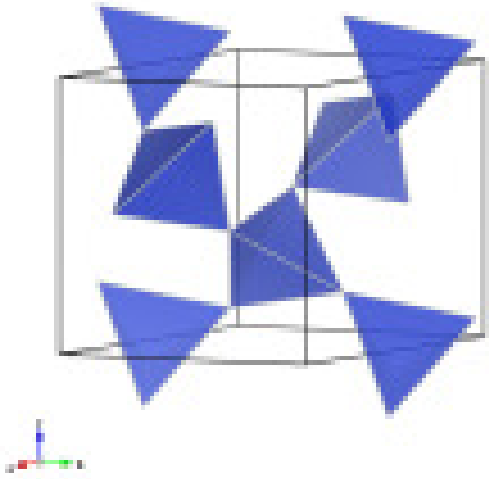

Fig. 2.16 Polyhedral of the crystal structure [19]

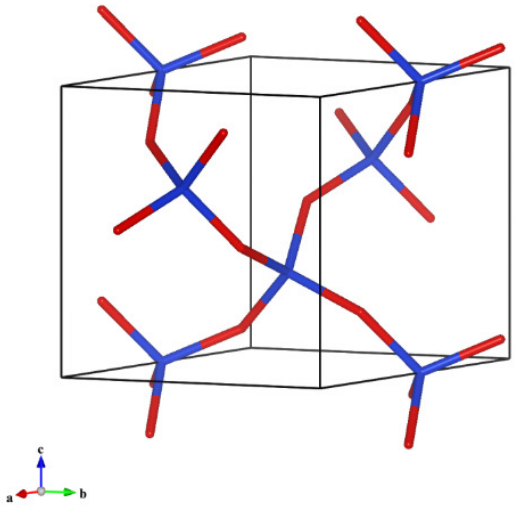

Fig. 2.17 Stick of crystal structure [19]

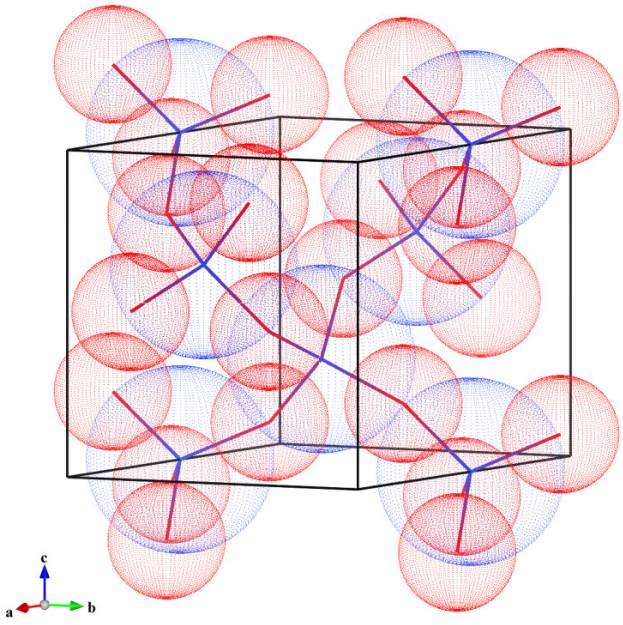

Fig. 2.18 Wireframe of the crystal structure [19]

Moreover, ball-and-stick, wireframe, and stick models can be overlapped with dotted surfaces corresponding to van der Waals radii. For ball-and-

stick and polyhedral models, thermal displacement of atoms can be presented as ellipsoids.

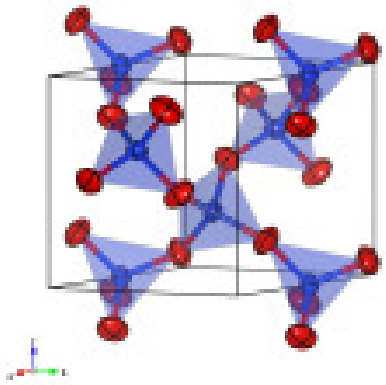

Fig. 2.19 Ellipsoids of the crystal structure [19]

1.2 Display crystallographic information

Variety of crystallographic information can be displayed easily by selecting the objects in the program. They consist of fractional coordinates, symmetry operations and translation vectors, site multiplicities, Wyckoff letters, site symmetry, information about principal axes and mean square displacements for anisotropic thermal motion, interatomic distances, bond angles, and torsion angles, information about coordination polyhedra including volumes, Baur's distortion indices, quadratic elongations, bond angle variances, bond valence sums of central metals, and bond lengths expected from bond valence parameters.

1.3 Lattice transformation

This program can convert general equivalent positions in a conventional setting into those in a non-conventional one with a transformation

matrix, which is also used for (primitive lattice)-(complex lattice) conversions and for creating superstructures.

1.4 Vectors on atoms

The magnetic moments or directions of static displacements can be attached to atoms.

2. For volumetric data

2.1 Visualization of volumetric data

Isosurfaces can be represented as smooth-shaded polygons, wireframes, and dot surfaces.

2.2 Surface coloring

VESTA has an attractive feature to colorize isosurfaces, whose typical application is to colorize isosurfaces of electron densities according to electrostatic potentials.

2.3 Peak search

Peak values and positions in 3D pixel data can be listed in the Text Area.

2.4 Display lattice planes

Lattice planes with variable opacities can be inserted. For 3D pixel data, both boundary sections and lattice planes are colorized on the basis of numerical values on them.

2.5 2D color & contour map

With a 2D Data Display window, 2D distribution of a physical quantity on a lattice plane can be visualized as a colored map with contour lines or Bird's-eye view.

3. Visualization of Crystal Morphologies

Crystal morphologies can be drawn by inputting Miller indices of faces.

The advantages of VESTA are:

- Deal with multiple structural models, volumetric data, and crystal morphologies in the same window.
- Visualize interatomic distances and bond angles that are restrained in Rietveld analysis.

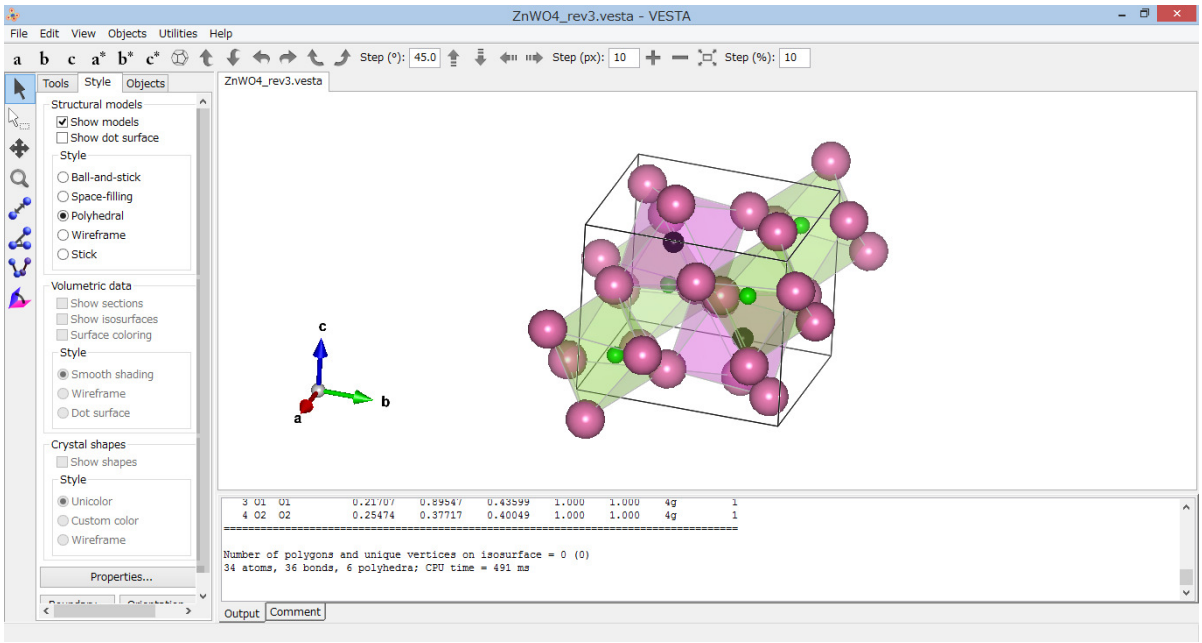

Fig. 2.20 Snapshot of VESTA program

References

[1] T. Oi, K. Takagi and T. Fukuzawa, Scintillation study of $ZnWO_4$ single crystals, Appl. Phys. Letts. 36 (1980) 278-279.

[2] V. N. Kolobanov, I. A. Kamenskikh, V. V. Mikhailin, I. N. Shpinkov, D. A. Spassky, B. I.Zadneprovsky, L. I. Potkin and G. Zimmerer, Optical and luminescent properties of anisotropic tungstate crystals, Nucl. Instrum. Methods Phys. Res. A 486 (2002) 496-503.

[3] H.Grassmann, H. Moser and E. Lorenz, Scintillation properties of $ZnWO_4$, J. Lumin. 33 (1985) 109-113.

[4] Y. C. Zhu, J. G. Lu, Y. Y. Shao, H. S. Sun, J. Li, S. Y. Wang, B. Z. Dong, Z. P. Zheng and Y. D. Zhou, Measurements of the scintillation properties of $ZnWO_4$ crystals, Nuclear Instruments and Methods in Physics Research Section A: Accelerators, Spectrometers, Detectors and Associated Equipment 244 (3) (1986) 579-581

[5] M. Yamaga, A. Marshall, K. P. O'Donnell and B. Henderson, Polarized photoluminescence from Cr^{3+} ions in laser host crystals III. $ZnWO_4$, Journal of Luminescence Volume 47, Issues 1–2, August–September 1990, Pages 65-70

[6] G. Huang, C. Zhang, and Y. Zhu, $ZnWO_4$ photocatalyst with high activity for degradation of organic contaminants, Journal of Alloys and Compounds Volume 432, Issues 1–2, 25 April 2007, Pages 269-276

[7] C. Zhang, H. Zhang, K. Zhang, X. Li, Q. Leng, and C. Hu, Photocatalytic Activity of $ZnWO_4$: Band Structure, Morphology and Surface Modification, ACS Appl. Mater. Interfaces, 2014, 6 (16), pp 14423–14432

[8] J. Yan, Y. Shen, F. Li, and T. Li, Synthesis and Photocatalytic Properties of ZnWO4 Nanocrystals via a Fast Microwave-Assisted Method, ScientificWorldJournal. 2013; 2013: 458106.

[9] P. Siriwong, T. Thongtem, A. Phuruangrat and S. Thongtem, Hydrothermal synthesis, characterization, and optical properties of wolframite $ZnWO_4$ nanorods, CrystEngComm, 2011,13, 1564-1569

[10] X. Wang, Z. Fan, H. Yu, H. Zhang, and J. Wang, Characterization of ZnWO4 Raman crystal, OPTICAL MATERIALS EXPRESS 1732, Vol. 7, No. 6 | 1 Jun 2017

[11] M. Bonanni, L. Spanhel, M. Lerch, E. Fuglein and G. Muller, Conversion of colloidal ZnO–WO_3 heteroaggregates into strongly blue luminescing $ZnWO_4$ xerogels and films, Chem. Mater. 10 (1998) 304-310.

[12] P. Belli, R. Bernabei1, F. Cappella, R. Cerulli, F. A. Danevich, S. D'Angelo, A. Incicchitti, V. V. Kobychev, D. V. Poda, V. I. Tretyak, Final results of an experiment to search for 2β processes in zinc and tungsten with the help of radiopure $ZnWO_4$ crystal Scintillators, J. Phys. G 38 (2011) 115107

[13] A. Alessandrello, V. Bashkirov, C. Brofferio, C. Bucci, D.V. Camin, O. Cremonesi, E. Fiorini, G. Gervasio, A. Giuliani, A. Nucciotti, M. Pavan, G. Pessina, E. Previtali, L. Zanotti, A scintillating bolometer for experiments on double beta decay, Phys. Lett. B 420 (1998) 109–113

[14] F. A. Danevich, V. V. Kobychev, S. S. Nagorny, D. V. Poda, V. I. Tretyak, S. S. Yurchenko, Y. G. Zdesenko, $ZnWO_4$ crystals as detectors for 2 β decay and dark matter experiments, Nuclear Instruments and Methods in Physics Research

Section A: Accelerators, Spectrometers, Detectors and Associated Equipment Volume 544, Issue 3, 1 June 2005, Pages 553-564

[15] R. Bernabei, P. Belli, F. Cappella, V. Caracciolo, R. Cerulli, F.A. Danevich, A. d'Angelo, A. Di Marco, A. Incicchitti V. M. Mokina, D.V. Poda, O.G. Polischuk, C. Taruggi, and V.I. Tretyak, $ZnWO_4$ anisotropic scintillator for Dark Matter investigation with the directionality technique, EPJ Web of Conferences 136, 05002 (2017)

[16] F. Cappella, R. Bernabei, P. Belli, V. Caracciolo, R. Cerulli, F. A. Danevich, A. d'Angelo, A. Di Marco, A. Incicchitti, D. V. Poda and V. I. Tretyak, On the potentiality of the $ZnWO_4$ anisotropic detectors to measure the directionality of Dark Matter, The European Physical Journal C, January 2013, 73:2276

[17] I. Bavykina, G. Angloher, D. Hauff, E. Pantic, F. Petricca, F. Proebst, W. Seidel and L. Stodolsky, Investigation of $ZnWO_4$ Crystals as Scintillating Absorbers for Direct Dark Matter Search Experiments, IEEE TRANSACTIONS ON NUCLEAR SCIENCE, VOL. 55, NO. 3, JUNE 2008

[18] C. S. Lim, Preparation and characterization of $ZnWO_4$ nanocrystallines and single crystals, Journal of the Korean Crystal Growth and Crystal Technology Vol. 20, No. 5 (2010) 197-201

[19] VESTA, http://jp-minerals.org/vesta/en/features.html

CHAPTER 3

FABRICATION OF POTASSIUM SALTS DOPED ZINC TUNGSTATES PREPARED WITH NITRATE, SULFATE, CHLORIDE AND THEIR PHOTOLUMINESCENCE PROPERTIES

ABSTRACT

In this work, we found the significant improvement of photoluminescence of zinc tungstate doped with potassium salts. The samples were prepared by solid-state reaction using ZnO, WO_3, KNO_3, K_2SO_4, and KCl as starting powders. The powders were mixed with the molar ratios of ZnO: WO_3: potassium salts = 1: 1: x and sintered at 800˚C for 3 h in air. The emission peak of photoluminescence excited at 275 nm was observed at 465 nm. With increasing potassium salts content, the intensity increased reached its maximum at x = 0.02 and decreased. The tendency of the luminescence intensity for KCl doping was almost the same as KNO_3 doping, whereas, for K_2SO_4 doping, the tendency of the decrease was less steep than other

doping. The order of each maximum intensity was $KNO_3 > K_2SO_4 > KCl$. It was considered that K replacing Zn in the crystal lattice enhanced the intrinsic luminescence in the blue wavelength region. Moreover, different anions doping had the different effect of the enhancement of the luminescence.

3.1 INTRODUCTION

Zinc tungstate ($ZnWO_4$) has been studied as promising materials for the photonic field such as scintillators [1-2], optical fiber [3], laser host [4], photocatalyst [5], and optical recording [6]. It is the wolframite lattice compounds having the intrinsic blue emission wavelength between 460 and 490 nm [7]. The studies of optical properties including light yield, emission wavelength, and the afterglow of $ZnWO_4$ have been reported [1, 8]. In scintillation applications, zinc tungstate crystals are very interesting and important detectors in fundamental physics: they are used in such principal investigations as searches for neutrinoless double beta decay [9, 10] and searches for dark matter [11] where the anisotropic properties of $ZnWO_4$ crystals are used. The advantages of $ZnWO_4$ are less hygroscopic, less toxic and cheaper than other materials such as CsI(Tl) and $CdWO_4$, a widely used scintillation crystals [7]. Single-crystal $ZnWO_4$ is usually grown by Czochralski technique [12], whereas its powder is synthesized by solid state reaction method [13].

Doping of $ZnWO_4$ can improve the photoluminescence activities. Many materials have been doped and investigated for their photoluminescence activities.

Wen et al. [14] has reported that $ZnWO_4$ crystals doped with Eu^{3+} show a significant energy transfer from WO_4^{2-} structure to Eu^{3+} ions. Dafinova et al. [15] has reported that the addition of SO_4^{2-}, F^-, and Cl^- ions from ammonium salts to the matrix leads to a substantial increase in the intensity of the self-activated blue emission in $ZnWO_4$. Kraus et al. [16] reported that Ca-doped $ZnWO_4$ could increase the scintillation light yield of samples. For alkali metal doping, it was reported that co-doping of Li_2CO_3, Sm, and B improved the extrinsic photoluminescence properties. And for Sodium salts such as NaCl, Na_2SO_4 doping, the destruction of the WO_6 structures occurs, which decreases the emission.

However, there have not been many studies of other alkali metals. In this research, we investigated the doping material which improved photoluminescence activities of $ZnWO_4$ and found that potassium salts affected to improve the intrinsic photoluminescence of zinc tungstate.

3.2 EXPERIMENTAL

Fig. 3.1 showed the sample preparation method in this experiment. $ZnWO_4$ powders were synthesized by solid-state reaction technique using starting powders of ZnO (99.99%, Furuuchi Chemical Co., Ltd.), WO_3 (99.99%, Kojundo Chemical Lab.), KNO_3, K_2SO_4 and KCl (>99.00%, Junsei Chemical Co., Ltd.). The powders were mixed with the molar ratios of ZnO: WO_3: potassium salts = 1: 1: x, where x is from 0 to 0.1. At first, the powder mixtures were ground in distilled water to dissolve salts for 20 minutes. After that, powders were mixed in 2-propanol for 2 h.

After drying, the mixtures were pressed into pellet (diameter 10 mm) under 100 MPa. The pellets were sintered at 800 °C for 3 h in air and ground into powders. The powders were compacted in 2x2 cm glass holders for testing. The crystalline phase was measured by X-ray diffractometer (XRD, RIGAKU Multiflex) using Cu Kα radiation (Kα= 1.5418 Å). The morphologies of the samples were observed using scanning electron microscope (SEM, JEOL JSM-5510). The luminescence of the samples was measured around 5-7 times using fluorescence spectrophotometer (Hitachi F-7000). After that, the normalized emission intensity of each sample by using following equation:

$$\text{Normalized PL intensity} = \frac{\textit{The highest of PL intensity of doped sample}}{\textit{The highest of PL intensity of undoped sample}} \quad (3.1)$$

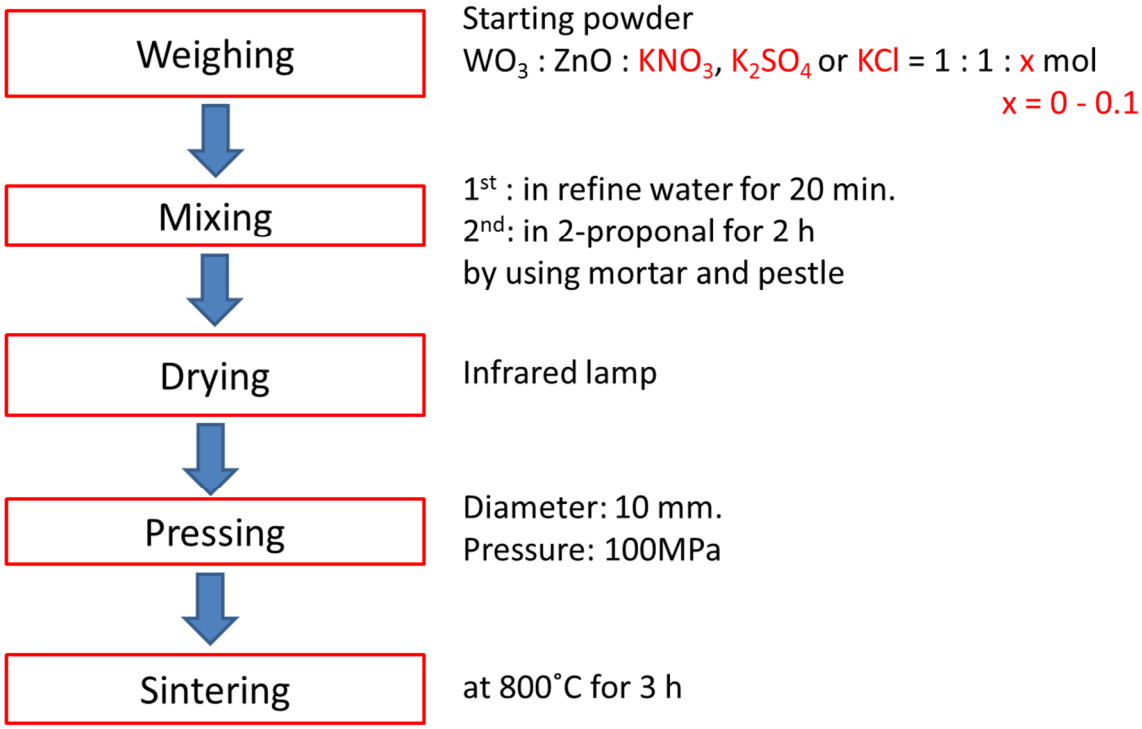

Fig. 3.1 The sample preparation method

3.3 RESULT AND DISCUSSION

Fig. 3.2 shows the SEM micrographs of undoped and doped samples after sintering at 800˚C. Undoped sample showed the formation of small crystals. The grain size of the doped potassium salt increased with increasing salt contents. The grain size of samples depended on the type of anions. The melting points of KNO_3, K_2SO_4, KCl are 334, 1,069 and 770 °C, respectively. In general, the grain growth is accelerated by the presence of liquid phase. For KNO_3 doping, some portion of KNO_3 would vaporize during sintering because melting point is lower than sintering temperature. Therefore, the grain size of 0.02 mol KNO_3 doping was smaller than K_2SO_4 and KCl doping. But for 0.1 mol KNO_3 doping, the large amount of dopant was supposed to increase the grain size of samples rapidly. The melting point of KCl is slightly lower than the sintering temperature, and the melting point of K_2SO_4 is higher than the sintering temperature. As a result, the crystallite size of KCl was larger than K_2SO_4.

Fig. 3.2 SEM of samples obtained under different doping conditions: (a) Undoped $ZnWO_4$; (b) doping with 0.02 mol KNO_3; (c) doping with 0.02 mol K_2SO_4; (d) doping with 0.02 mol KCl; (e) doping with 0.10 mol KNO_3; (f) doping with 0.10 mol K_2SO_4; (g) doping with 0.10 mol KCl , respectively.

The XRD patterns for all sample powders prepared with different potassium salt are shown in Fig. 3.3, 3.4, 3.5. All the peaks in the patterns were indexed on the basis of the crystallographic data of $ZnWO_4$ (ICDD code 89-0774). In the XRD pattern of the $ZnWO_4$ powders, the peak was slightly shifted in 2θ depending on salt doping. Their lattice constants and unit cell volume were determined using XRD peaks and Bragg's law and shown in Fig. 4.6. From the data, with increasing content of potassium salts, the lattice constant a decreased whereas b and c increased. Moreover, the density of the samples was shown in Fig. 3.7. In this figure, the density was increased when potassium salts doping contents were increased. XPS data in Fig. 3.8 and Fig. 3.9 shows the content of Zn^{2+}, W^{6+}, O^{2-}, K^{+}, and anions in the samples. From the data of lattice parameter and XPS, potassium ions and anions were considered to have dissolved into the samples after the sintering. Jenkins, et al. [17] reported that the ionic radii of Zn^{2+}, W^{6+}, K^{+}, N^{3-}, S^{2-}, Cl^{-} and O^{2-} were 0.074, 0.042, 0.138, 0.171, 0.184, 0.184 and 0.140 nm, respectively. It was considered that the potassium ion, which is the cation, could be highly possible to substitute for Zn^{2+} of $ZnWO_4$ rather than W^{6+} because the ionic radius for K^{+} are larger than Zn^{2+} and much larger than W^{6+}, moreover and there is a huge charge difference between K^{+} and W^{6+}. For N^{3-}, S^{2-}, Cl^{-} anions, they were supposed to substitute for O^{2-} of $ZnWO_4$. The ionic radii of N^{3-}, S^{2-}, Cl^{-} is larger than O^{2-}, so that the shifting of XRD peak in 2θ which result in the changing of lattice constants occurred. This result was explained as same as fluorine [18] and chloride [19] anions doping.

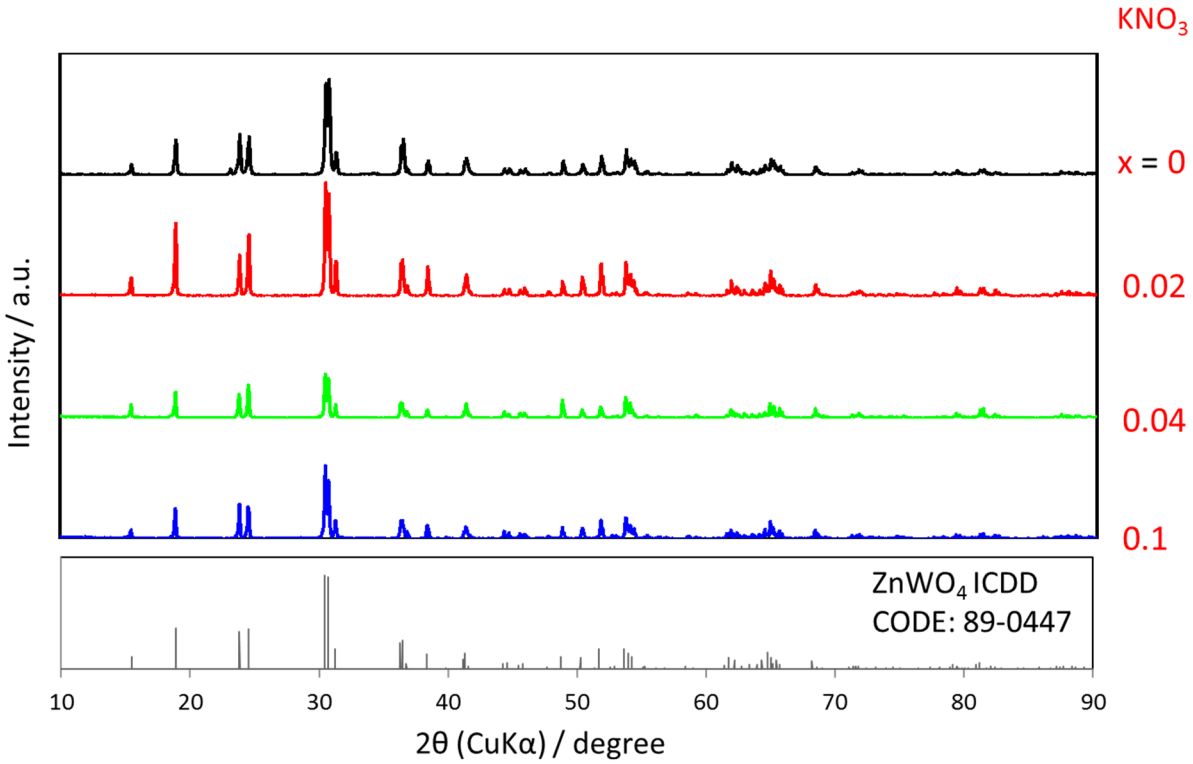

Fig. 3.3 XRD patterns f samples obtained under different KNO_3 doping contents.

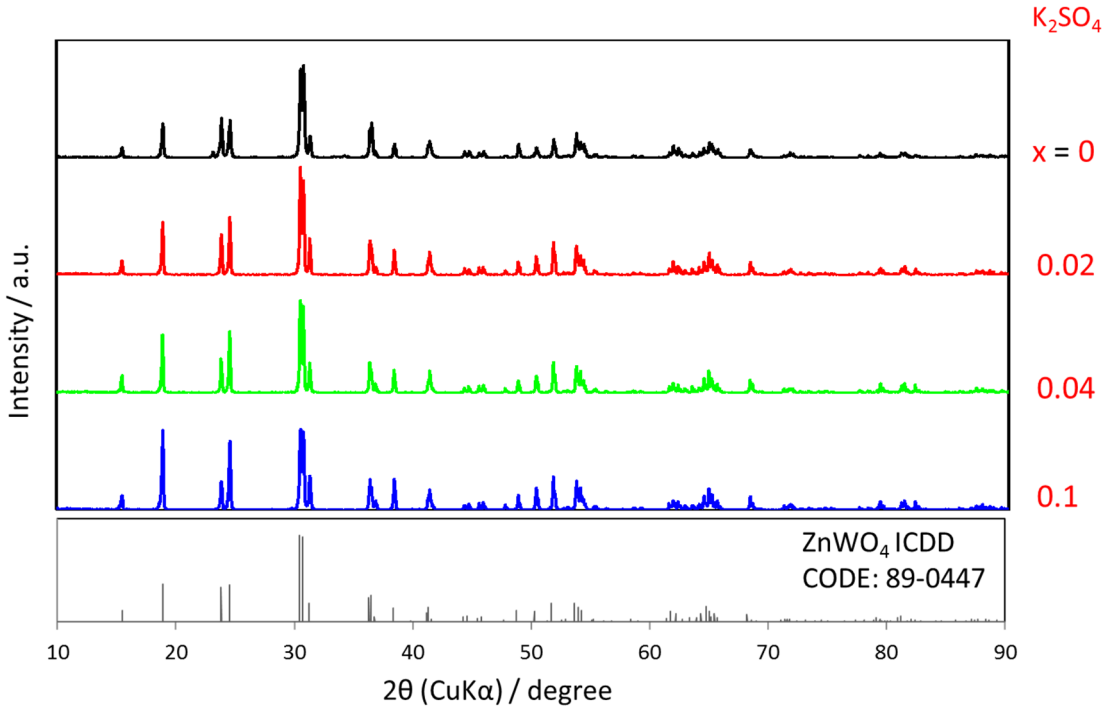

Fig. 3.4 XRD patterns of samples obtained under different K_2SO_4 doping contents.

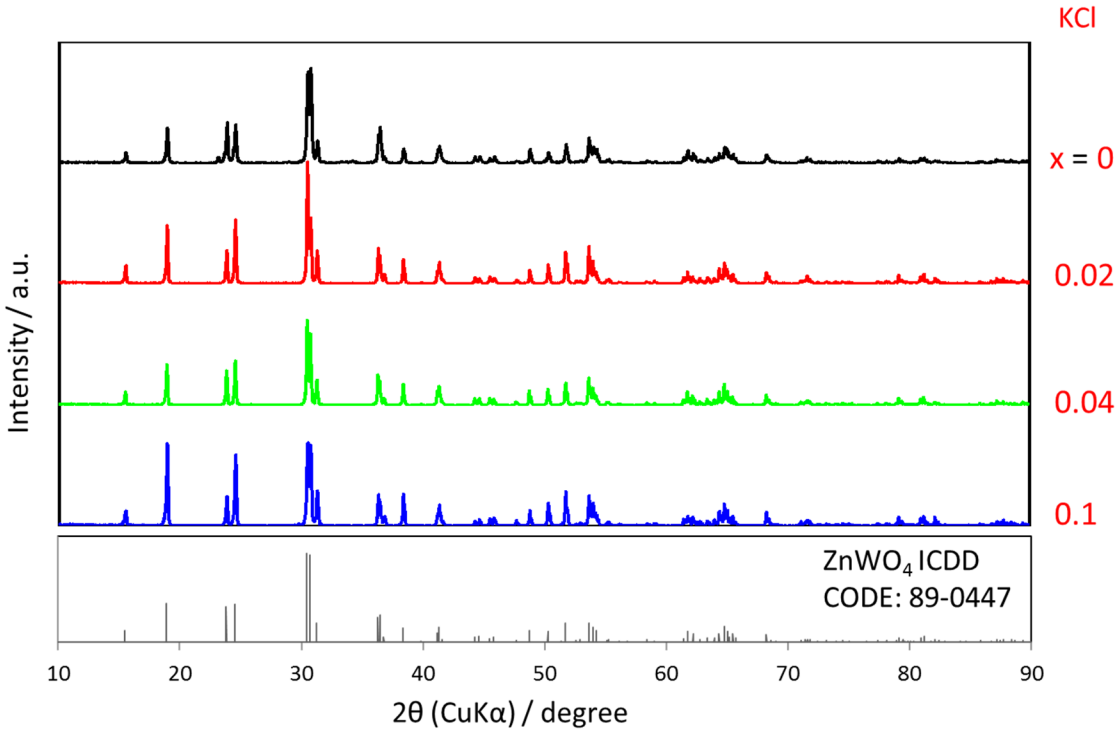

Fig. 3.5 XRD patterns of samples obtained under different KCl doping contents.

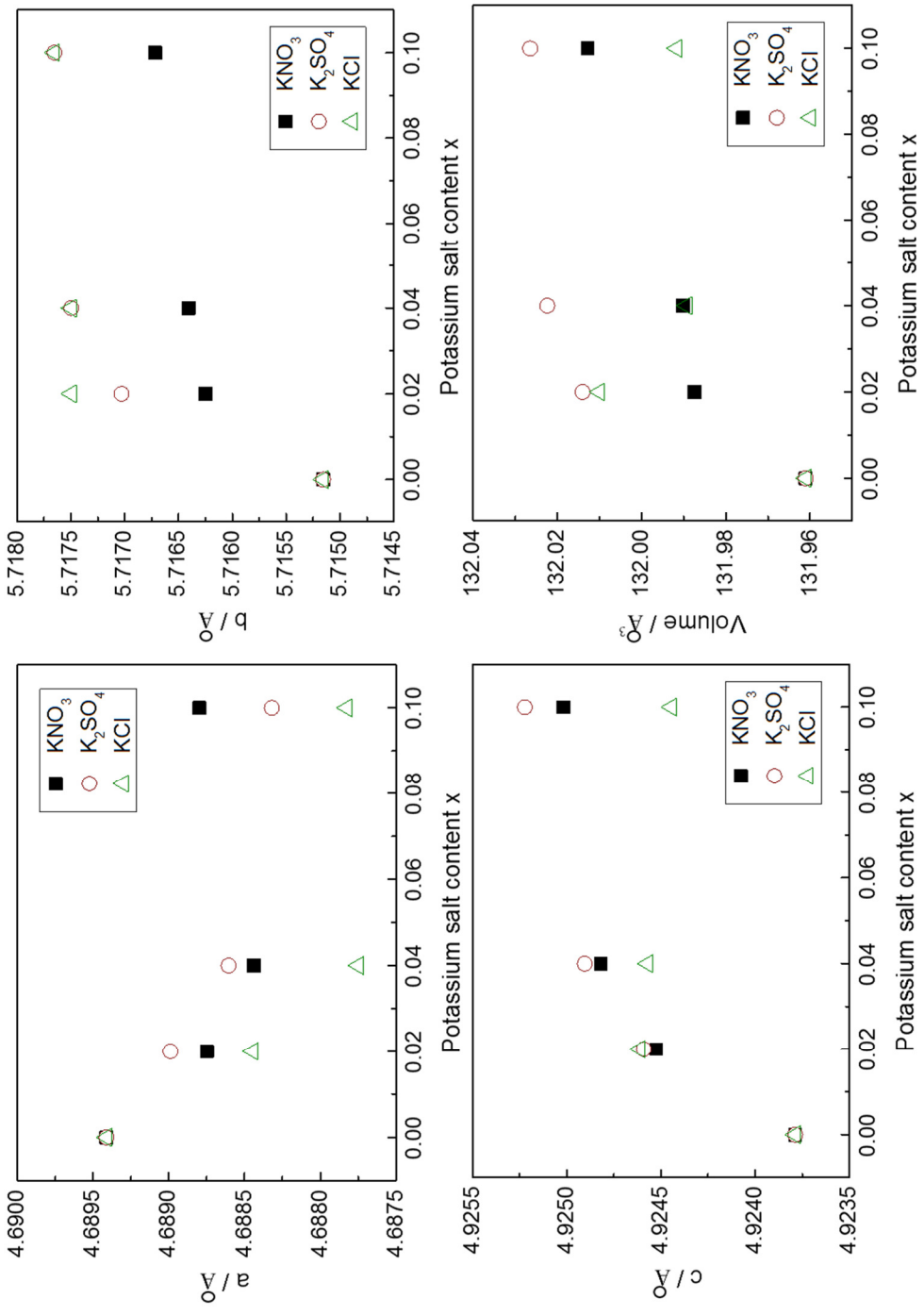

Fig. 3.6 Lattice constants and unit cell volume of potassium salts doped.

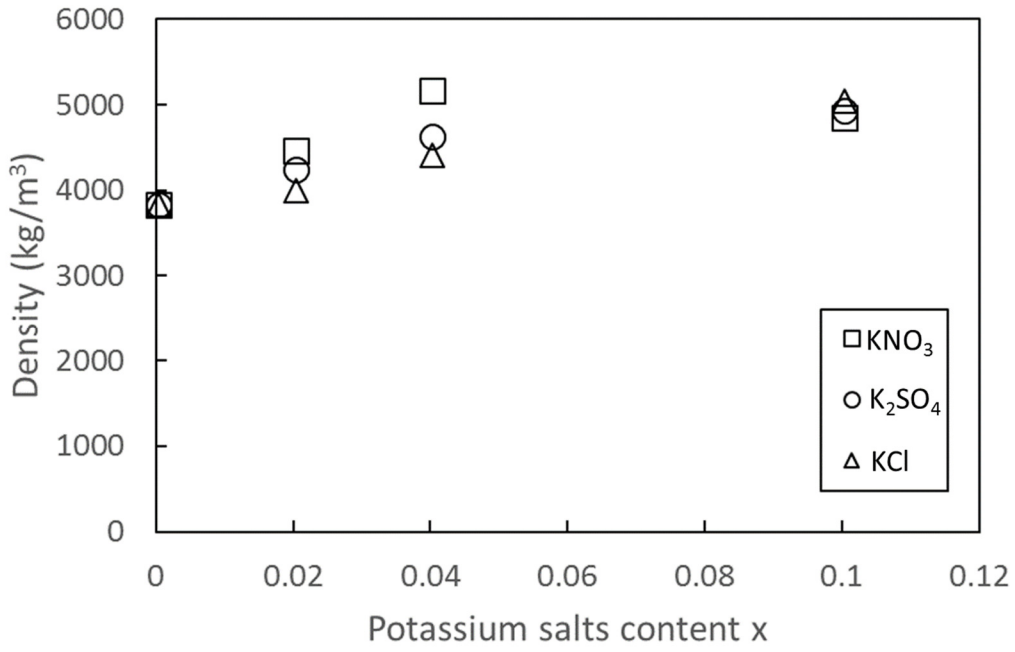

Fig. 3.7 Density of the potassium salts doped samples

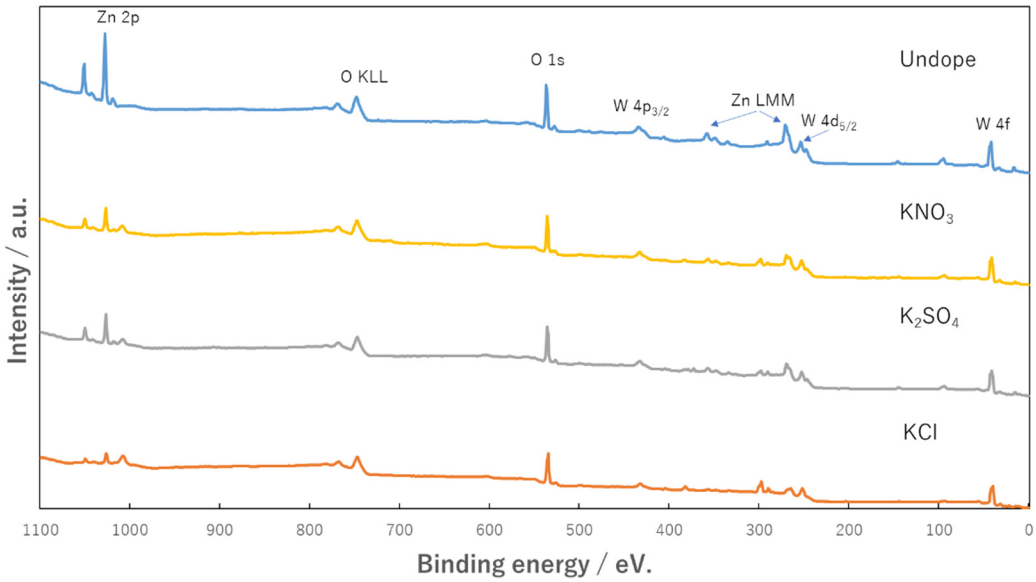

Fig. 3.8 Wide XPS scan of the potassium salts doped sample

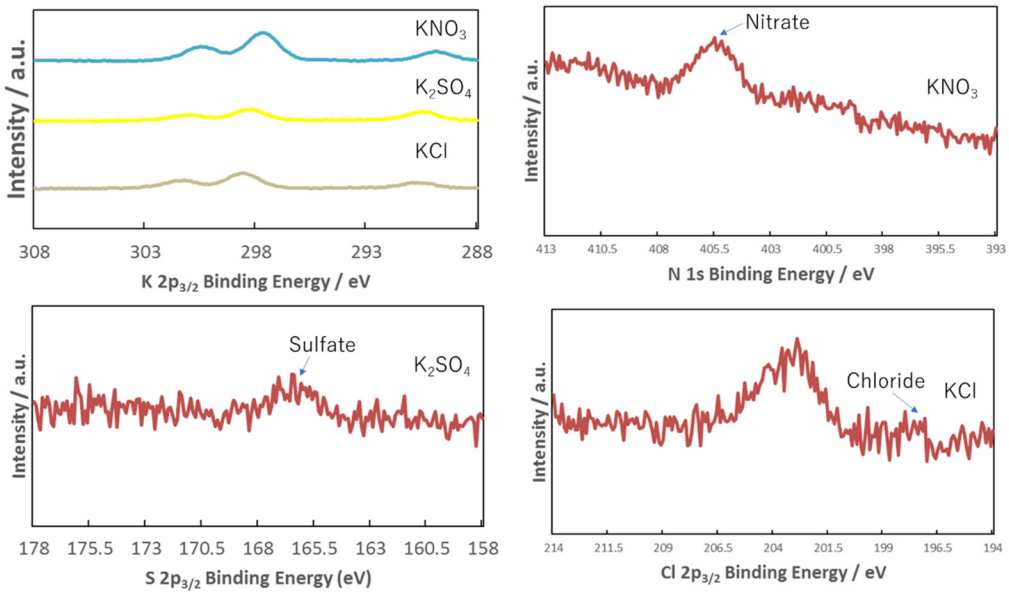

Fig. 3.9 Narrow XPS scan of the potassium salts doped sample

Photoluminescence activities such as excitation peak and the emission peak of all samples are shown in Fig. 3.10. The result showed that emission peak occurred at 465 nm, but excitation peak wavelength s appeared at 275-285 nm. With increasing KNO_3 (a), the intensity increased reached its maximum at about x = 0.02 and decreased as same as K_2SO_4 (b) and KCl (c) doping. From Fig. 3.11, the tendency of the intensity for KCl doping was almost the same as KNO_3 doping. But for K_2SO_4 doping, the tendency of the decrease was less steep than other doping. The order of each maximum photoluminescence intensity was $KNO_3 > K_2SO_4 >$ KCl. From these results and Fig. 3.12, it is considered that the excitation peak wavelength and the increasing of emission peak intensity were depended on anions and doping content. Moreover, the fact that the emission peak wavelength did not change suggested that emission mechanism was not

changed by doping. Fig. 3.13 shows the relationship between normalized peak intensity and FWHM of XRD which was estimated from the distance between the curve points at the peak half maximum level of $\bar{1}\,1\,1$ peak. Compared with undoped sample, doping with potassium salts had the lower FWHM which reflected the increasing of the crystallinity in $ZnWO_4$.

According to related researches [20], the WO_6 structure has 6 oxygen atoms surrounding by tungsten atom. The crystal structure of $ZnWO_4$ is shown in Fig.3.14. The positions of two shared oxygen atoms in the WO_6 structure were close to the tungsten atom and participated in the optical transitions between W and O atoms. Oosterhout [21] explained that the optical transition of WO_6 structure occurred from a charge transfer transition between the oxygen 2p-orbitals and the tungsten d-orbitals. In this work, K and anions are considered to replace Zn^{2+} and O^{2-}, respectively. The K and anions are supposed to deform the WO_6 structure which increases the photoluminescence activities of $ZnWO_4$. The fact that the emitted peak intensity of the samples prepared with KNO_3, K_2SO_4 was higher than that prepared with KCl suggests that the N^{3-} from nitrate and S^{2-} from sulfate penetrated into the sample structure by replacing with O^{2-} of $ZnWO_4$ and affected the luminescence more than Cl^-. Moreover, when K^+ is inserted together with the respective anions in the sample structure, it can maintain these optical transitions. However, the increasing potassium salt doping contents could decrease the photoluminescence because the destruction of the WO_6 structures occurred.

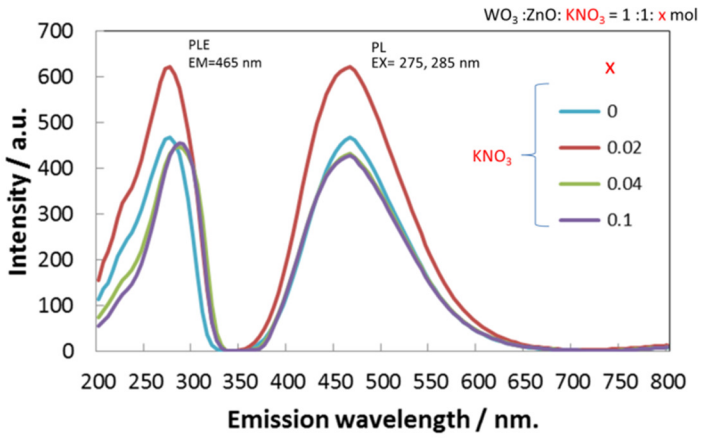

(a)

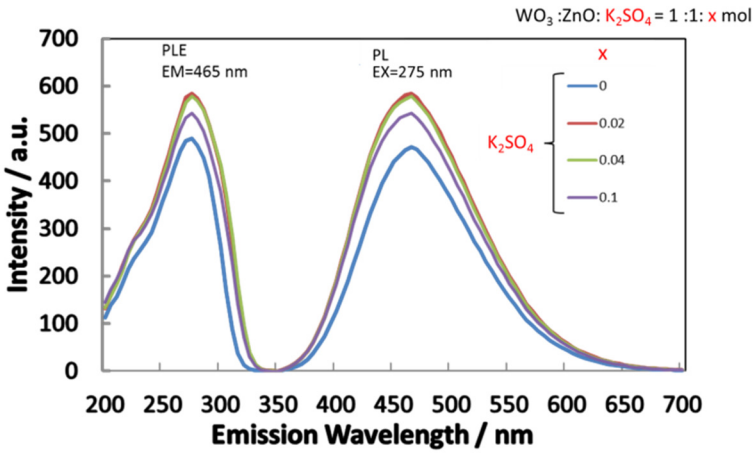

(b)

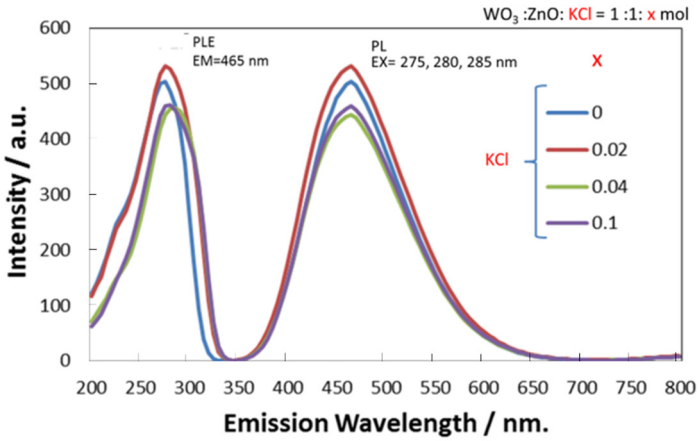

(c)

Fig. 3.10 Emission and excitation spectra of all samples: (a) doped with KNO_3; (b) doped with K_2SO_4; (c) doped with KCl, respectively.

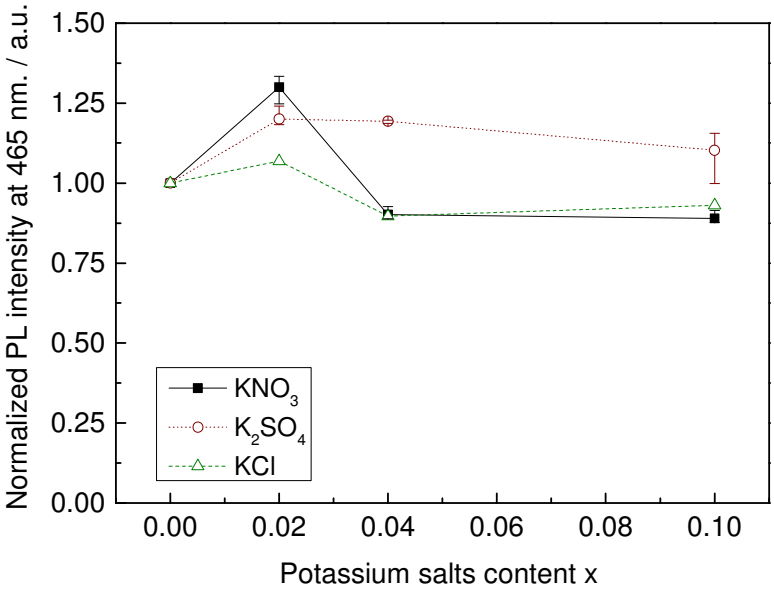

Fig. 3.11 Emission mechanism of all samples prepared with potassium nitrate, potassium sulfate and potassium chloride.

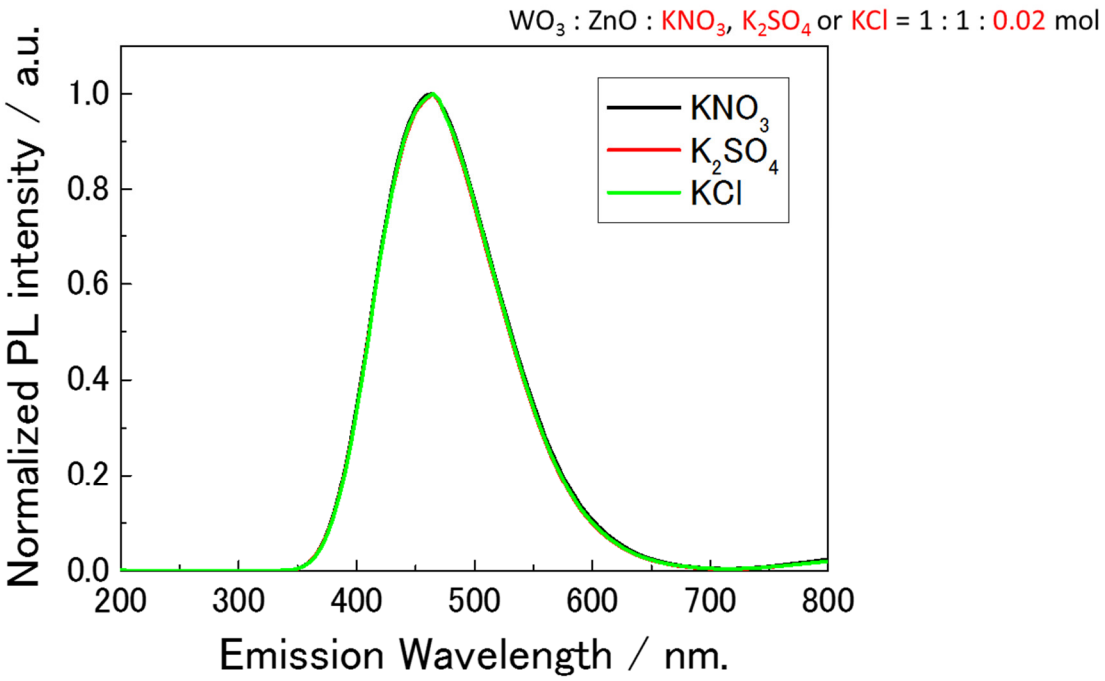

Fig. 3.12 Emission mechanism of all samples prepared with potassium nitrate, potassium sulfate and potassium chloride.

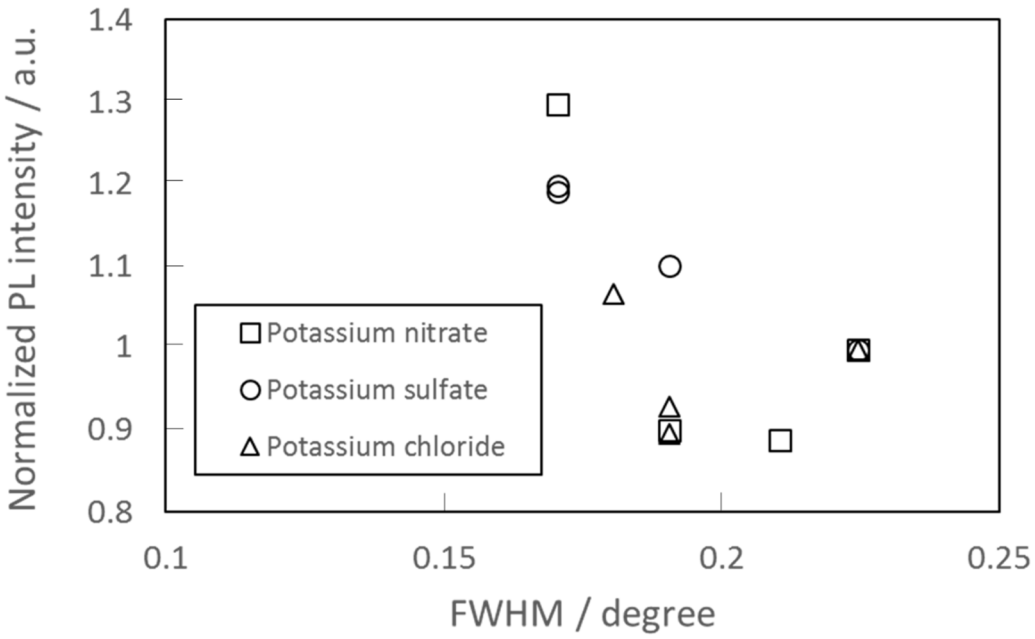

Fig. 3.13 FWHM of all samples prepared with potassium nitrate, potassium sulfate and potassium chloride.

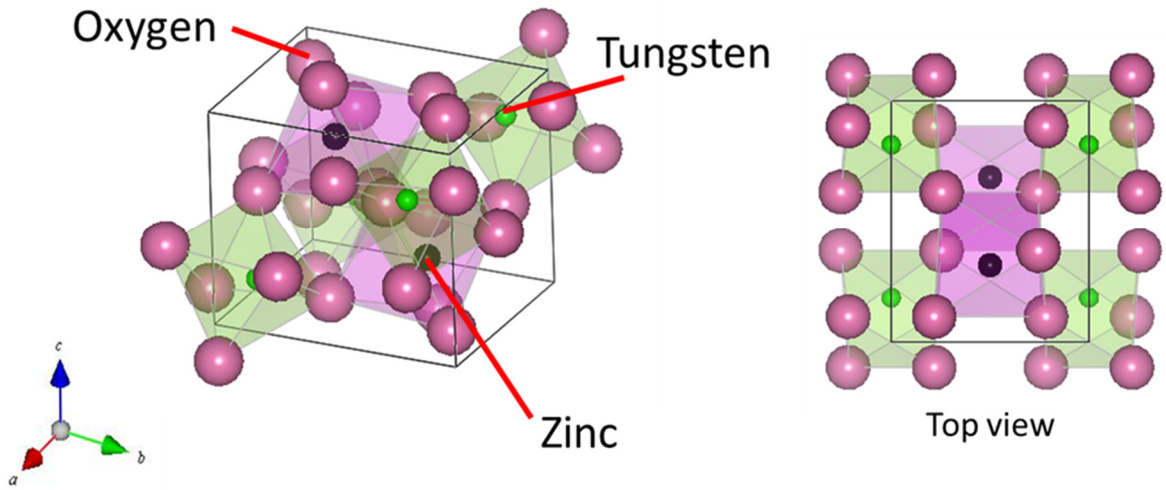

Fig. 3.14 Crystal structure of zinc tungstate and area which potassium and anions can place in.

3.4 CONCLUSION

We have successfully fabricated potassium salts doped zinc tungstates confirmed their structure and evaluated their optical properties. The powders were mixed with the molar ratios of ZnO: WO_3: potassium salts = 1: 1: x and sintered at 800˚C for 3 h in air. The grain size of samples increased when potassium salts were doped. Potassium and anions were considered to dissolve in $ZnWO_4$ and change the lattice constants. The photoluminescence intensity of the samples was significantly increased when potassium salt content x was 0.02. The order of each maximum photoluminescence intensity was KNO_3, K_2SO_4, KCl. The different cations and anions doping changed the structure of the sample and affected the emission peak intensity. It could be concluded that the radiative transitions between tungsten and oxygen can be enhanced by doping with potassium and anions.

References

[1] T. Oi, K. Takagi and T. Fukuzawa, Scintillation study of $ZnWO_4$ single crystals, Appl. Phys. Letts. 36 (1980) 278-279.

[2] V.N. Kolobanov, I.A. Kamenskikh, V.V. Mikhailin, I.N. Shpinkov, D.A. Spassky, B.I.Zadneprovsky, L.I. Potkin, G. Zimmerer, Optical and luminescent properties of anisotropic tungstate crystals, Nucl. Instrum. Methods Phys. Res. A 486 (2002) 496-503.

[3] H.Grassmann, H. Moser, E. Lorenz, Scintillation properties of $ZnWO_4$, J. Lumin. 33 (1985) 109-113.

[4] Hulliger, A.A. Kaminskii, H.J. Eichler, Molecular inorganic, organic crystalline, and glassy materials for Raman laser converters, Adv. Funct. Mater. 11 (2001) 243-250.

[5] G. Huang, Y. Zhu, Synthesis and photocatalytic performance of $ZnWO_4$ catalyst, Mater. Sci. Eng. B 139 (2007) 201-208.

[6] A. Kuzmin, R. Kalendarev, A. Kursitis, J. Purans, Confocal spectromicroscopy of amorphous and nanocrystalline tungsten oxide films, J. Non-Cryst. Solids 353 (2007) 1840-1843.

[7] M. Bonanni, L. Spanhel, M. Lerch, E. Fu¨glein, G. Muller, Conversion of colloidal $ZnO–WO_3$ heteroaggregates into strongly blue luminescing $ZnWO_4$ xerogels and films, Chem. Mater. 10 (1998) 304-310.

[8] W. Kolbe, K. Petermann, and G. Huber, Optical properties of planar waveguides on $ZnWO_4$ formed by carbon and helium ion implantation and effects of annealing, IEEE J. Quantum Electron. 21(10) (1985) 1596–1599.

[9] P. Belli, R. Bernabei1, F. Cappella, R. Cerulli, F. A. Danevich, S. D'Angelo, A. Incicchitti, V. V. Kobychev, D. V. Poda, V. I. Tretyak, Final results of an experiment to search for 2β processes in zinc and tungsten with the help of radiopure $ZnWO_4$ crystal Scintillators, J. Phys. G 38 (2011) 115107

[10] A. Alessandrello, V. Bashkirov, C. Brofferio, C. Bucci, D.V. Camin, O. Cremonesi, E. Fiorini, G. Gervasio, A. Giuliani, A. Nucciotti, M. Pavan, G. Pessina, E. Previtali, L. Zanotti, A scintillating bolometer for experiments on double beta decay, Phys. Lett. B 420 (1998) 109–113

[11] F. Cappella, R. Bernabei, P. Belli, V. Caracciolo, R. Cerulli, F. A. Danevich, A. D'Angelo, A. Di Marco, A. Incicchitti, D. V. Poda, V. I. Tretyak, On the potentiality of the $ZnWO_4$ anisotropic detectors to measure the directionality of Dark Matter, Eur. Phys. J. C73 (2013) no.1, 2276

[12] S. O'Hara, G. M. McManus, Czochralski growth of low-dislocation-density zinc tungstate crystals, J. Appl. Phys. 36 (1965) 1741-1746.

[13] A.R. Phani, M. Passacantando, L. Lozzi, S. Santucci, Structural characterization of bulk $ZnWO_4$ prepared by solid state method, J. Mater.Sci. 35 (2000) 4879-4883

[14] Fu-Shan Wen, Xu Zhao, Hua Huo, Jie-Sheng Chen, E. Shu-Lin, Jia-Hua Zhang, Hydrothermal synthesis and photoluminescent properties of $ZnWO_4$ and Eu^{3+}-doped $ZnWO_4$, Materials letters 55 (2002) 152-157

[15] R. Dafinova, K. Papazova, A. Bojinova, Photoluminescence of Eu^{3+} and SO_4^{2-} doped tungstate systems, Journal of Luminescence 75 (1997) 51-55

[16] H. Kraus, V. B. Mikhailik, L. Vasylechko, D. Day, K. B. Hutton, J. Telfer, Yu. Prots, Effect of Ca doping on the structure and scintillation properties of $ZnWO_4$, Phys. Stat. Sol. (a) 204, No. 3 (2007) 730-736.

[17] H.D.B. Jenkins and K.P. Thakur, Reappraisal of thermochemical radii for complex ions, J. Chem. Educ. 56 (1979) 576-577.

[18] Guangli Huang and Yongfa Zhu, Enhanced photocatalytic activity of $ZnWO_4$ catalyst via fluorine doping, J. Phys. Chem. C, 111 (32) (2007) 11952-11958

[19] Guangli Huang and Yongfa Zhu, Synthesis and photoactivity enhancement of $ZnWO_4$ photocatalysts doped with chlorine, CrystEngComm, 14 (2012) 8076–8082

[20] Y. Liu, H. Wang, G. Chen, Y. D. Zhou, B. Y. Gu and B. Q. Hu, Analysis of Raman spectra of $ZnWO_4$ single crystals, J. Appl. Phys. 64 (1988) 4651-4653

[21] A. B. van Oosterhout, An ab initio calculation on the WO_6^{6-} octahedron with an application to its luminescence, The Journal of Chemical Physics 67 (1977) 2412-2418

CHAPTER 4

SYNTHESIS AND PHOTOLUMINESCENCE PROPERTIES OF ALKALI METAL-DOPED ZINC TUNGSTATE PREPARED BY NITRATE

ABSTRACT

In this work, the significant improvement of photoluminescence was found by doping alkali metal nitrates in zinc tungstate. The samples were prepared by solid state reaction at 800˚C in air. The grain size of the doped samples was large compared with undoped one. Lattice parameters of zinc tungstate phase increased with increasing ionic radius of alkali metal ions. The intrinsic emission peak of photoluminescence excited at 275 nm was observed at 465 nm. Compared with undoped sample, the samples doped with alkali metal nitrate exhibited the higher emission intensity except $LiNO_3$ doping. The order of peak emission intensity was $RbNO_3$ > $CsNO_3$ > KNO_3 > $NaNO_3$ > undoped > $LiNO_3$. The alkali metal ions and N^{3-} were considered to replace

Zn^{2+} and O^{2-}, respectively, and modify the crystallinity of $ZnWO_4$, which resulted in the changing of the luminescence activity. Moreover, an increase of atomic ordering along c-axis and reduced emission was observed from $LiNO_3$ doped sample.

4.1 INTRODUCTION

Zinc tungstate ($ZnWO_4$) has been attracted the attention of researchers in optical applications such as scintillators [1-2], optical fibers [3], laser hosts [4], photocatalysts [5], and optical recording materials [6]. It is the wolframite crystal structure having intrinsic blue emission wavelength between 460 and 490 nm [7]. In scintillation applications, the advantages of $ZnWO_4$ are non-hygroscopic and non-toxic. Many studies about optical properties including absorption, light yield, emission wavelength, and afterglow of $ZnWO_4$ have been reported [1, 8]. Generally, pure $ZnWO_4$ crystals emit reasonably well without any dopants but its photoluminescence properties are likely to be enhanced by doping. Minh et al. [9] has reported that $ZnWO_4$ crystals doped with Er^{3+} shows a significant optical transition from WO_4^{2-} structure. Dafinova et al. [10] has reported that the addition of ammonium and sodium salts into the $ZnWO_4$ leads to a substantial increase in the intensity of the intrinsic blue emission. Sheng Deng et al. [11] reported that co-doping of Ca and Dy showed higher UV absorption efficiency of sample. For alkali metal and alkali earth metal doping, it was reported that co-doping of Li, Sm and Bi improved the

white light emission which is the extrinsic photoluminescence properties of sample. The enhanced luminescence comes from the improved crystalline and from the charge compensation of Li^+ ions by the co-doping of Li and Pr [12]. And for sodium salts doping, the decreasing of photoluminescence activities in the samples occurs because Na^+ hamper the transition [10].

However, for other alkali metal salts, there have not been many studies yet. In this research, we investigated the doping materials which would improve photoluminescence activities and found that alkali metal nitrates had an effect to improve the intrinsic blue-green photoluminescence of zinc tungstate.

4.2 EXPERIMENTAL

The sample preparation was shown in Fig. 4.1. Alkali metal nitrate doped zinc tungstate samples were fabricated by solid state reaction technique. The starting powders were ZnO (99.99%, Furuuchi Chemical Co., Ltd.), WO_3 (99.99%, Kojundo Chemical Lab.), $LiNO_3$, $NaNO_3$, $RbNO_3$, $CsNO_3$ (>99.00%, Wako Pure Chemical Industries, Ltd.) and KNO_3 (>99.00%, Junsei Chemical Co., Ltd.). The powders were mixed in the molar ratios of Zn: W: alkali metal = 1: 1: 0.02. At first, the powder mixtures were ground in distilled water to dissolve the nitrate for 20 minutes, mixed in 2-propanol for 2 hours and dried by using infrared lamp. After drying, the mixtures were pressed into pellet (diameter 10 and 20 mm) under 100 and 400 MPa, respectively. and sintered at 800 °C for 3 h in air. The heating rate is 4°C per minute. After sintering, the

morphologies of the 10 mm pellet samples were characterized using scanning electron microscope (SEM, JEOL JSM-5510). Some 10 mm pellets were ground into the powders. The powders were compacted in 2×2 cm^2 glass holders for XRD and photoluminescence testing. The crystalline phase was measured using X-ray diffractometer (XRD, RIGAKU Multiflex) with Cu Kα radiation (λ= 1.5418 Å). XRD was operated at 30kV and 20mA in the 2θ range from 10˚ to 80˚ with a scan speed of 2˚ per minute. After that, the lattice constants and unit cell volumes of samples were calculated using XRD results, Bragg's law and equations:

$$\lambda = 2\, d_{hkl} \sin\theta \tag{1}$$

$$\frac{1}{d_{hkl}^2} = \frac{h^2}{a^2 sin^2\beta} + \frac{k^2}{b^2 sin^2\beta} - \frac{2hkcos\beta}{absin^2\beta} + \frac{l^2}{c^2} \tag{2}$$

$$V = abcsin\beta \tag{3}$$

where λ is the wavelength of the rays, d_{hkl} is the spacing between layers of atoms, θ is the angle between the incident rays and the surface of the crystal, h, k and l are miller indices of the samples, a, b and c are the lattice parameters of the samples, β is the angle between a and c and V is unit cell volume.

After lattice constants and unit cell volumes calculation, the content of alkali metals in the 20 mm pellets was confirmed by X-ray fluorescence (XRF, ZSX Primus II). The photoluminescence of the powder samples was measured using fluorescence spectrophotometer (Hitachi F-7000).

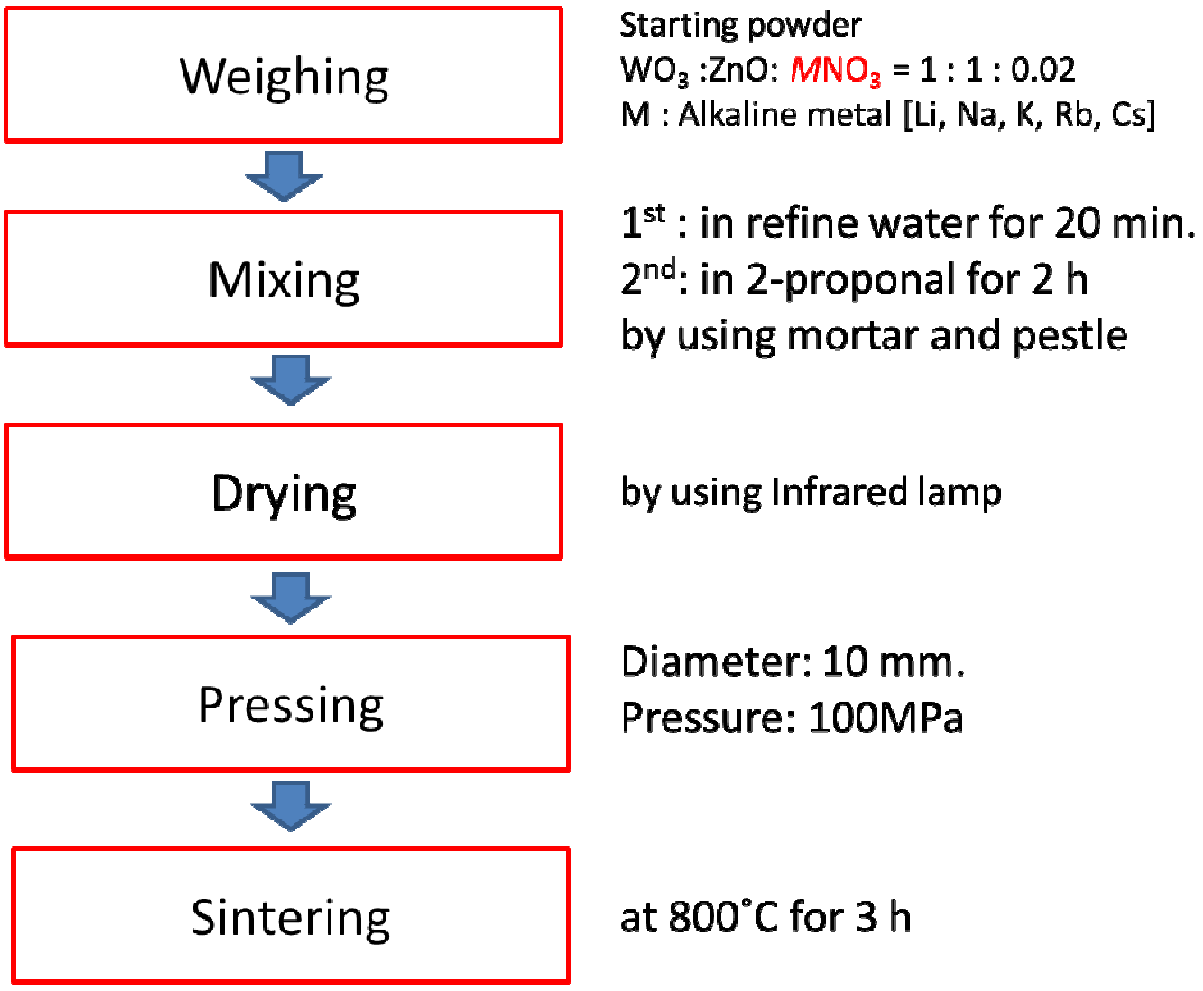

Figure 4.1 The sample preparation method

4.3RESULT AND DISCUSSION

Fig. 4.2 shows the SEM micrographs of undoped and alkali metal nitrate doped samples after sintering at 800˚C. Doped sample showed the formation of crystals with diameter lower than 1 μm. The grain size of the doped samples was large compared with undoped sample. The grain size of doped samples appeared to depend on boiling/melting points which are 600/255, 380/308, 400/334, 578/310 and -/414 °C for $LiNO_3$, $NaNO_3$, KNO_3, $RbNO_3$, $CsNO_3$ respectively, as shown in Fig. 4.3. Generally, the grain growth is accelerated by the presence of liquid phase. The fact that the grain size for $LiNO_3$ doping was the largest among the samples seems to be because of its wide temperature range between boiling and melting points.

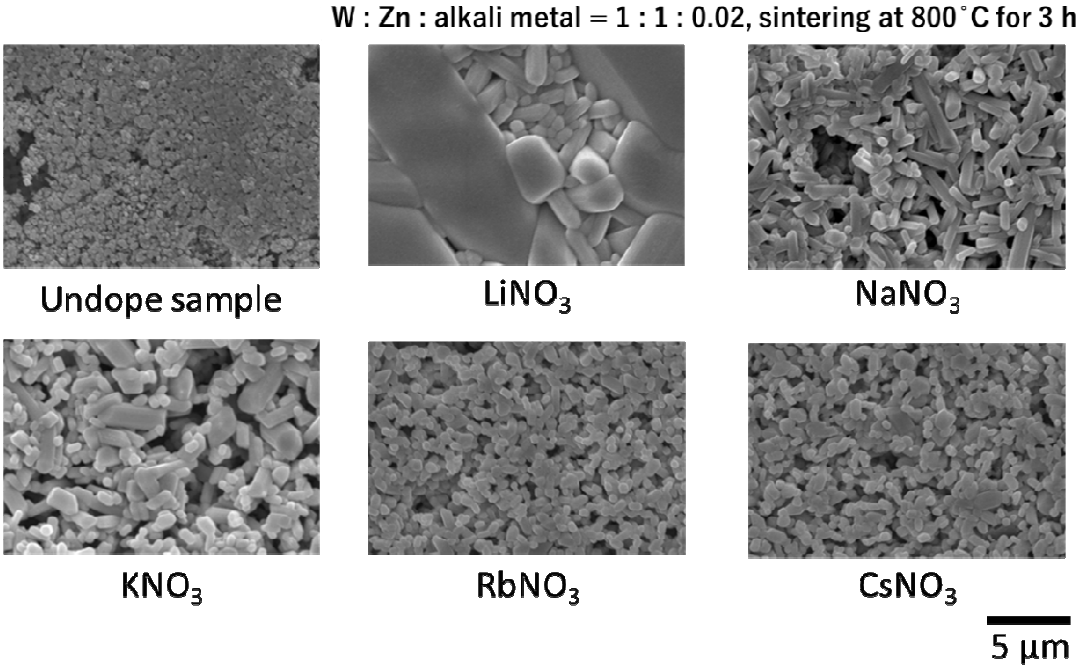

Figure 4.2 SEM images of samples doped with various alkali metal nitrates.

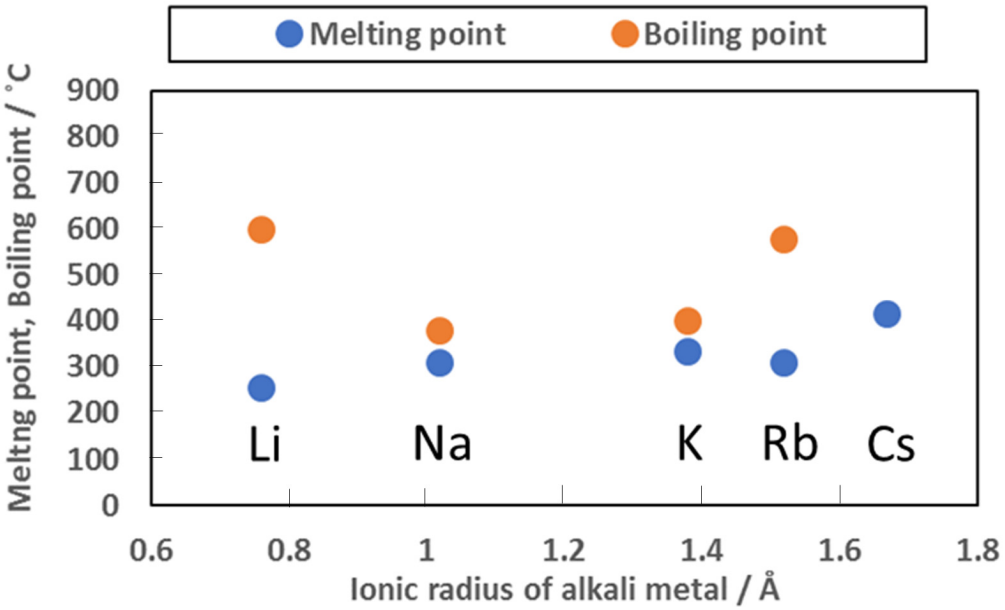

Figure 4.3 Melting point and boiling point of various alkali metal nitrates.

Fig. 4.4 shows XRD patterns for all the sample powders prepared with various alkali metal nitrates. The peaks in the patterns were indexed on the basis of the crystallographic data of $ZnWO_4$ (ICDD code 89-0774). For $LiNO_3$ doped sample, the increase of h k 0 diffraction peak intensity was observed, which implied the increase of atomic ordering along c-axis. XRD peaks were slightly shifted in 2θ depending on the alkali metal nitrate. Their lattice constants and unit cell volumes were determined using eq. (1), (2) and (3) (Fig. 4.5). The lattice constants a, b, c and the unit cell volume showed the tendency of increasing with increasing ionic radius. XRF data in Fig.4.6 shows the amount of K^+, Rb^+, Cs^+ content existed in the doped samples. Li^+ and Na^+ cannot be detected because of the limitation of XRF equipment. From these results, alkali metal nitrates were considered to dissolve in the samples.

Jenkins, et al. [13] reported that the ionic radii of Zn^{2+}, W^{6+}, Li^{+}, Na^{+}, K^{+}, Rb^{+}, Cs^{+}, O^{2-} and N^{3-} were 0.074, 0.042, 0.076, 0.102, 0.138, 0.152, 0.167, 0.140 and 0.171 nm, respectively. The alkali metal ions (Li^{+}, Na^{+}, K^{+}, Rb^{+}, Cs^{+}) are possible to substitute for Zn^{2+} of $ZnWO_4$ rather than W^{6+}, because the ionic radii for alkali metal ions are nearly the same as or larger than Zn^{2+} and much larger than W^{6+}. Moreover, charge difference of alkali metal ions from Zn^{2+} is smaller than that from W^{6+}. N^{3-} anion of nitrate were supposed to substitute for O^{2-} of $ZnWO_4$ since the ionic radii of N^{3-} is nearly the same as or larger than O^{2-}, so that the XRD peaks shift in 2θ. This was explained as same as other anions doping such as chloride and fluoride ions [14, 15].

Photoluminescence activities of all the samples are shown in Fig.4.7. The result showed that emission peak occurred at 465 nm and excitation peak appeared at 275 nm. The fact that the emission peak wavelength did not change suggested that emission mechanism was not changed by doping. Compared with undoped sample, those doped with alkali metal nitrates exhibited the higher emission intensity except $LiNO_3$ doping as shown in Fig. 4.8. The order of peak emission intensity was $RbNO_3$ > $CsNO_3$ > KNO_3 > $NaNO_3$ > undoped > $LiNO_3$. Fig. 4.9 shows the relationship between normalized peak intensity and FWHM of XRD which was estimated from the distance between the curve points at the peak half maximum level of $\bar{1}\,1\,1$ peak. The order of FWHM was $RbNO_3$ < $CsNO_3$ = KNO_3 < $NaNO_3$ = $LiNO_3$<<undoped. Compared with undoped sample, doping with alkali metal

nitrate had the lower FWHM which reflected the increasing of the crystallinity in $ZnWO_4$.

According to related researches [16, 17, 18, 19], the emission of $ZnWO_4$ is related to the intrinsic emission of WO_6^{6-} complexes. The four shared oxygen atoms in the WO_6 structure are close to the tungsten atom and participate charge transfer between the O 2p orbitals and empty 5d W orbitals. It was considered that the distance between W and O atoms and crystallinity of $ZnWO_4$ has a significant impact on the instinct fluorescence intensity. The increasing of instinct emission intensity occurs from the short distance between W and O atoms and high crystallinity [16]. Fig.5.13 shows the relationship between normalized photoluminescence intensity and distance between W and O_{II}. From these results, all samples which can improve the photoluminescence intensity have short distance between W and O atoms. From all results in this work, it was considered that the alkali metal ions and N^{3-} ions replacing Zn^{2+} and O^{2-} modify the WO_6 structure and crystallinity in $ZnWO_4$, which resulted in the increasing of the luminescence activity. For $LiNO_3$ doping, the photoluminescence was weaker than the undoped sample and other doped sample, which might be related to high atomic ordering along c-axis. Alkali metal ions such as Na^+, K^+, Rb^+, Cs^+ which ionic radii are larger than Zn^{2+} may gave a decrease in distance between O^{2-} and W^{6+} and an increase of the optical transition between the d orbitals of W and the p orbitals of the O. For $RbNO_3$ doping, the highest photoluminescence intensity occurred because of the highest crystallinity which showed the lowest FHWM.

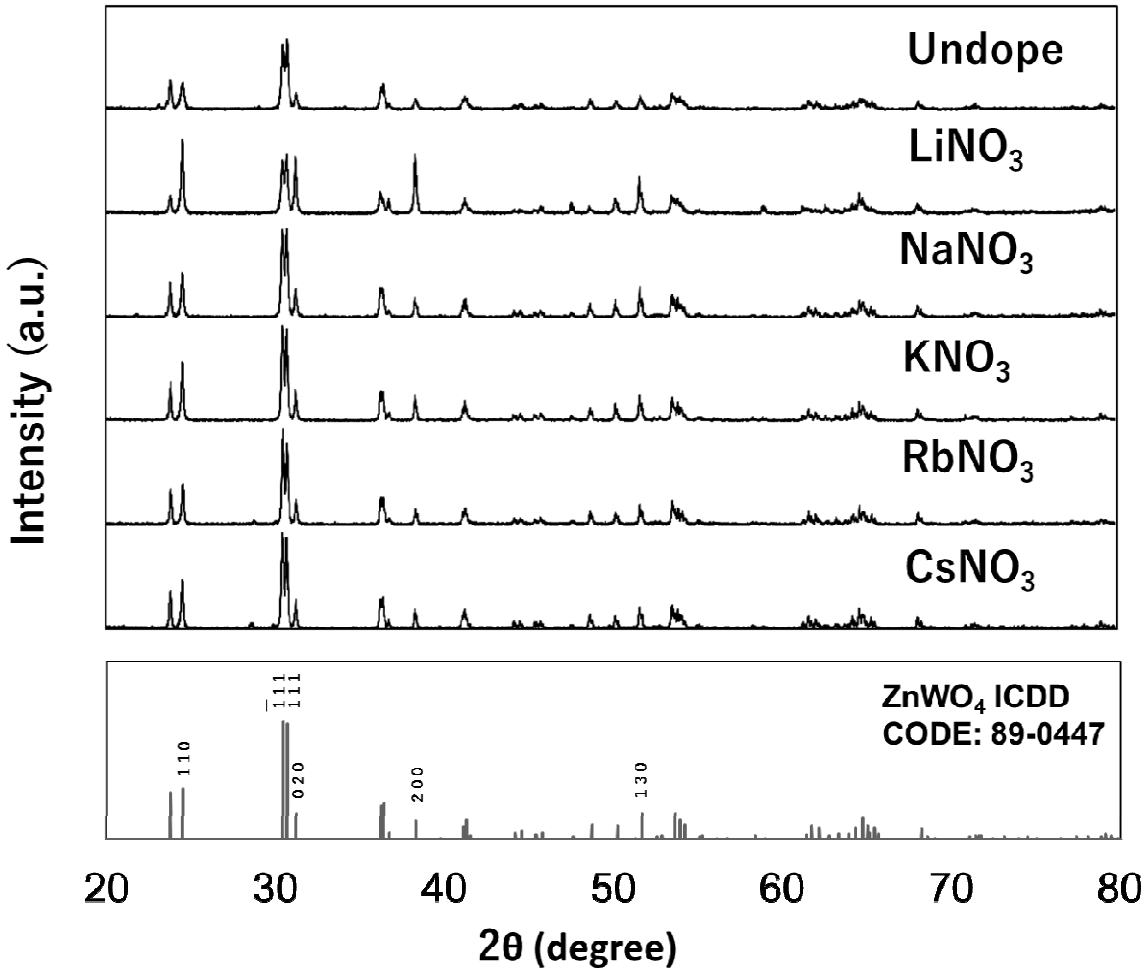

Figure 4.4 XRD patterns of samples doped with various alkali metal nitrates.

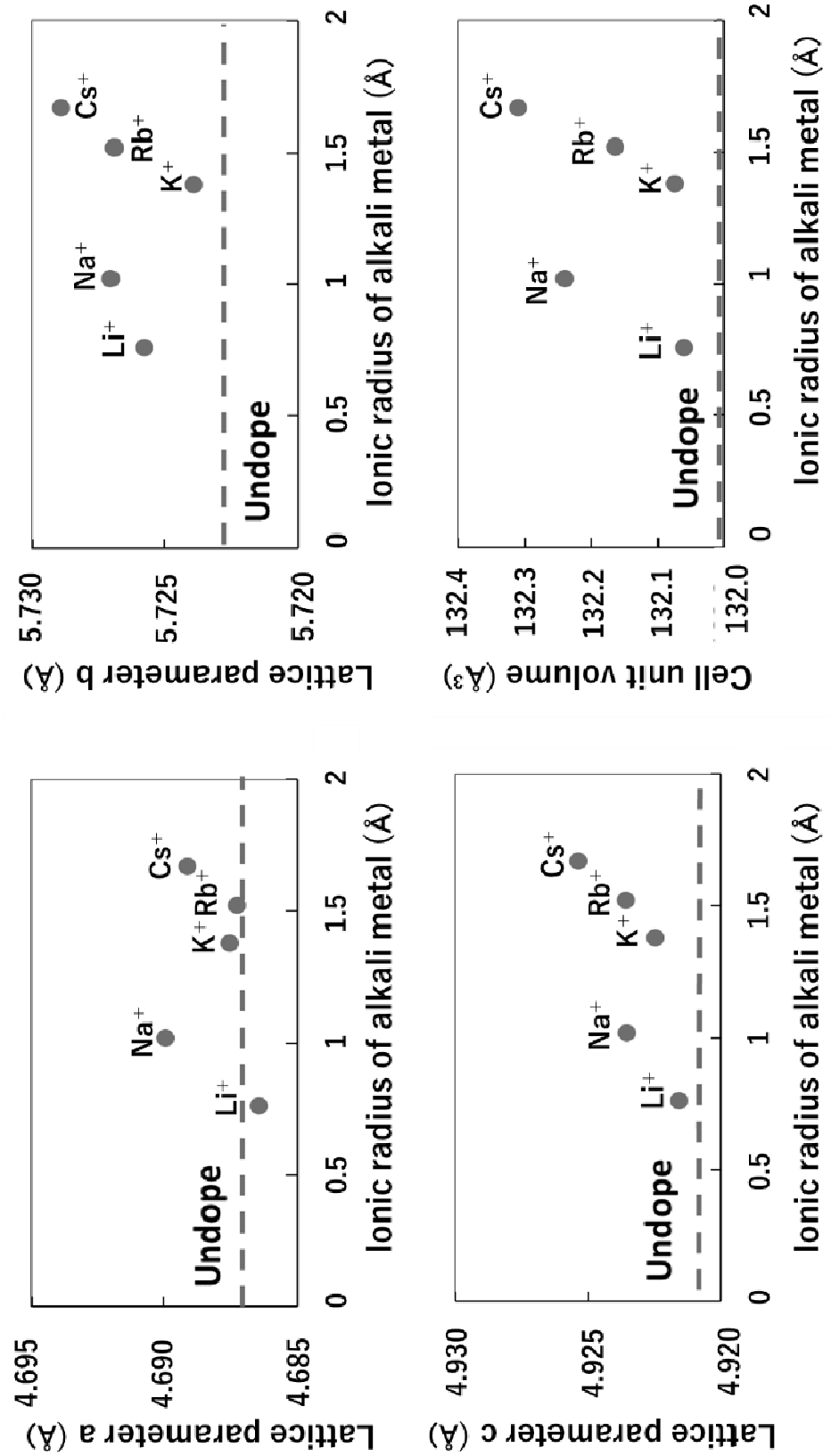

Fig. 4.5 Lattice constants and unit cell volume of alkali metal nitrate doped.

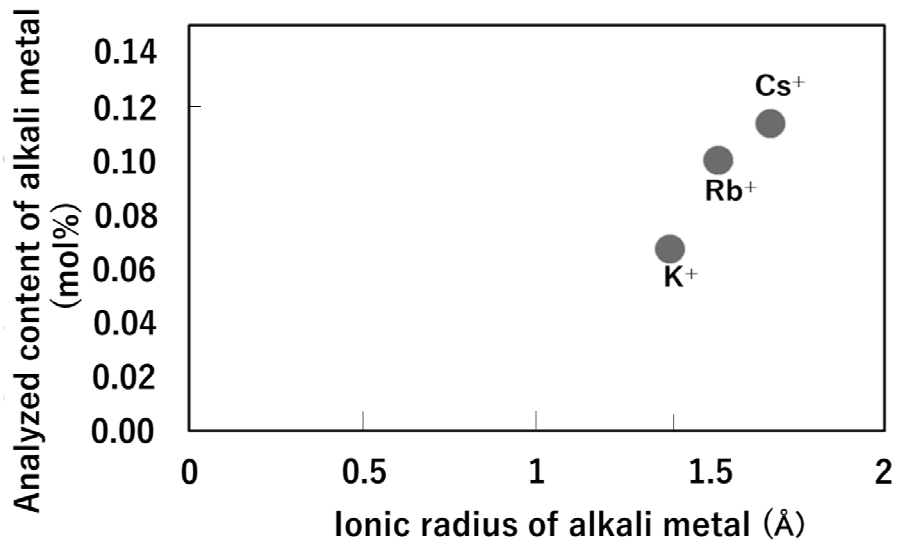

Figure. 4.6 Alkali metal content analyzed by XRF for the doped samples.

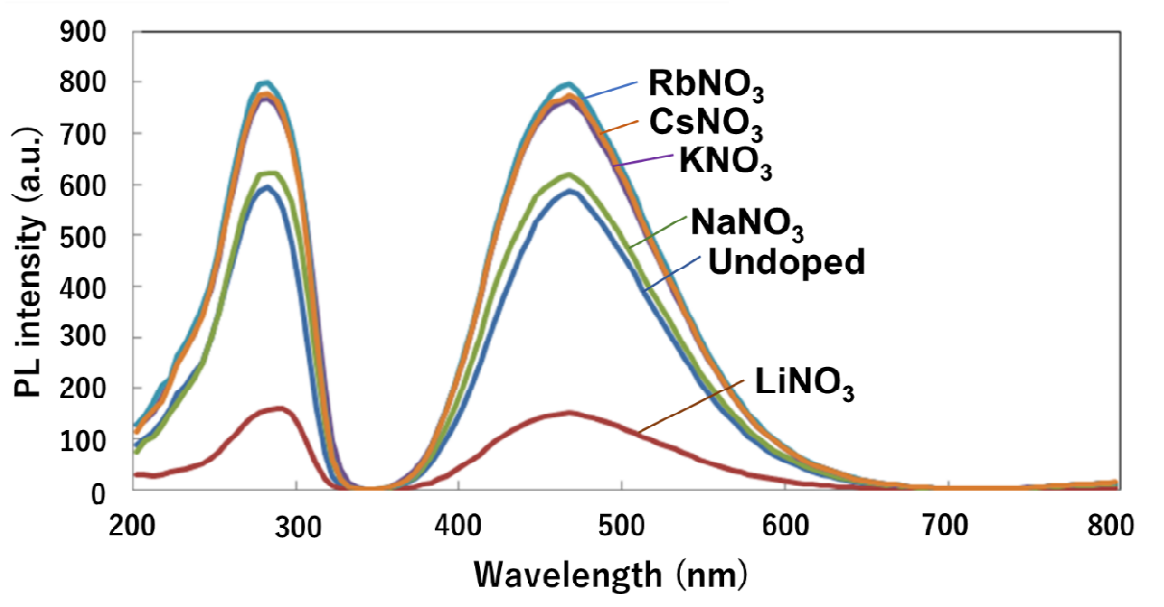

Figure 4.7 Emission and excitation spectra of samples doped with various alkali metal nitrates

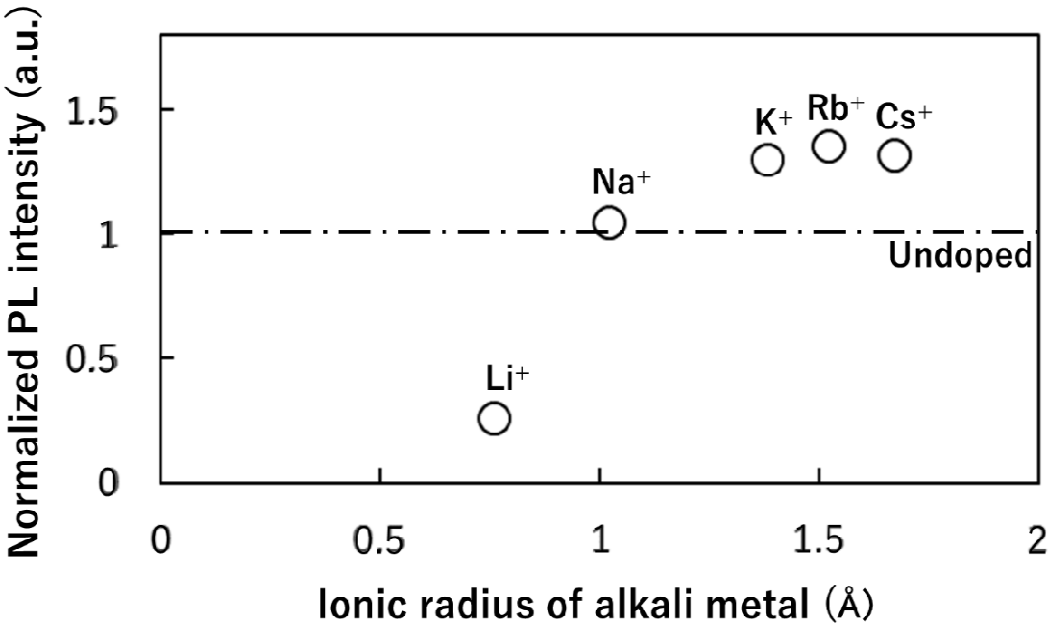

Figure 4.8 Normalized peak intensity of all samples prepared with alkali metal nitrate.

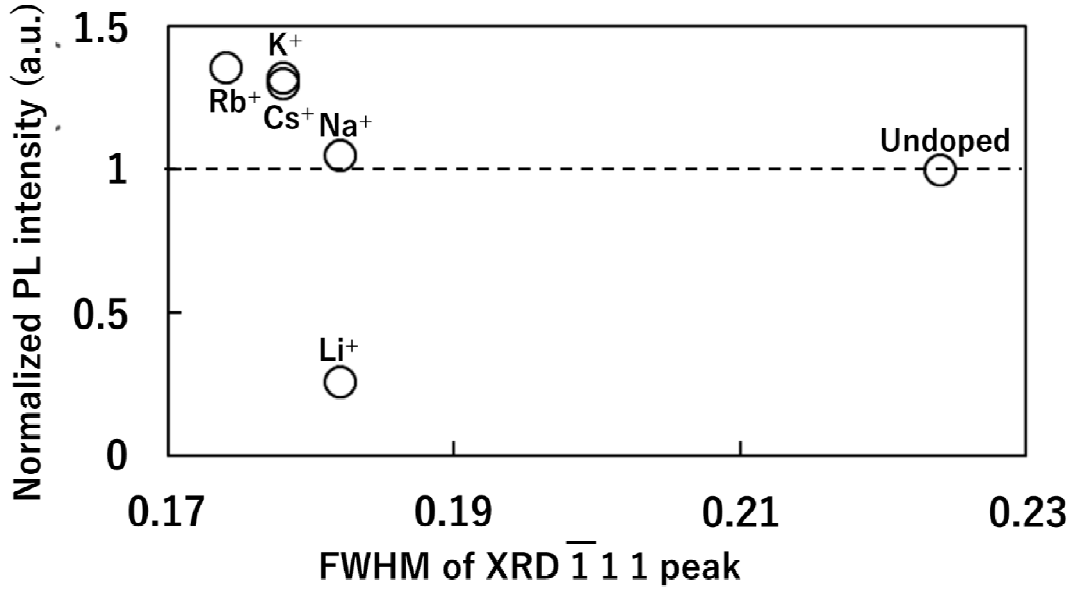

Figure 4.9 Relationship between normalized PL peak intensity and FWHM of XRD $\bar{1}$ 1 1 peak for samples doped with various alkali metal nitrates.

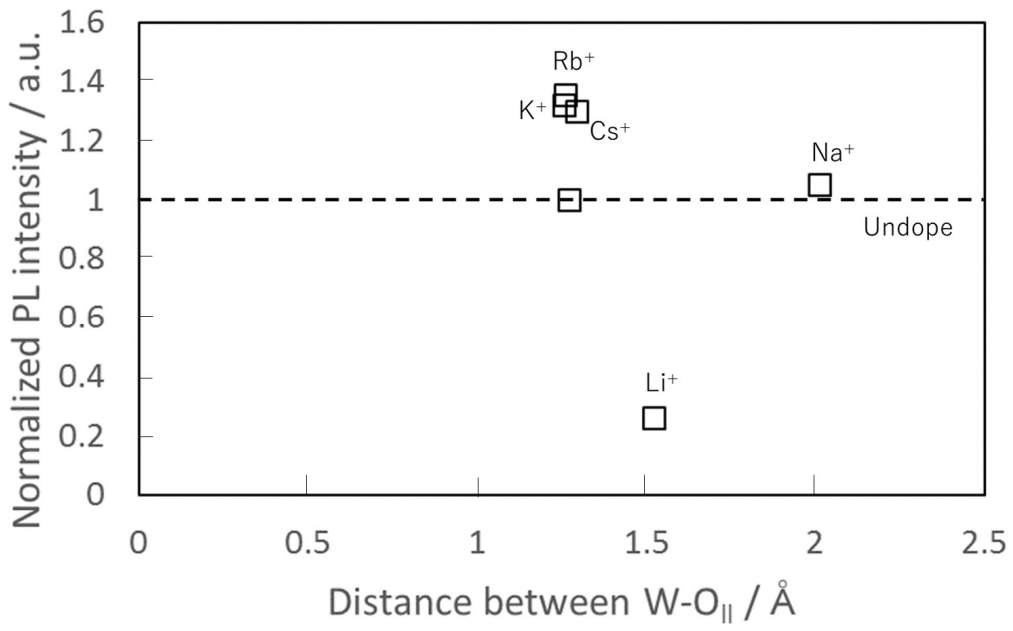

Fig. 4.10 Atomic distance between W and O_{II} of alkali metal nitrates doped.

4.4 CONCLUSION

We fabricated alkali metal nitrates doped $ZnWO_4$, confirmed their structure and evaluated their optical properties. For morphology, the grain size of the samples after doping was increased, and the lattice parameter of zinc tungstate phase changed. It was confirmed that dopant was dissolved into the samples and changed their crystal structure. For photoluminescence properties, the intrinsic emission peak of the samples excited at 275 nm was observed at 465 nm. The photoluminescence intensity of the samples was significantly increased when $NaNO_3$, KNO_3, $RbNO_3$, $CsNO_3$ were used as dopants.

Moreover, the different cation doping changed the crystal structure of sample and affected the emission peak intensity. $RbNO_3$ doping gave the highest crystallinity which resulted in the highest photoluminescence intensity. But $LiNO_3$ doping gave the photoluminescence weaker than the undoped sample and other doped sample, which may be related to the high atomic ordering along c-axis. It could be concluded that the radiative transitions between oxygen and tungsten can be enhanced by doping with alkali metal nitrates except $LiNO_3$.

References

[1] T. Oi, K. Takagi, T. Fukuzawa, Appl. Phys. Letts. 36, 278 **(1980)**.

[2] V.N. Kolobanov, I.A. Kamenskikh, V.V. Mikhailin, I.N. Shpinkov, D.A. Spassky, B.I.Zadneprovsky, L.I. Potkin, G. Zimmerer, Nucl. Instrum. Methods Phys. Res. A 486, 496 **(2002)**.

[3] H.Grassmann, H. Moser, E. Lorenz, J. Lumin. 33, 21 **(1985)**.

[4] J. Hulliger, A. A. Kaminskii, H. J. Eichler, Adv. Funct. Mater. 11, 243 **(2001)**.

[5] G. Huang, Y. Zhu, Mater. Sci. Eng. B 139, 201 **(2007)**.

[6] A. Kuzmin, R. Kalendarev, A. Kursitis, J. Purans, J. Non-Cryst. Solids 353, 1840 **(2007)**.

[7] M. Bonanni, L. Spanhel, M. Lerch, E. Fu¨glein, G. Muller, Chem. Mater. 10, 304 **(1998)**.

[8] W. Kolbe, K. Petermann, and G. Huber, IEEE J. Quantum Electron. 21, 1596 **(1985)**.

[9] N.V. Minh, N.M. Hung, D.T.X. Thao, M. Roeffaers, J. Hofkens, spectrosc., **(2013)**.

[10]R. Dafinova, K. Papazova, A. Bojinova, J. Lumin. 75, 51 **(1997)**.

[11]S. Deng, W. Zhange, Z.F. Hu, Z.Y. Feng, L. Ma, Y.M. Pan, X. Sheng, L. Luo, Authors. Photoluminescence and Photocatalytic Activity in Ca^{2+} and Dy^{3} Co-doped $ZnWO_4$ System. Proceeding of 2017 Joint International Conference on Materials Science and Engineering Application (ICMSEA

2017) and International Conference on Mechanics, Civil Engineering and Building Materials (MCEBM 2017), **(2017)** April 21–23; Nanjing, China.

[12] Ke Wang, Wenlin Feng, Xu Feng, Yao Li, Peng Mi, Shasha Shi, Spectrochim. Acta A 154, 72 **(2016)**.

[13] H.D.B. Jenkins, K.P. Thakur, J. Chem. Educ. 56, 576 **(1979)**.

[14] G. Huang, Y. Zhu, J. Phys. Chem. C 111, 11952 **(2007)**.

[15] G. Huang, Y. Zhu, CrystEngComm 14, 8076 **(2012)**.

[16] P.F.S. Pereira, A.F. Gouveia, M. Assis, R.C. de Oliveira, I.M. Pinatti, M. Penha, R.F. Gonçalves, L. Gracia, J. Andrés, E. Longo, Phys. Chem. Chem. Phys. 20,1923 **(2018)**

[17] A. B. van Oosterhout, J. Chem. Phys. 67, 2412 **(1977)**.

[18] G. He, H. Fan, L. Ma, K. Wang, D. Ding, C. Liu, Z. Wang, Mater. Sci. Semicond. Process. 41, 404 **(2016)**

[19] M. Hojamberdiev, G. Zhu, Y. Xu, Mater. Res. Bull. 45, 1934 **(2010)**

CHAPTER 5

FABRICATION OF ALKALI METAL SULFATE–DOPED ZINC TUNGSTATE AND THEIR PHOTOLUMINESCENCE

ABSTRACT

The enhancement of photoluminescence of alkali metal sulfate-doped zinc tungstate was investigated. All samples were prepared by solid-state reaction at 800˚C using ZnO, WO_3, and alkali metal sulfates as starting powders. The zinc tungstate phase was confirmed from the samples by X-ray diffraction. The emission peak of the samples excited at 275 nm was observed at 465 nm. Rb_2SO_4 > K_2SO_4 > Cs_2SO_4 > undoped > Na_2SO_4 > Li_2SO_4 was the order of peak emission intensity of alkali metal sulfate-doped samples. Alkali metals with a large ionic radius (K, Rb, Cs) enhanced the emission of intrinsic luminescence in the blue wavelength region. Moreover, sulfates had the potential to change the luminescence activities of the samples.

5.1 INTRODUCTION

Zinc tungstate ($ZnWO_4$) is a promising material for optical applications because of its luminescence and afterglow properties. It is normally studied and used for scintillator [1, 2], lasers [3], acoustics [4], optical fibers [5] and gas sensors for the detection of hydrogen gas [6]. In addition, zinc tungstate has the advantage of not being hygroscopic and is much cheaper than those normally used for scintillator materials such as $Bi_4Ge_3O_{12}$ (BGO). Kraus et al. [7] explained that $ZnWO_4$ exhibits a ~10% higher light yield scintillation at a low temperature than $CaWO_4$ which indicates that $ZnWO_4$ can be the suitable material for a scintillator. Klamra et al. [8] investigated the scintillation properties of $ZnWO_4$ at LN_2 temperature compared with room temperature and suggested that $ZnWO_4$ has good scintillation parameters at room temperature. In recent years, doping with other materials has been investigated in order to improve the performance of $ZnWO_4$. The doping technique creates defects in the structure which resulted in luminescence properties. The related researches [9, 10] explained that oxygen vacancies which occurred from a defect in the structure create luminescence centers whose emission is shifted to the red region in comparison with the main band 470-500 nm at 355 nm excitation wavelength. For anions, Dafinova et al. [11] explained that the addition of anions, such as SO_4^{2-} , F^-, Br^-, I^- and Cl^- ions from ammonium salts to the structure, can create an increase in the photoluminescence intensity of the blue emission in $ZnWO_4$. Additionally, for alkali metal and alkali metal earth doping, co-doping of Li and Pr improved the

crystallinity of the samples and charge compensation of Li^+ ions which resulted in enhanced luminescence [12]. For Na salts doping, the emission decreases because of the destruction of the WO_6 structures [11]. An increase in the light yield has been found in the scintillation properties after Ca was doped in the samples [13].

However, for alkali metals and anions, there are a few studies which investigated the luminescence properties after doping in $ZnWO_4$ [14]. In this research, we doped $ZnWO_4$ with various alkali metal sulfates and found that alkali metal with a large ionic radius and sulfates had an effect whereby the blue-green intrinsic photoluminescence of zinc tungstate was enhanced.

5.2 EXPERIMENTAL

Fig. 5.1 shows the sample preparation methods. The samples were prepared by solid-state reaction [14]. ZnO (99.99%, Furuuchi Chemical Co., Ltd.), WO_3 (99.99%, Kojundo Chemical Lab.), alkali metal sulfates (>99.00%, Junsei Chemical Co., Ltd.) were mixed as the starting powders in the molar ratios of ZnO : WO_3 : dopant (Li_2SO_4, Na_2SO_4, K_2SO_4, Rb_2SO_4 or Cs_2SO_4) = 1 : 1 : 0.02 which can obtain the highest improvement of photoluminescence as shown in our previous research [14]. The starting powder mixtures were ground in distilled water to dissolve salts for 20 minutes and were then mixed in 2-propanol for 2 h. After mixing, the powder mixtures were pressed into 10 and 20 mm diameter pellets under 100 and 300 MPa, respectively. The pellets were sintered at 800 °C for 3 h in air. After that, the 10 mm diameter pellets were ground into powders which were prepared in 2x2 cm glass holders for XRD and photoluminescence

testing. The crystalline phase of the samples was measured by X-ray diffractometer (XRD, RIGAKU Multiflex) using Cu Kα radiation (Kα= 1.5418 Å). The amount of dopant in the samples was confirmed by X-ray fluorescence (XRF, ZSX Primus II). The morphologies of the samples were observed using a scanning electron microscope (SEM, JEOL JSM-5510). Laser Raman spectroscopy (JASCO, NRS-7200) was used to investigate the effects of structural order-disorder on the properties of the samples. The photoluminescence of the samples was measured by using a fluorescence spectrophotometer (Hitachi F-7000) and the normalized photoluminescence emission intensity of each of the samples was calculated.

5.3 RESULT AND DISCUSSION

Fig. 5.2 shows the SEM micrographs of undoped and alkali metal sulfate-doped samples after sintering at 800˚C. The undoped sample shows the formation of crystals with a diameter lower than 1 μm. The grain size of the doped samples was large compared with the undoped one. The melting points were 859, 884, 1069, 1050, and 1010 °C for Li_2SO_4, Na_2SO_4, K_2SO_4, Rb_2SO_4, Cs_2SO_4, respectively. Generally, the grain growth is accelerated by the presence of the liquid phase. Some portions of alkali metal sulfates would melt during sintering and the grain size of the samples would increase rapidly. Moreover, the melting points of all alkali metal sulfates were higher than the sintering temperature (800°C). Hence, the grain growth of alkali metal sulfate doped samples is nearly the same.

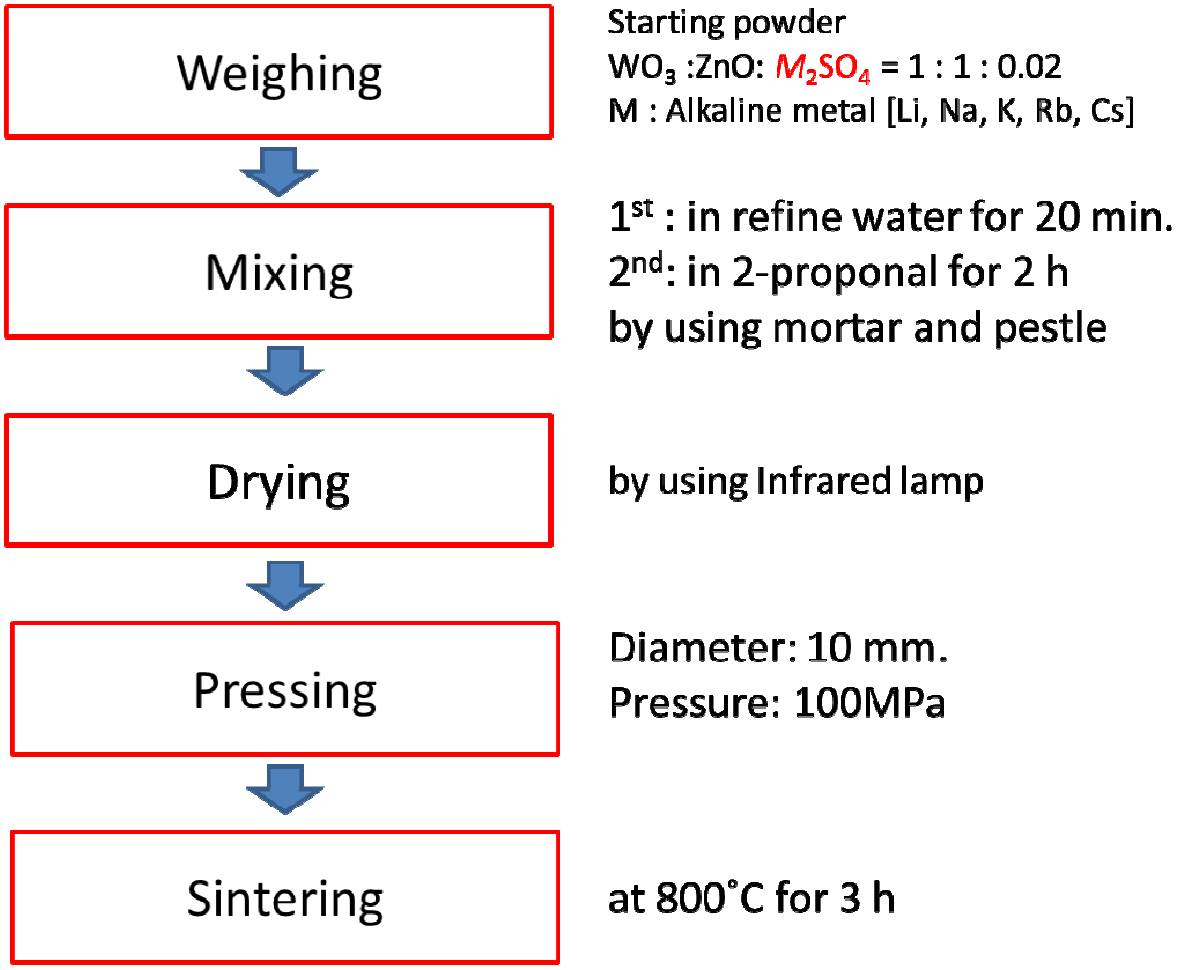

Fig. 5.1 The sample preparation method

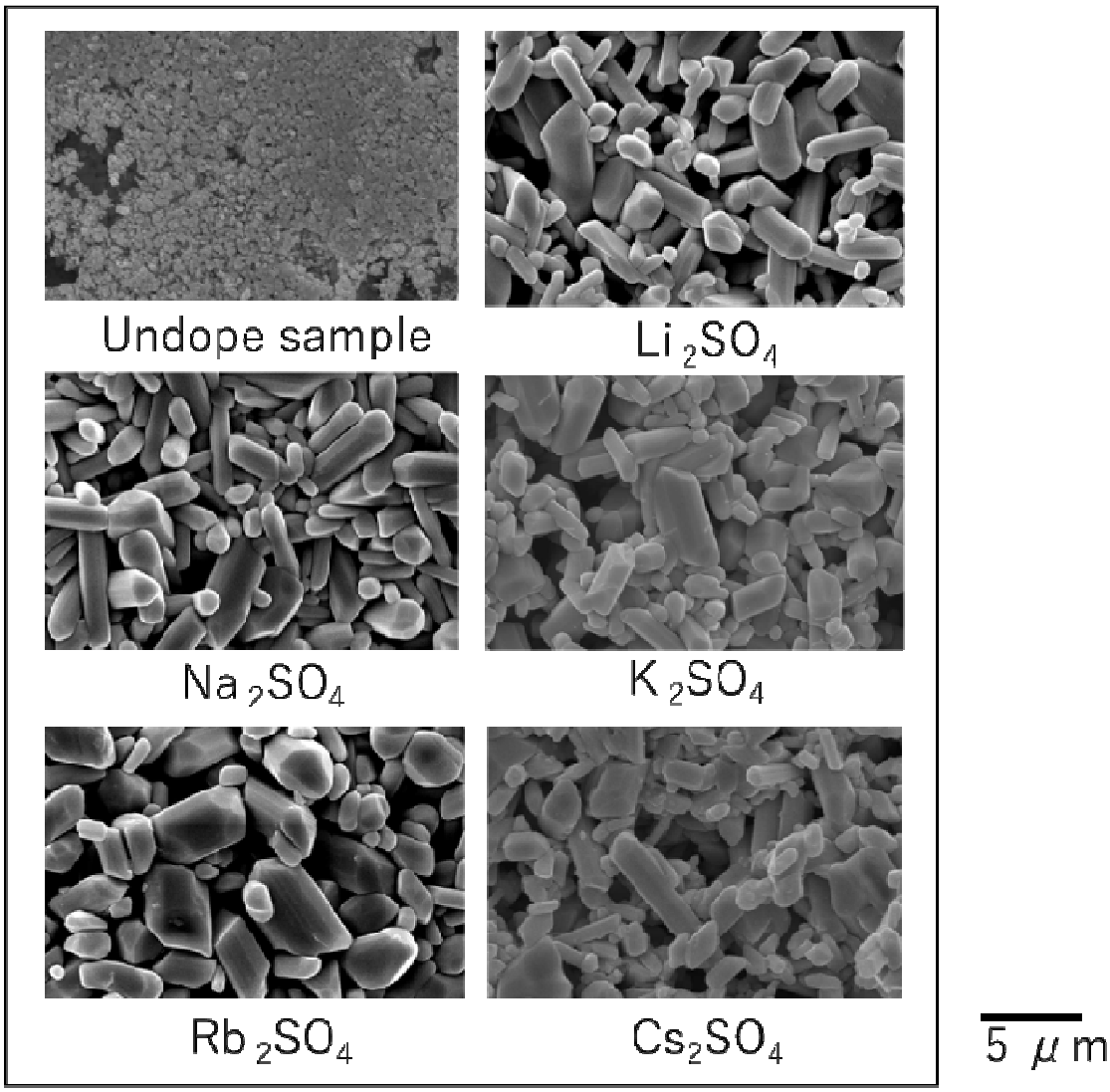

Fig. 5.2 SEM of samples doped with various sulfates

Fig. 5.3 shows XRD patterns of the sample powders prepared with various alkali metal sulfates. The peaks in the patterns were indexed on the basis of the crystallographic data of $ZnWO_4$ (ICDD code 89-0774). All samples presented well-defined diffraction peaks which were sharp and very clear peaks showing a good degree of structural order. The peaks slightly shifted in 2θ depending on the

alkali metal sulfates. The structural analysis was calculated to observe the structure of the sample by Profex program which is a graphical user interface for Rietveld refinement of X-ray diffraction data of the powder samples. The lattice constants and atomic coordinates of the samples were determined using XRD peaks and Rietveld refinement, as shown in Table 5.1, 5.2. The lattice constants a, b, c and unit cell volume were increased and the atomic coordinates of atoms in the samples were changed when alkali metal sulfates were doped, as shown in Fig. 5.4. From Table 5.2, the crystal structure of the samples was simulated using VESTA program, as shown in Fig. 5.5. These results indicate that the octahedral ZnO_6 and WO_6 complex were distorted which results in the generation of structural disorder in the samples and the changing of the lengths for W−O bonds, bonds between oxygen complex and the symmetry of the WO_6 complex, as shown in fig. 5.6 and table 5.3. Moreover, the XRF data in Fig. 5.7 shows the content of K^+, Rb^+, Cs^+ and S^{2-} in the samples. Li^+ and Na^+ cannot be detected because of the limitation of the XRF equipment. From the data of lattice parameter and XRF, alkali metal and sulfate ions were considered to have dissolved into the samples after the sintering. The ionic radii of Zn^{2+}, W^{6+}, Li^+, Na^+, K^+, Rb^+, Cs^+, O^{2-}, S^{2-} were 0.074, 0.06, 0.076, 0.102, 0.138, 0.152, 0.167, 0.140, and 0.184 nm, respectively. Li^+, Na^+, K^+, Rb^+, and Cs^+ were supposed to substitute for Zn^{2+} of $ZnWO_4$ rather than W^{6+}, because the difference of the ion charge between alkali metal ions and Zn^{2+} is smaller than W^{6+} and the ionic radii for alkali metal ions are nearly the same as or larger than Zn^{2+} and much larger than W^{6+}. S^{2-} anions were supposed to substitute for O^{2-} of $ZnWO_4$. The ionic radii of alkali metal and S^{2-} is

larger than Zn^{2+} and O^{2-}, so that the shifting of XRD peak in 2θ occurred which resulted in the change of lattice constants.

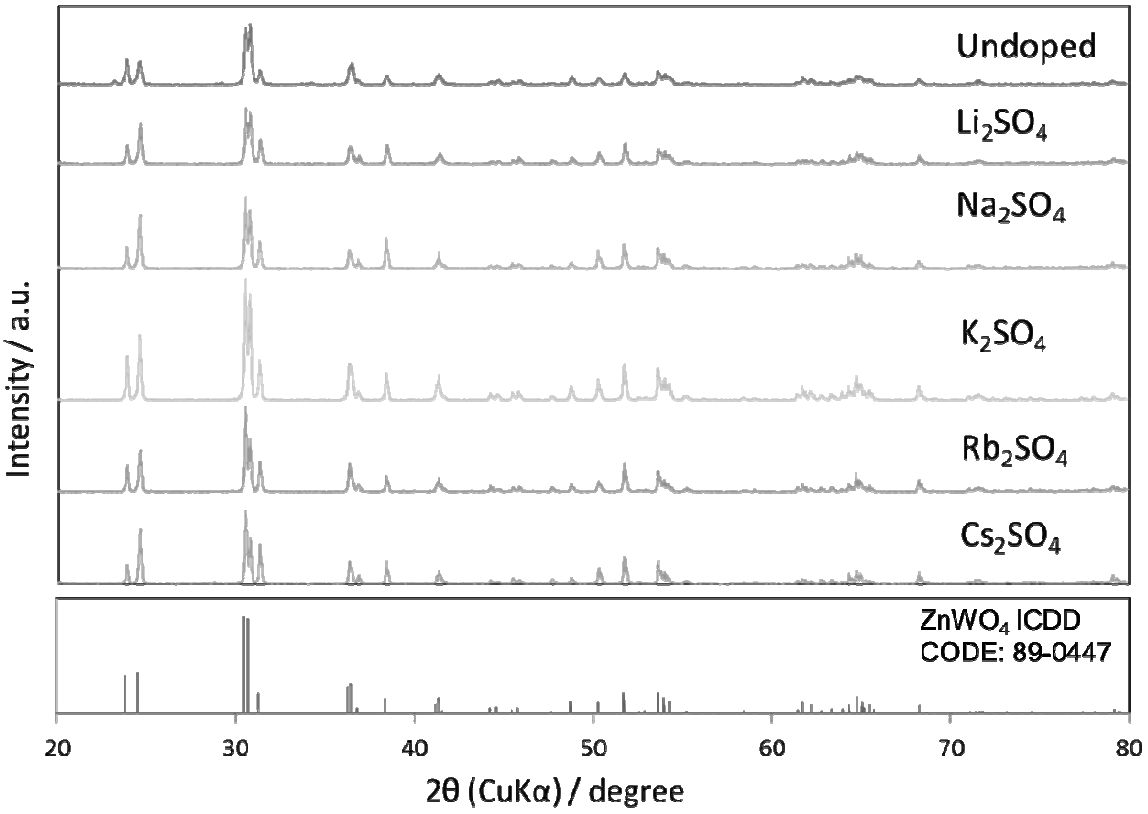

Fig. 5.3 XRD patterns of samples doped with various alkali metal sulfates.

Table 5.1 Lattice parameter and statistical parameters of the samples doped with various alkali metal sulfates.

	a (Å)	b (Å)	c (Å)	β (Degree)	Unit cell volume (Å^3)	χ^2	Rwp (%)	Rexp (%)
Undope	4.68648	5.71342	4.92222	90.6414	131.7882607	1.4289	32.49	27.18
Li_2SO_4	4.68575	5.71333	4.92296	90.6204	131.7859981	1.4608	32.5	26.89
Na_2SO_4	4.68844	5.71606	4.92493	90.6189	131.9774905	1.5034	31.34	25.56
K_2SO_4	4.68753	5.71531	4.92397	90.6234	131.9087312	1.2194	50.51	45.74
Rb_2SO_4	4.68825	5.7156	4.92436	90.6225	131.9461589	1.4913	31.8	26.04
Cs_2SO_4	4.68825	5.71519	4.92404	90.618	131.9282325	1.5201	32.66	26.49

Table 5.2 Atomic coordinates of the samples doped with various alkali metal sulfates.

	Zn			W			O_I			O_{II}			W-O_{Ia} (Å)	W-O_{Ib} (Å)	W-O_{II} (Å)
	x	y	z	x	y	z	x	y	z	x	y	z			
Undope	0.5	0.6886	0.25	0	0.1787	0.25	0.2029	0.3	0.35	0.15	0.8223	0.5	2.33811	1.43498	1.27133
Li_2SO_4	0.5	0.6806	0.25	0	0.1818	0.25	0.2	0.3	0.35	0.15	0.8605	0.5	2.35512	1.44426	1.25167
Na_2SO_4	0.5	0.6773	0.25	0	0.1834	0.25	0.3	0.3652	0.45	0.15	0.85	0.5	2.37142	1.43724	1.99962
K_2SO_4	0.5	0.6864	0.25	0	0.1816	0.25	0.2016	0.3	0.35	0.15	0.8747	0.5	2.25111	1.46017	1.25828
Rb_2SO_4	0.5	0.6854	0.25	0	0.1792	0.25	0.2	0.3	0.35	0.15	0.8624	0.5	2.29564	1.44412	1.2603
Cs_2SO_4	0.5	0.6855	0.25	0	0.1805	0.25	0.2	0.3	0.35	0.15	0.8602	0.5	2.31133	1.44316	1.25624

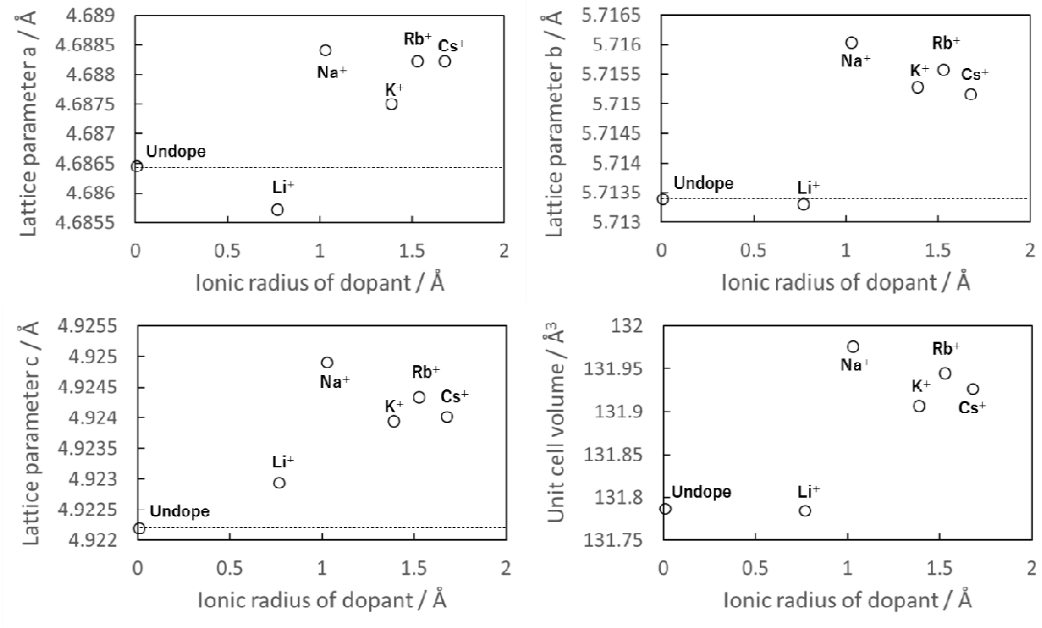

Fig. 5.4 Lattice constants and unit cell volume of alkali metal sulfates doped.

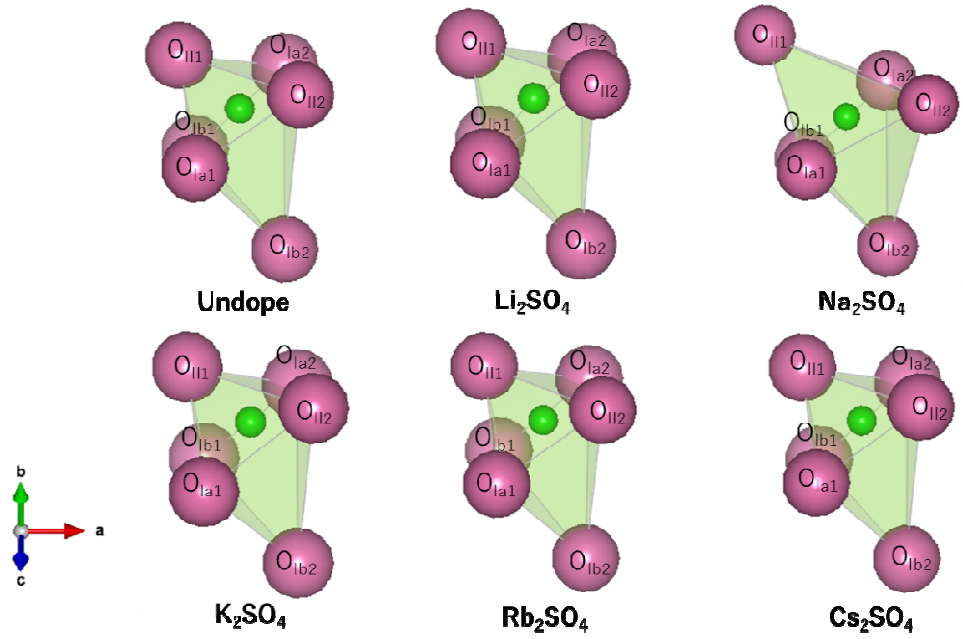

Fig. 5.5 Simulation of W-O complex of the samples from rietveld refinement

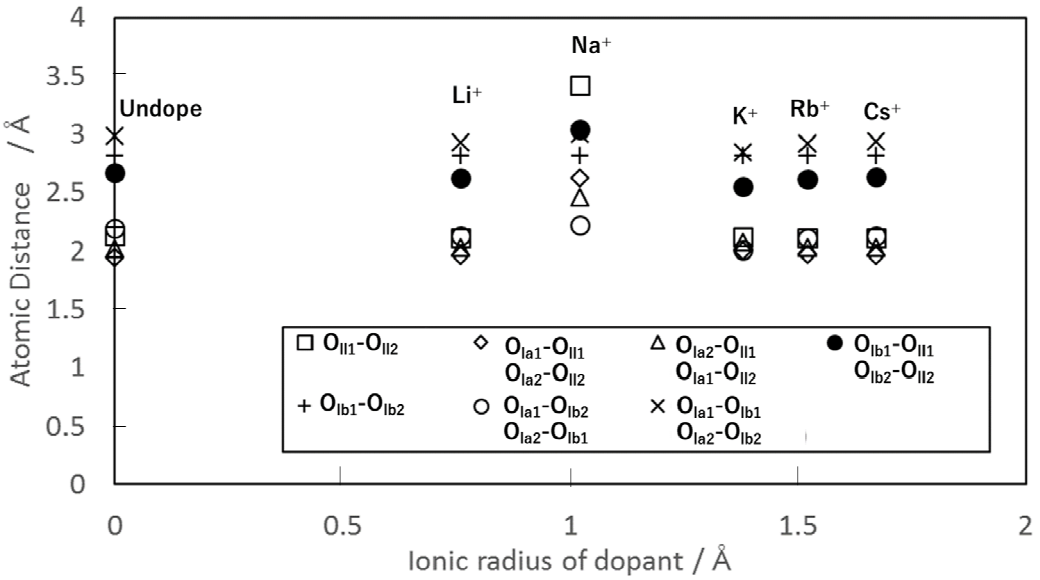

Fig. 5.6 The relationship between atomic distance between O_I and O_{II} and ionic radius of dopant of alkali metal sulfates doped.

Table 5.3 Atomic distance between O_I and O_{II} of alkali metal sulfates doped

	Ionic radius of alkali metal ion (Å)	O_{II1}-O_{II2} (Å)	O_{Ia1}-O_{II1} O_{Ia2}-O_{II2} (Å)	O_{Ia2}-O_{II1} O_{Ia1}-O_{II2} (Å)	O_{Ib1}-O_{II1} O_{Ib2}-O_{II2} (Å)	O_{Ib1}-O_{Ib2} (Å)	O_{Ia1}-O_{Ib2} O_{Ia2}-O_{Ib1} (Å)	O_{Ia1}-O_{Ib1} O_{Ia2}-O_{Ib2} (Å)
Undope	0	2.13166	1.94346	2.01616	2.67461	2.82069	2.19662	2.98422
Li_2SO_4	0.76	2.10771	1.96364	2.02535	2.62852	2.82135	2.12531	2.93254
Na_2SO_4	1.02	3.41678	2.62406	2.45668	3.03834	2.82283	2.21787	3.00072
K_2SO_4	1.38	2.12167	2.00411	2.0701	2.55271	2.82198	2.00722	2.84829
Rb_2SO_4	1.52	2.10869	1.96934	2.03127	2.61917	2.82228	2.11005	2.92172
Cs_2SO_4	1.67	2.10873	1.96333	2.02546	2.63099	2.82224	2.12877	2.93514

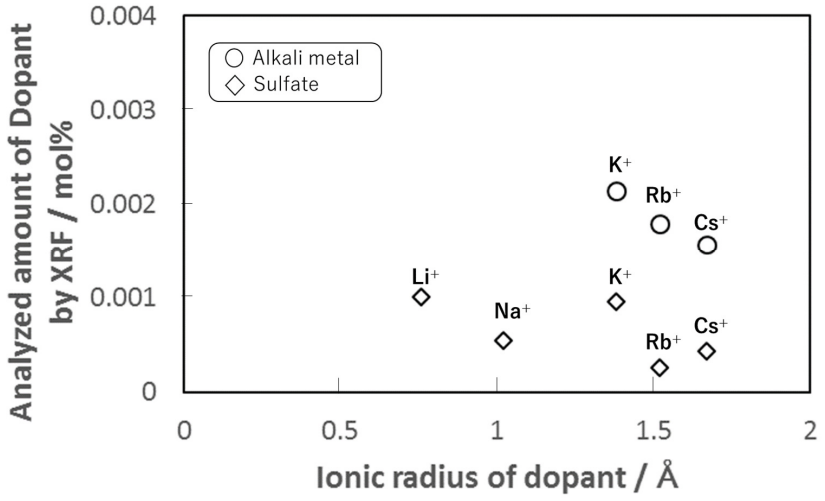

Fig. 5.7 XRF of alkali metal and sulfate content in the doped samples.

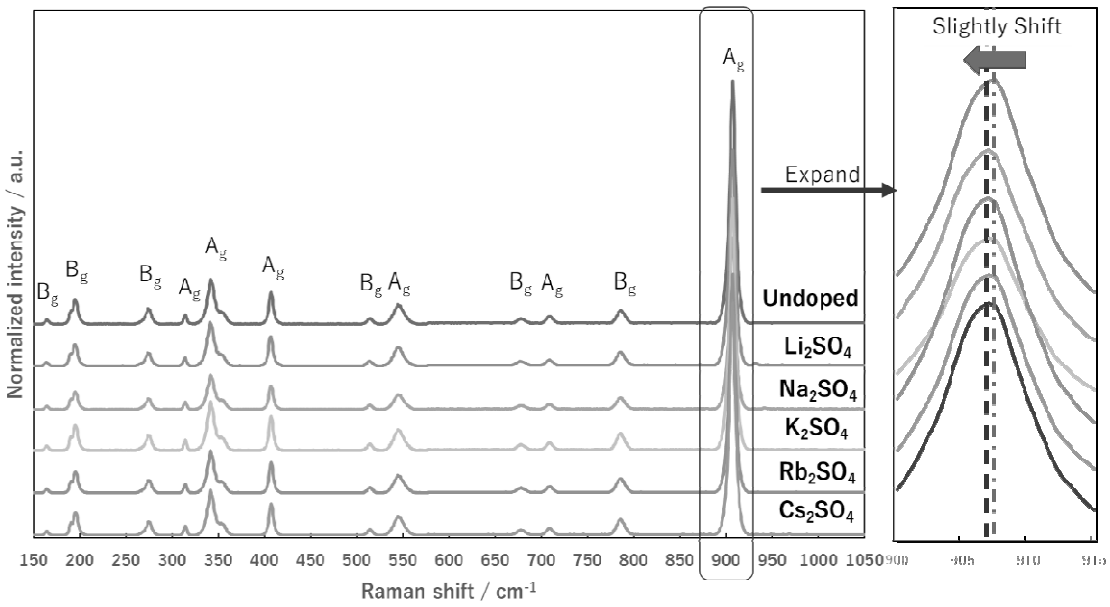

Fig. 5.8 Laser raman spectroscopy of samples doped with various alkali metal sulfates.

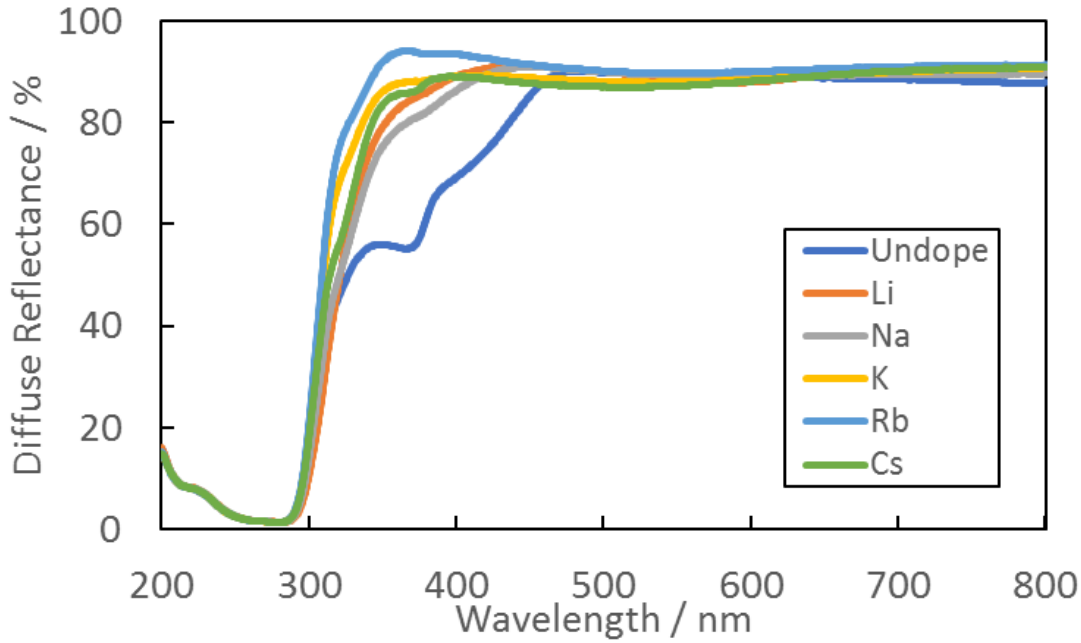

Fig. 5.9 UV-Vis diffuse reflectance spectra of samples

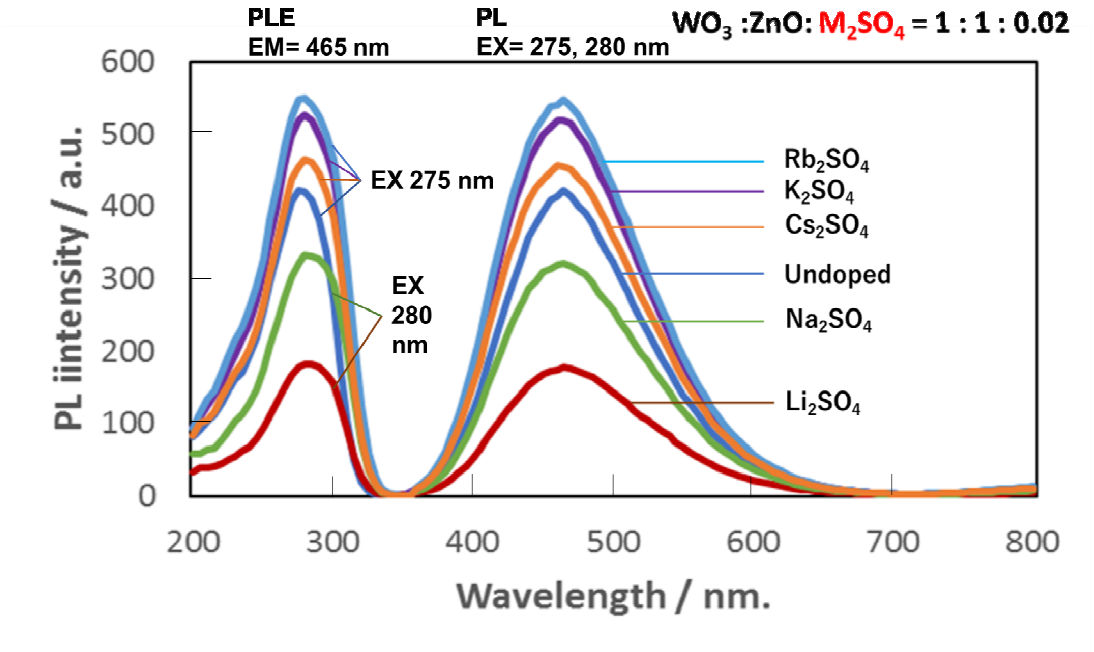

Fig. 5.10 Emission and excitation spectra of samples doped with various alkali metal sulfates.

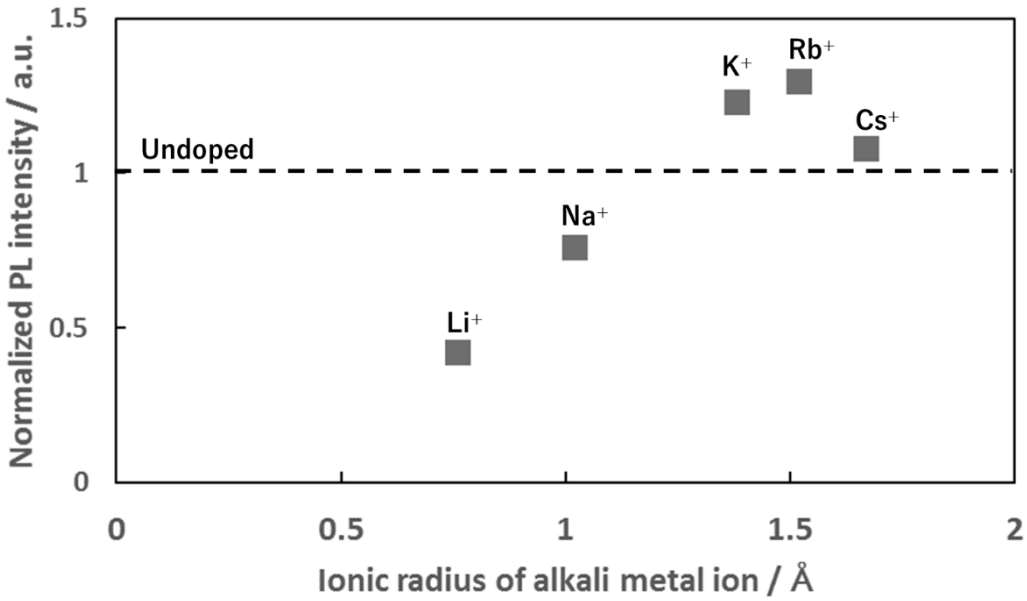

Fig. 5.11 Relationship between normalized peak intensity and ionic radius of alkali metal ion

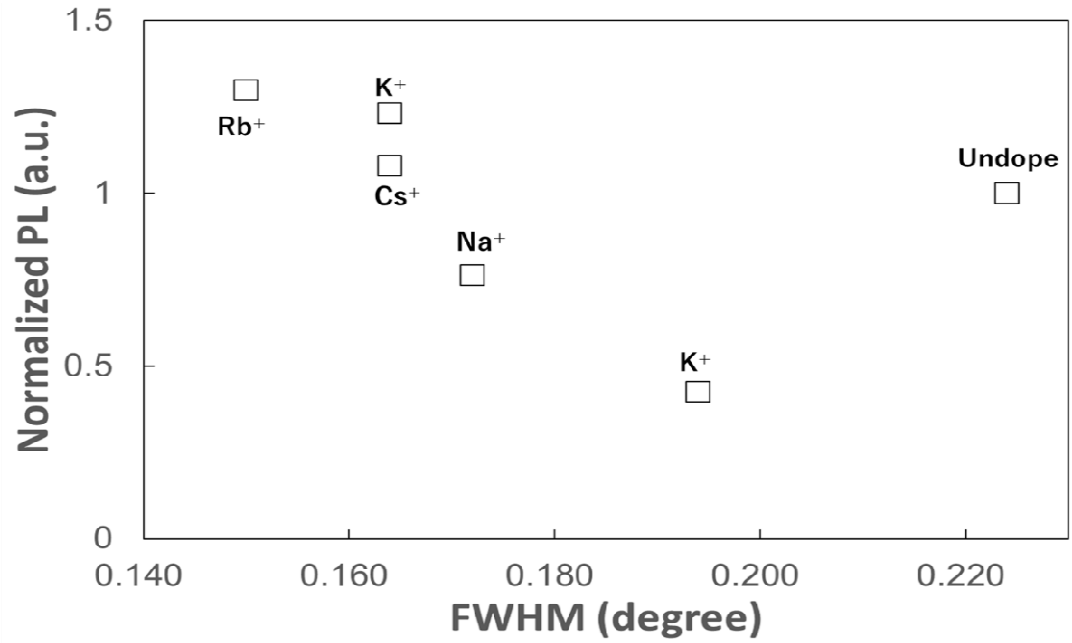

Fig. 5.12 Relationship between normalized peak intensity of samples doped with various alkali metal sulfate and FWHM of XRD $\bar{1}\,1\,1$ peak

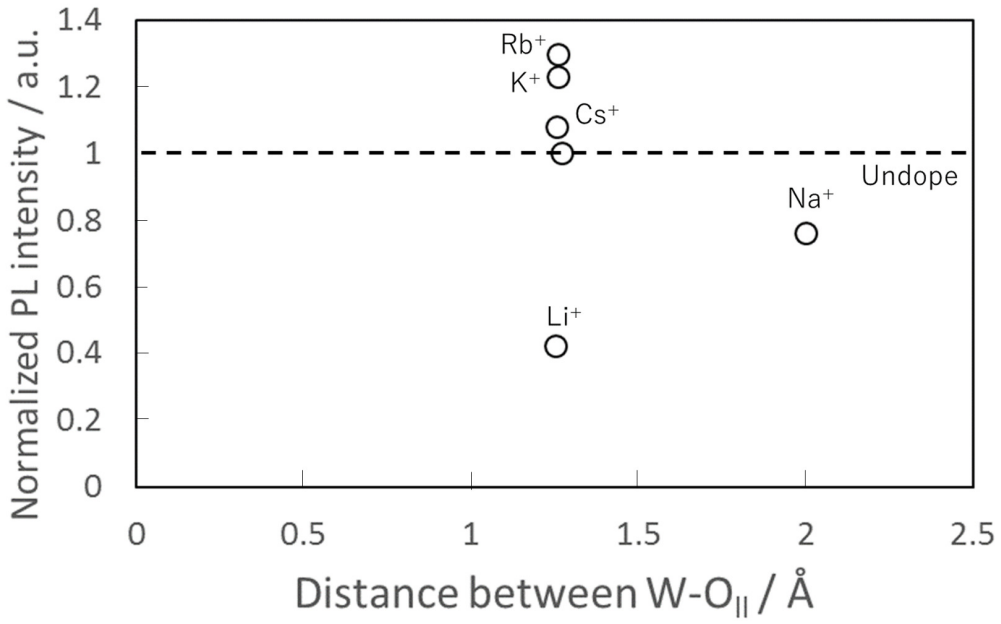

Fig. 5.13 Atomic distance between W and O_{II} of alkali metal sulfates doped.

Figure 5.8 shows the laser Raman spectra of the samples which have the vibrational Raman active modes between 50 and 1150 cm−1. For wolframite-type monoclinic structures, the Raman spectra of tungstate structures will exhibit 18 active vibrational modes which can be classified into external modes, which correspond to the movement of distorted ZnO_6 complex in the unit cell, and internal modes, which correspond to the vibrations of distorted WO_6 complex. From Fig. 5.8, for the well-defined Raman peaks, it is considered that the crystals have good structural order in the same way as XRD data. From related researches [15, 16], all Raman-active modes in the samples were designated as Ag or Bg. The Raman bands observed at 905 and 344 cm^{-1} correspond to the vibrations of W–O bonds in the WO_6. The motions of the WO_6 against Zn^{2+} were observed at 707 and 675 cm^{-1} while the bands ranging between 500 and 600 cm^{-1} show the symmetry of W–O–W in the stretching mode. However, when the particle size increases, an effect on the vibrational transitions of the samples might occur. In vibrational transitions, the wavenumber changes in proportion to k1/2 as shown in eq. (1)

$$\nu = \frac{1}{2\pi}\left(\frac{k}{m}\right)^{\frac{1}{2}} \quad (1)$$

, where ν is the wavenumber, k is the force constant and m is mass. Consequently, the Raman bands shift towards a lower wavenumber due to the decreasing force constants which resulted to bond distance, atomic coordinate in the crystal structure of the samples and related to the disorder in the crystal structure.

Fig. 5.9 shows the UV-Vis diffuse reflectance spectra of samples. From this

result, absorption edge is investigated and found that absorption edge of all samples occurred about 295 nm.

Fig. 5.10 shows there is photoluminescence intensity of all samples. The emission peak occurred at 465 nm and excitation peak appeared at 275 nm. Compared with the undoped sample, doping with alkali metal sulfates exhibited a higher emission intensity except for Li_2SO_4, and Na_2SO_4 doping (as shown in Fig. 5.8). Rb_2SO_4 > K_2SO_4 > Cs_2SO_4 > undoped > Na_2SO_4 > Li_2SO_4 was the order of peak emission intensity of alkali metal sulfate-doped samples. When investigated the effect between ionic radius of dopant and photoluminescence intensity, Fig. 5.11 shows the increasing photoluminescence intensity of the sample with the increasing ionic radius of dopants. Fig. 5.12 shows the relationship of normalized peak intensity and FWHM of XRD $1^{-}1\ 1$ peak. The order of FWHM of sulfate was Rb_2SO_4 < K_2SO_4 < Cs_2SO_4 < Na_2SO_4 < Li_2SO_4 << undoped. Compared with the undoped sample, doping with alkali metal sulfate had a lower FWHM which resulted in the crystallinity in $ZnWO_4$ and photoluminescence properties to increase. Morevoer, fig.5.13 shows the relationship between normalized photoluminescence intensity and distance between W and O_{II}. According to related researches [16, 17, 18, 19], the four shared oxygen atoms surrounding the tungsten atom in the WO_6 structure participate in charge transfer between the O 2p orbitals and empty 5d W orbitals. It was considered that the distance between W and O, crystallinity and oxygen vacancy of $ZnWO_4$ has a significant impact on the photoluminescence intensity. Increasing instinct emission intensity occurs from the short distance between W and O, high crystallinity and some simultaneous order-

disorder in the system while the decrease of emission occurs from the total disorder or highly crystalline structures [16]. Some researches [9, 10, 20, 21, 22] have explained that the photoluminescence of tungstate system occurred as a result of the defects, such as oxygen vacancies and interstitial atoms. From all of the results in this work, it is considered that the alkali metal ions replacing Zn^{2+}, which created the oxygen vacancy from charge compensation, deform the WO_6 structure and crystallinity in $ZnWO_4$, which resulted in the changing of the luminescence activity. From the related research [16], oxygen vacancies can appear in different charge states in the disordered lattice, such as $[WO_5 \cdot V_o^x]$ and $[ZnO_5 \cdot V_o^x]$ or $[WO_4 \cdot 2V_o^x]$ and $[ZnO_4 \cdot 2V_o^x]$, where the vacancies donate electrons and are neutral in relation to the lattice. These oxygen vacancies induce the generation of new energy states in the band gap attributed to the $[WO_6]$ and $[ZnO_6]$ structure. For Li and Na doping, the photoluminescence was weaker than the undoped sample and other doped samples, which might be related to the changing of the crystal structure which is shown in Rietveld refinement (Fig. 5.3, 5.4 ,5.5). Alkali metal ions such as K^+, Rb^+, Cs^+ which have a larger ionic radius than Zn^{2+} may provide a symmetrical W-O structure and short distance between W and O atoms which was shown in Rietveld refinement (Table 5.2, Fig. 5.5 and Fig. 5.13), increased the crystallinity which affects the optical transition between the d orbitals of W and the p orbitals of the O atoms. For Rb doping, the highest photoluminescence intensity occurred because of the highest crystallinity which showed the lowest FHWM. However, for Li_2SO_4 and Na_2SO_4 doping, the distortion of WO_6 complex as a non-symmetrical structure which is shown from Rietveld refinement (Table

5.1, 5.2 and Fig. 5.5) had an effect of decreasing the photoluminescence of the sample. It is considered that different cations will give different enhancement in the luminescence activities of the samples. This result was explained in the same way as results in related research [11]. Moreover, the S^{2-} from sulfate penetrated the structure by replacing with O^{2-} and affected the photoluminescence activities of the samples.

5.4 CONCLUSION

In this study, we fabricated alkali metal sulfate-doped $ZnWO_4$, confirmed their structure and evaluated their optical properties. The photoluminescence intensity of the samples was significantly increased when K_2SO_4, Rb_2SO_4, Cs_2SO_4 were used as dopants. Moreover, the different cation and anion doping changed the crystal structure of the sample and affected the emission peak intensity. It could be concluded that doping alkali metal sulfates could change the optical transition between tungsten and oxygen which resulted in higher photoluminescence intensity of the samples. Alkali metal sulfates, except Li and Na, could enhance the photoluminescence of the samples.

References

[1] T. Oi, K. Takagi, T. Fukuzawa, Appl. Phys. Letts. 36, 278 (1980).

[2] V.N. Kolobanov, I.A. Kamenskikh, V.V. Mikhailin, I.N. Shpinkov, D.A. Spassky, B.I. Zadneprovsky, L.I. Potkin, G. Zimmerer, Nucl. Instrum. Methods Phys. Res. A 486, 496 (2002).

[3] J. Hulliger, A. A. Kaminskii, H. J. Eichler, Adv. Funct. Mater. 11, 243 (2001).

[4] Yu. V. Pisarevskii, I. M. Silvestrova, R. Voszka, A. Peter, I. Foldvlri, J. Janszky, Phys. Stat. Sol. (a) 107, 161 (1988).

[5] H. Grassmann, H. Moser, E. Lorenz, J. Lumin. 33, 21 (1985).

[6] Zhaoyun Tang, Xiaogan Li, Jianhang Yang, Jun Yu, Jing Wang, Zhenan Tang, Sensors and Actuators B 195 (2014) 520–525

[7] H. Kraus, V. B. Mikhailik, Y. Ramachers, D. Day, K. B. Hutton, J. Telfer, Phys. Lett. B 610, 37 (2005)

[8] W. Klamra, T. Szczesniak, M. Moszynski, J. Iwanowska, L. Swiderski, A. Syntfeld-Kazuch, V. N. Shlegel, Y. V. Vasiliev, E. N. Galashov, Journal of Instrumentation 7 (2012)

[9] A.E. Ovechkin, V.D.Ryzhikov, G.Tamulaitis, Phys.stat.sol. (a) 103, 285 (1987)

[10] I.A. Tupitsyna, P.O. Maksimchuk, A.G. Yakubovskaya, Y.V. Malyukin, V.S. Zvereva, O.M. Vovk, Functional Materials 23, 535 (2016)

[11] R. Dafinova, K. Papazova, A. Bojinova, Journal of Luminescence 75, 51 (1997).

[12] Ke Wang, Wenlin Feng, Xu Feng, Yao Li, Peng Mi, Shasha Shi, Spectrochimica Acta Part A: Molecular and Biomolecular Spectroscopy 154 72–75 (2016).

[13] F. A. Danevich, S. Henry, H. Kraus, R. McGowan, V. B. Mikhailik, O. G. Shkulkova, J. Telfer, Phys. Stat. Sol. (a) 205, No. 2, 335–339 (2008)

[14] Prinya Lorchirachoonkul, Masaya Nakata, Yasuyuki Yamada, Tomoichiro Okamoto, Journal of Luminescence 197, 131 (2018)

[15] R. F. Gonçalves, E. Longo, A. P. A. Marques, M. D. P. Silva, L. S. Cavalcante, I. C. Nogueira, I. M. Pinatti, P. F. S. Pereira, M. J. Godinho, J Mater Sci: Mater Electron 28, 15466 (2017)

[16] P. F. S. Pereira, A. F. Gouveia, M. Assis, R. C. de Oliveira, I. M. Pinatti, M. Penha, R. F. Gonçalves, L. Gracia, J. Andrés, E. Longo, Phys Chem Chem Phys. 20(3),1923 (2018)

[17] A. B. van Oosterhout, The Journal of Chemical Physics 67, 2412 (1977).

[18] G. He, H. Fan, L. Ma, K. Wang, D. Ding, C. Liu, Z. Wang, Mater Sci Semicond Process. 41, 404 (2016)

[19] M. Hojamberdiev, G. Zhu, Y. Xu, Mater. Res. Bull. 45, 1934 (2010)

[20] B. Ding, C. Han, L. Zheng, J. Zhang, R. Wang, Z. Tang, Scientific Reports 5, 9443 (2015)

[21] A. Magraso, R. Haugsrud, A Review. J. Mater. Chem. A. 2, 12630 (2014)

[22] M. A. Santos, Phys. Rev. B. 75, 165105 (2007).

CHAPTER 6

CONCLUSIONS AND RECOMMENDATIONS

6.1 CONCLUSIONS

This study aimed to develop the zinc tungstate by doping with other materials. In the first part of this thesis, potassium salts in different contents were added into zinc tungstate. After that, the samples were investigated the effect in photoluminescence properties of the sample and confirm the highest content which obtains the highest photoluminescence intensity. In the second part of this thesis, zinc tungstate was doped with alkali metal salts. By using the data from the first part, the alkali metal salts contents were decided.

Alkali metal salts doped zinc tungstates were confirmed for their structure and were evaluated for their optical properties. First, for potassium salts doping, the powders were mixed with the molar ratios of ZnO: WO_3: potassium salts = 1: 1: x and sintered at 800˚C for 3 h in air. The grain size of samples increased when potassium salts were doped. Potassium and anions were considered to dissolve in $ZnWO_4$ and change the lattice constants. The photoluminescence intensity of the samples was significantly increased when potassium salt content x was 0.02. The order of each maximum photoluminescence intensity was KNO_3, K_2SO_4, KCl. The

different cations and anions doping changed the structure of the sample and affected the emission peak intensity. It could be concluded that the radiative transitions between tungsten and oxygen can be enhanced by doping with potassium and anions.

For alkali metal nitrate and sulfate, the grain size and the lattice parameter of the samples was increased after doping. It was confirmed that dopant was dissolved into the samples and changed the crystal structure. For photoluminescence properties, the intrinsic emission peak of the samples excited at 275 nm was observed at 465 nm. The photoluminescence intensity of the samples was significantly increased when $NaNO_3$, KNO_3, $RbNO_3$, $CsNO_3$ were used as dopants. Moreover, the different cation doping changed the crystal structure of the sample and affected the emission peak intensity. $RbNO_3$ doping gave the highest crystallinity which resulted in the highest photoluminescence intensity. But $LiNO_3$ doping gave the photoluminescence weaker than the undoped sample and other doped samples, which may be related to the high atomic ordering along c-axis. For alkali metal sulfate doping, the photoluminescence intensity of the samples was significantly increased when K_2SO_4, Rb_2SO_4, Cs_2SO_4 were used as dopants.

Moreover, the different cation and anion doping changed the crystal structure of the sample and affected the emission peak intensity. It could be concluded that the doping alkali metal salts could change the optical transition between tungsten and oxygen which resulted in the photoluminescence intensity of the samples.

6.2 RECOMMENDATIONS FOR FURTHER RESEARCH

(1) Other luminescence activities such as absorptance, transmittance, band gap after alkali metal doping.

(2) Investigate more the photoluminescence mechanism of $ZnWO_4$ by using Rietveld refinement to analyze.

AUTHOR PUBLICATIONS

Journal

Prinya Lorchirachoonkul, Masaya Nakata, Yasuyuki Yamada, Tomoichiro Okamoto, Journal of Luminescence 197, 131 (2018). IF: 2.732.

Prinya Lorchirachoonkul, Masaya Nakata, Tomoichiro Okamoto, Nanoscience and Nanotechnology Letters, Volume 10, Numbers 5-6, May 2018, pp. 854-857(4). IF: 2.917.

Prinya Lorchirachoonkul, Masaya Nakata, Tomoichiro Okamoto, Journal of Luminescence 207, 333 (2019). IF: 2.732.

Conference

Prinya Lorchirachoonkul, Masaya Nakata, Yasuyuki Yamada, Tomoichiro Okamoto, Annual Meeting of the ceramic society of Japan, 2016, Tokyo, Japan. (in Japanese)

Prinya Lorchirachoonkul, Masaya Nakata, Yasuyuki Yamada, Tomoichiro Okamoto, The 29th Fall meeting, 2016, Hiroshima, Japan. (in Japanese)

Prinya Lorchirachoonkul, Masaya Nakata, Yasuyuki Yamada, Tomoichiro Okamoto, The 8th Thailand-Japan International Academic (TJIA) (TJIA2016), Tokyo, Japan.

Prinya Lorchirachoonkul, Masaya Nakata, Yasuyuki Yamada, Tomoichiro Okamoto, The The 5th international Gigaku conference in Nagaoka, 2016, Nagaoka, Japan. (Poster)

Prinya Lorchirachoonkul, Masaya Nakata, Yasuyuki Yamada, Tomoichiro Okamoto, The The 6th international Gigaku conference in Nagaoka, 2017, Nagaoka, Japan. (Poster)

Prinya Lorchirachoonkul, Masaya Nakata, Tomoichiro Okamoto, The 5th International Conference on Engineering, Energy, and Environment (ICEEE 2017), Thailand. [Award]

Prinya Lorchirachoonkul, Masaya Nakata, Tomoichiro Okamoto, - The 4th International Symposium on Hybrid Materials and Processings (Hymap 2017), Korea.